UNIVERSITÀ DEGLI STUDI DI NAPOLI PARTHENOPE

DIPARTIMENTO DI INGEGNERIA

CORSO DI DOTTORATO IN ENERGY SCIENCE AND ENGINEERING

XXXVIII CICLO

Techno-Economic and Environmental Analysis of innovative Proton-Conducting Ceramic Electrolyzers for sustainable hydrogen production.

Relators:

Prof. Minutillo Mariagiovanna

Prof. Jannelli Elio

Candidate:

Romano Fabiana

Matr. DR06000070

ACCADEMIC YEAR 2024/2025

Alle Donne,

Figlie della rivoluzione.

INDEX

ABSTRACT

According to the *Fit for 55 package*, *REPowerEU plan*, and *Renewable Energy Directive III*, sustainable hydrogen production constitutes a strategic priority for decarbonizing hard-to-abate sectors. As an energy carrier, hydrogen must be produced. While conventional water electrolysis technologies (Alkaline, Proton Exchange Membrane, and Anion Exchange Membrane Electrolyzers) are mature, they present significant technical and economic barriers to large-scale deployment.

Proton-Conducting Ceramic Electrolyzers (PCCELs) offer innovative potential: operating at intermediate temperatures (400–600°C) enables non-precious materials for cost savings. Separate hydrogen production eliminates downstream separators and compressors, reducing plant size and installation costs. However, operation at such temperatures still accelerates material degradation, limiting efficiency and productivity. Research thus focuses on materials and single-cells, lacking integrated stack/system assessments, economic feasibility studies, and environmental impact evaluations. The scalability of PCCEL technology represents another unresolved challenge, requiring further research to achieve full commercialization.

This thesis addresses these gaps through a *Techno-Economic* and *Environmental Analysis* of a 1 MW PCCEL system under development within the *European PROTOSTACK project.*

Chapter one outlines the regulatory framework, emphasizing green hydrogen's role in the energy transition.

Chapter two provides a comparative analysis of various electrolysis technologies, illustrating the thermodynamic principles, performance profiles, and industrial landscape.

Chapter three characterizes PCCEL technology through description of planar and tubular configurations, electrode and electrolyte materials, and current technical limitations.

In *chapter four*, *Techno-Economic feasibility Analysis (TEA)* is conducted. The PCCEL system, modeled in Aspen Plus^{TM} environment, shows 0.045 MWh/kg H_2 energy consumption. The estimated *Levelized Cost of Hydrogen (LCOH)* is approximately 5.44 €/kg H_2, calculated based on the average electricity cost in Europe in 2024 (75 €/MWh) and assuming oxygen is emitted into the atmosphere. Operating and maintenance costs dominate the total *LCOH* (3.94 €/kg H_2), primarily due to the high energy consumption required by the electrolyzer. Thus, to assess the fluctuations in *LCOH* due to variations in electricity prices, a sensitivity analysis is performed. This analysis considers different prices across the European countries examined and various temporal scenarios (current and future, including renewable energy integration). Finally, since the specific costs of some components are estimates provided by PROTOSTACK partners, they are categorized as "*Class 3*", which has an accuracy range of -10% to +10%. Applying this

variation, the *LCOH* is further estimated; it changes by only ± 0.16 €/kg H_2, confirming the robustness of the Techno-Economic model and underscoring the dominant role of operating and maintenance costs.

Finally, in *chapter five*, a *Life Cycle Assessment (LCA)* is performed in compliance with ISO (International Organization for Standardization) 14040 and 14044, International Reference Life Cycle Data System Handbook (ILCD), and Specific Guidelines for Hydrogen and Fuel Cells (SH2E), applied to the 20-year life cycle of the 1 MW PCCEL system. The functional unit is defined as the production of 1 kg of 99.99% pure hydrogen, available at 30 bar and 30°C. System boundaries include raw material acquisition and pre-processing, manufacturing of the system (electrolyzer, combustion chamber, BoP), and a 20-year operational phase, excluding end-of-life treatment (cradle-to-gate analysis).

According to the Environmental Footprint 3.1 methodology across 16 environmental impact categories, the manufacturing phase contributes 7.10% to total impact (0.117 mPt per functional unit), while the operating phase represents 92.9% (1.54 mPt)—a result consistent with literature recognizing operational impacts as the primary driver of overall sustainability.

Although electrolytic hydrogen is still expensive, when combined with renewable energy sources, it represents the most promising solution for significant emission reductions. Conversely, to effectively mitigate the environmental footprint of the PCCEL system, it is recommended to optimize the design of critical components (cathode, electrolyte, interconnections) and adopt circular economy strategies for recovery and recycling of strategic materials at end-of-life. *These findings provide guidance for PCCEL technology development within the PROTOSTACK project*, with continuous monitoring of environmental performance serving as an essential element to ensure optimization efforts remain aligned with critical bottlenecks while maintaining technical and economic feasibility.

CHAPTER 1: THE KEY ROLE OF HYDROGEN IN THE ENERGY TRANSITION

I.1 Greenhouse gas emissions trends: a global and European analysis

Currently, about 80% of the world's energy is produced from fossil fuels, with coal remaining the most common and polluting source. Global energy demand is expected to rise in the coming years due to the expansion of human activities, leading to significant environmental risks and an increase in greenhouse gas (GHG) emissions [1], [2].

In 2023, the global GHG emissions reached 53 gigatons of CO_2 equivalent (Gt CO_2eq), an increase of 1.9% compared to 2022. In particular, about 73.7% carbon dioxide (CO_2), 18.9% methane (CH_4), 4.7% nitrous oxide (N_2O), and 2.7% fluorinated gases (HFCs, PFCs, SF6) were emitted. The largest increases were recorded in India (+6.1%), China (+5.2%), and Indonesia (+4.1%) while other countries such as the United States (-1.4%), Japan (-6.0%), South Korea (-2.2%), Germany (-10.5%), and Pakistan (-0.7%) reported lower GHG emissions [2]. Consequently, the global average temperature increased by 1.58 degrees Celsius (°C), approaching the 1.5°C long-term target set by the UN′s Paris Agreement on climate change [3]. In the European Union (EU27), the necessary emission reductions have only just begun. GHG emissions have shown a decreasing trend over the past three decades. As shown in Figure 1, in 2023, GHGs amounted to approximately 3.22 Gt CO_2eq, representing a 34% reduction from 1990 and a 7.5% decrease from 2022 [2], [3].

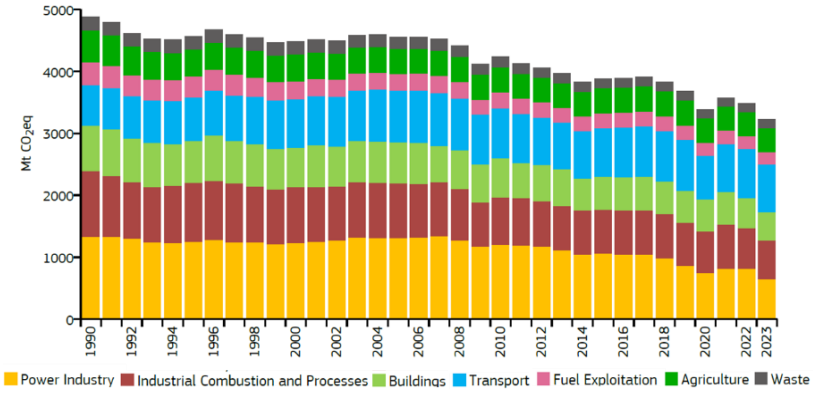

Figure 1. Total annual GHG emissions trend from 1990 to 2023 in the EU27 [2], [3].

The energy sector was the main driver with a 20% reduction between 2022 and 2023, followed by the industrial sector (iron/steel and cement industries), which contributed an 8.1% reduction in GHG emissions thanks to ETS coverage (Emission Trading System), and the transport sector,

with a 2% reduction. Finally, considering direct emissions from fossil fuel combustion in the residential sectors, the buildings sector achieved a 6% reduction in GHG emissions in 2023 compared to the previous year. The agriculture sector was the only one to emit the same GHG amount compared to 2022. These results were obtained primarily by the continued development of renewable electricity production and a combination of reduced output and efficiency gains in industrial sectors. In 2023, renewable energy accounted for about 24% of the EU's total energy mix, marking an increase of 1% compared with 2022 [3].

While the EU27 demonstrates a strong commitment and concrete results in decarbonization and reducing GHG emissions, fossil fuels are continuing to dominate the global energy mix. Therefore, faster energy transition policies and greater investment in renewable technologies are needed. The share of fossil fuel use is expected to gradually decline to 73% by 2030 [4].

I.2 Regulatory framework

The *Kyoto Protocol*, adopted in 1997 under the United Nations Framework Convention on Climate Change (UNFCCC), was the first international accord aimed at reducing global GHG emissions. It required the 192 signatory countries to reduce their emissions by about 5% below 1990 levels by 2012, and up to 20% by 2020. To assist these countries, the Kyoto Protocol introduced the use of several market-based mechanisms [5], [6]:

- The Joint Implementation (JI), which allowed countries to purchase carbon credits from emission reduction projects in other industrialized countries.
- The Emission Trading System (ETS), which allowed to create a carbon market where countries exceeding emission cuts could sell excess allowances to those struggling to meet their limits.
- The Clean Development Mechanism (CDM), allowing industrialized and transitional countries to invest in emission reduction projects in developing countries, generating Certified Emission Reduction credits.

The Kyoto Protocol was limited to developed countries, excluding major emerging economies such as China and India, which led to criticisms of effectiveness and fairness.

To address these limitations and the evolving global context, the *Paris Agreement* was adopted in 2015 (COP21). This Agreement set the goal of limiting global temperature increase well below 2°C and ideally to 1.5°C [7].

To ensure these climate objectives were achieved, in 2019 the European Union presented the "*Green Deal*", a set of political and legislative proposals aimed at reducing GHG emissions from 40% to 55% by 2030 and achieving climate neutrality by 2050.

Focusing on the 2030 climate target, the European Commission has proposed the "*Fit for 55 package*", strengthening the existing regulatory framework. Particular attention has been paid to the ETS: this directive has been extended not only to the aviation sector, as established in the Kyoto Protocol, but also to the maritime sector. A new carbon cap has also been set for CO_2 emissions, with the aim of reducing them by 62% by 2030 relative to 2005 levels. Starting in 2027, a new and separate ETS is expected in order to cover CO_2 emissions from fuel combustion in buildings, road transport, and other sectors. All hydrogen production methods with a capacity exceeding 5 tons per day, including electrolyzers, have been included in the revised ETS Directive. This allows renewable and low-carbon hydrogen production systems to receive free allowances as an incentive.

The *Renewable Energy Directive* (RED), initially introduced in 2010, laid the basis for increasing renewable energy use in the EU. Over time, this directive has been revised, and the latest version, adopted in 2023 (known as *RED III*) as part of the Fit for 55 package, established a binding target of 42.5% renewable energy share by 2030 [3], [8], [9].

Following Russia's invasion of Ukraine, the European Commission introduced the *REPowerEU plan* in 2022 to quickly cut the EU's reliance on Russian fossil fuels by replacing them with cleaner energy sources. **Green hydrogen** (H_2) is proposed as an essential energy carrier to support the EU's commitment to reach carbon neutrality by 2050. The strategy for the development of renewable hydrogen is based on three steps:

- The first phase (2020 - 2024) consists of the installation of electrolyzers with at least 6 GW capacity to produce up to 1 million tons of green hydrogen on site and to serve industrial processes and bus refuelling stations. In addition, the CCUS (carbon capture, utilization, and storage) infrastructure is implemented to capture CO_2 emitted from existing plants, thereby reducing CO_2 emissions in the hard-to-abate sectors and enabling the production of low-carbon hydrogen.
- The second phase (2025 - 2030) aims to increase electrolyzers capacity to 40 GW for production of 10 million tons of green hydrogen and to extend the use of hydrogen in the railway and maritime sectors.
- Finally, in the third phase (2030 - 2050), the goal is to use renewable hydrogen on a large scale.

Although hydrogen is a key priority in Europe as a symbol of a breakthrough for decarbonization, today, it represents only a few percent of the global and EU energy mix. It is produced mainly from fossil fuels and is associated with the release of at least 70 million tons of CO_2 per year. The transition to green hydrogen production and the use of renewable resources

for power generation is a hard challenge. The main obstacle is often the high cost of dedicated hydrogen production and utilization equipment, storage, and refuelling plants [10], [11].

I.3 Hydrogen as a strategic energy carrier for decarbonization

Hydrogen is the lightest chemical element and offers high energy density, efficiency, and versatility. Since the 1970s, hydrogen has been recognized as a potential alternative fuel to fossil fuels in the transport sector. However, due to high investment and production costs, the use of hydrogen did not spread rapidly. Nonetheless, the growing need for countries to reduce GHG emissions and use cleaner fuels has allowed hydrogen to re-emerge as one of the most promising solutions to support decarbonization in various sectors by meeting both the rising energy needs and environmental concerns [12].

While the decarbonization of light transport and residential heating and cooling is now a widely shared and established goal, reducing GHG emissions from heavy transport (road, maritime, and air), and energy-intensive industries (such as steel, chemical, and petrochemical sectors) is a much more complex challenge.

It is forecast that by 2050 global heavy truck activity will account for over 75% of total road transport GHG emissions. To address this growth, the adoption of battery electric vehicles and heavy trucks powered by renewable hydrogen, alongside the use of biofuels, constitutes an effective strategy to achieve net-zero emissions.

Similarly, maritime transport shows an increasing emissions trend, expected to rise by 130% compared to 2008 levels by 2050. This highlights the need to overcome dependence on fossil fuels by shifting to green hydrogen-based fuels such as green methanol, ammonia, and synthetic methane. These fuels reduce environmental impact while maintaining adequate performance for maritime logistics.

In aviation, decarbonization primarily involves adopting technological solutions aimed at improving aerodynamic efficiency, reducing aircraft weight, and integrating lower energy consumption engines. Additionally, modal shifts towards more sustainable means, like rail transport, are favored for short-distance travel. Low-carbon biofuels represent the most technologically straightforward and immediate option for sector decarbonization, while e-kerosene and green hydrogen are expected to have significant roles in medium and long-term transitions, respectively.

Regarding the steel industry, characterized by high energy demands, hydrogen can be serves two purposes: as a primary reducing agent, replacing natural gas in chemical reduction

processes, and as a fuel for generating high-temperature heat required in furnaces. However, hydrogen adoption requires technological adjustments in furnaces and burners due to its distinct chemical properties compared to traditional fuels.

In the chemical and petrochemical sectors, hydrogen is used in synthesis and chemical production, complemented by biomass, synthetic hydrocarbons, and clean CO_2 sources [13], [14], [15], [16], [17].

As shown in Figure 2, approximately 280 European projects are in the planning and development phase, aiming to consume more than 7 million tons of clean hydrogen per year by 2030. The greatest share of hydrogen consumption is expected in the ammonia and steel sectors, with approximately 2 million tons/year of clean hydrogen demand for each [8].

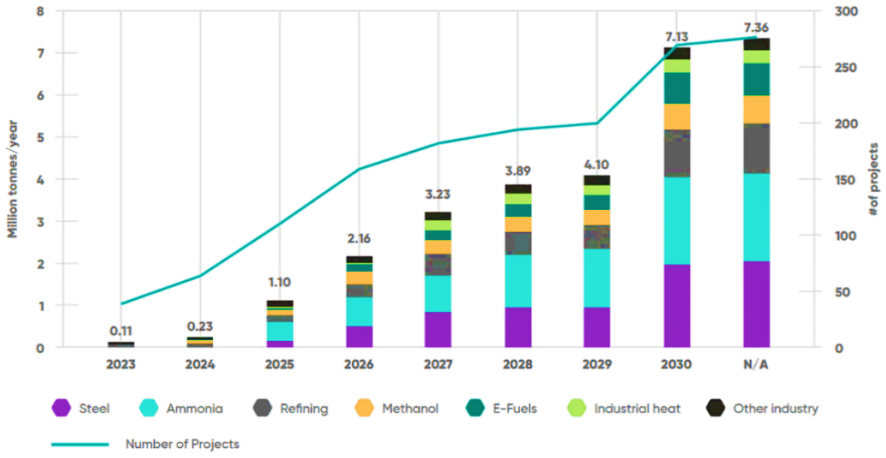

Figure 2. Expected clean hydrogen consumption in industry sectors by 2030 in Europe [8].

In conclusion, green hydrogen is recognized as the most promising solution for decarbonizing these energy-intensive sectors, although its widespread operational and industrial deployment remains distant in time.

I.4 Hydrogen supply chains

All the related environmental advantages achieved by using hydrogen are highly dependent on the production methods and primary sources used (Figure 3) [12].

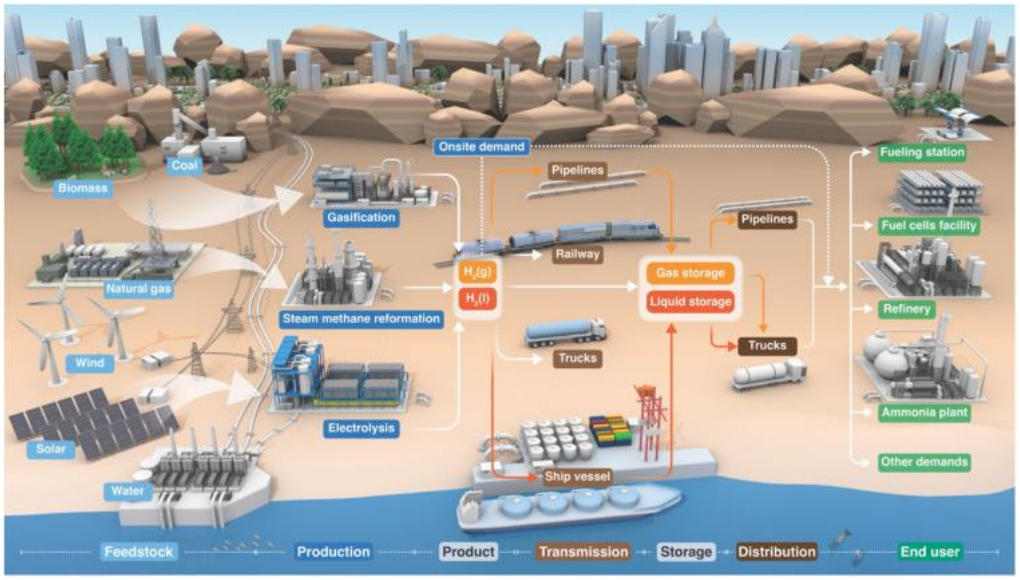

Figure 3. Hydrogen supply chain [12].

Fossil fuels dominate global hydrogen production: in 2022, about 96% of hydrogen was produced by these fuels [18]. The most used fossil fuel-based technologies are methane reforming and pyrolysis. Steam reforming of methane (SMR) is a widely developed and used process: carbon monoxide and grey hydrogen are obtained from steam and methane, giving rise to synthesis gas. Through a further water-gas shift reaction, carbon monoxide is converted into carbon dioxide, and more grey hydrogen is obtained, reaching an overall of about 76% of hydrogen. To maximize hydrogen production, high performance catalysts are required, which are often based on nickel supported by ceramic oxides or oxides stabilized by hydraulic cement. This process has a high environmental impact, as the carbon dioxide produced is released into the atmosphere. Coupling this process with CCUS techniques to reduce atmospheric emissions, it is possible to produce blue hydrogen. These technologies are considered as bridging before a full transition to green hydrogen.

In the methane pyrolysis process, the light liquid hydrocarbons are converted into elemental carbon and turquoise hydrogen without CO_2 production. However, the solid carbon produced is deposited on the active sites of the catalysts, causing both the deactivation of these components and reactor blockage. Therefore, it is not always the best solution for producing hydrogen [18], [19], [20], [21].

There is a growing interest in biological and renewable sources for brown and green hydrogen production, respectively. The biological sources, derived from organic materials, are an eco-friendly, cost-effective, and efficient strategy to solve the energy crisis. Given current technological advancements and economic conditions in many developed nations, the technical

and economic viability of brown hydrogen production is well-established. It is forecasted that about 10% - 50% of the energy consumption in the world will be produced from biomass until 2050.

Another highly promising and environmentally sustainable method is the electrochemical process using nuclear or renewable energy sources. The electrolysis process, the most significant primary electrochemical method for producing molecular hydrogen, involves splitting water into hydrogen and oxygen without generating harmful emissions. If nuclear energy sources power the electrolyzer, yellow hydrogen is obtained. It is expected to produce more than 200,000 t of hydrogen per year for a single 1,000 MW nuclear reactor [20].

On the other hand, if electrolyzers are powered by renewable energy sources such as solar and wind, it is possible to obtain green hydrogen.

The hydrogen produced (whether with low or zero carbon emissions) can then be used directly onsite, storing it in liquid or gaseous form, and distributing it locally or transporting it long distances [12]. Road transport is considered more suitable for local distribution, given the limited transport volumes that can be achieved. Pipelines and ship vessels are recommended for national and regional transport. Hydrogen can be transformed into methane through the methanation process and transported as green natural gas or synthetic natural gas (SNG) via existing liquefied natural gas (LNG) infrastructure. It is possible to use existing LNG pipelines, but this involves considerable effort and expense. Therefore, there is the possibility of importing liquid hydrogen via shipping. In Europe, both new and existing pipelines are used to transport hydrogen over distances of up to 10,000 km, as this is the most cost-effective option. The estimated cost of pipeline transport is approximately 0.16 €/kg for every 1,000 km [22].

At terminals, hydrogen is stored in liquid or gaseous form until distributed to end-users. The steel industry employs hydrogen both as a primary reducing agent and as a fuel for high-temperature heat generation. In the first case, since hydrogen would replace natural gas, specific components would need to be added to ensure the operation of the combustors and furnaces, given its different chemical characteristics as a fuel. In the second case, hydrogen would be burned instead of, or in a mixture with, other fossil fuels to provide heat [17].

Haber-Bosch (HB) process is the most widely used method for ammonia production; however, it is also the most expensive, energy-intensive, and the largest global emitter of greenhouse gases. Generally, the primary feedstocks for producing ammonia in this process are natural gas (50%), oil (31%), or coal (19%). The methane-fueled Haber-Bosch process is considered the most efficient technique, given its higher energy efficiency and lower carbon emissions. It is possible to produce green ammonia by replacing methane reforming and steam turbine

compressors with renewable technologies: hydrogen can be generated through water electrolysis and then converted into ammonia using an HB reactor similar to the conventional process [23].

Finally, hydrogen can be utilized in the transportation sector. To support green mobility, fuel cell electric vehicles (FCEVs) fueled by hydrogen can be adopted. Hydrogen is typically stored onboard as a compressed gas at 350 bar or 700 bar to produce electric power, which is then supplied to an electric motor for propulsion. Light FCEVs consume between 1 and 1.4 kg of H_2 per 100 km and typically store less than 10 kg of H_2 onboard. In contrast, heavy vehicles can consume around 10 kg of H_2 per 100 km and can hold 30-35 kg of hydrogen [24].

Typically, on board ships, electricity is produced by diesel generators, in which chemical energy is converted into electricity through thermal and mechanical energy. In contrast, fuel cells, powered by hydrogen, convert chemical energy directly into electrical energy, thus omitting the indirect path through thermal energy in combustion engines [25].

To utilize hydrogen in the aviation sector, there are two primary options: hydrogen fuel cell systems, which convert hydrogen into electricity to power propellers via electric motors, or the direct combustion of hydrogen in gas turbines with turboprop or turbofan engines. The first option involves a complex systems design that includes compressing ingested air, the fuel cell, heat exchangers, and power electronics. Because of the size effects of the various components in an aircraft fuel cell power system, this setup is considered practical for regional aircraft but less likely to be feasible for short- and medium-range aircraft. For such applications, combusting hydrogen directly in gas turbines is a viable alternative. This method enables turboprop or turbofan propulsion systems to power larger aircraft [26].

In conclusion, all these solutions can be considered fully sustainable if the hydrogen used in industries and the transport sector is produced from renewable resources. It is expected that green hydrogen production will rapidly increase following the expansion of energy production from renewable sources.

CHAPTER 2: LOW AND HIGH TEMPERATURE ELECTROLYSIS TECHNOLOGIES

II.1 History of water electrolysis

In 1789, water electrolysis was first demonstrated by A. Troostwijk and J. Deiman using an electrostatic generator and gold electrodes in a water-filled tube to produce hydrogen gas.

In 1800, W. Nicholson and A. Carlisle performed electrolysis experiments using the voltaic pile (discovered by Alessandro Volta) with copper electrodes, observing oxide formation on the anode. Therefore, their work did not lead to significant practical improvements. Just a month later, J. Ritter worked on the first true water electrolysis. He succeeded in separately collecting oxygen and hydrogen gases from the oxidation-reduction of water.

In 1888, Russian engineer D. Lachinov developed an industrial method for the synthesis of gases via water electrolysis.

Despite these promising early developments, the industrial application of water electrolysis did not become seriously widespread until the late 19th century. By 1902, over 400 electrolysis units with alkaline electrolytes were already in operation. The first membranes were made of asbestos, while the cathodes were based on nickel alloys. However, asbestos proved to be poorly resistant to corrosion in highly alkaline environments at high-temperatures, whereas nickel-based alloys demonstrated superior corrosion resistance and efficiency.

Figure 4 shows the timeline of the water electrolysis development [27], [28], [29].

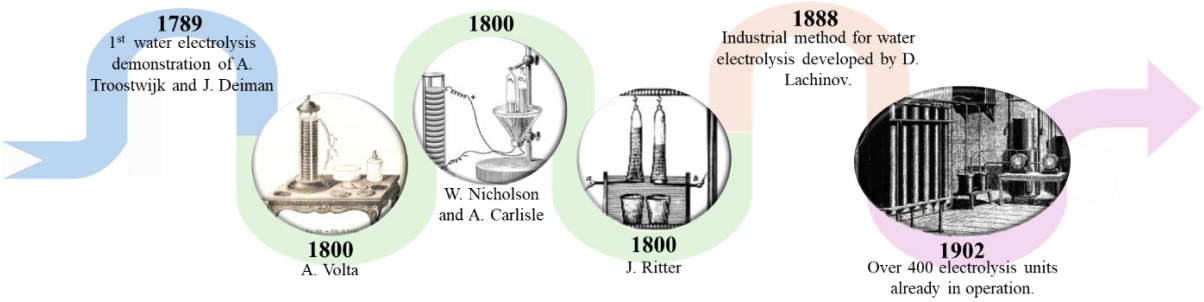

Figure 4. Water electrolysis technology timeline from 1789 to 1902 [28], [29], [30], [31].

Despite great advances in water electrolysis technology, widespread adoption of electrolyzers occurred almost a century later due to several technical and engineering challenges. Among these, it was necessary to develop reliable and efficient direct current power sources and diaphragms to separate the anode and cathode chambers to prevent mixing of the produced

gases. Furthermore, hydrogen production via the electrolysis process required significant improvement in energy efficiency, safety, durability, operability, and reduction in installation and operation costs. During the 20th century, these challenges stimulated important research and developments, resulting in substantial technological advances in water electrolysis [27], [28], [29].

II.2 Thermodynamics and Electrochemistry of electrolytic cells

Water electrolysis uses electricity to decompose water molecules into their constituent elements. The overall chemical reaction, regardless of the specific electrolysis method used, can be represented as [32]:

$$H_2O \rightarrow H_2 + \frac{1}{2}O_2 \quad (1)$$

The total energy demand (ΔH) for this reaction is provided by heat (ΔQ) and electricity (Gibbs energy change ΔG) [32].

$$\Delta H = \Delta Q + \Delta G \quad (2)$$

As shown in Figure 5, the kinetics improves as temperature increases because thermal integration rises; consequently, electrical energy demand decreases [32].

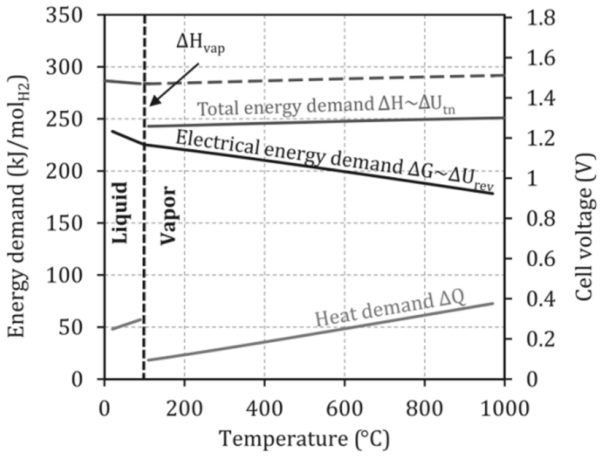

Figure 5. Total energy demand of an ideal electrolysis process as a function of the temperature [32].

The theoretical minimum cell voltage of electrolysis operation, also called reversible cell voltage U_{rev}, is calculated by applying Equation 3. It is directly proportional to the change in Gibbs free energy and decreases with rising operating temperature of the electrolyzer.

The parameters z and F are the number of electrons transferred per reaction (z equal to 2) and Faraday's constant (96,485 C/mol), respectively [32]. U_{rev} assumes values in the range of 1.25–0.91 V.

$$U_{rev} = \frac{\Delta G}{zF} \quad (3)$$

In contrast, the thermoneutral cell voltage U_{tn} represents the minimum voltage required for electrolysis in an ideal cell without heat integration [32]. U_{tn} is about 1.47–1.48 V (284–286 kJ/molH_2) when liquid water below 100°C is considered (dashed blue line), while it is 1.26–1.29 V (243–249 kJ/mol H_2) if feed steam in the temperature range of 100–1,000 °C is taken into account.

$$U_{tn} = \frac{\Delta H}{zF} \quad (4)$$

Thermoneutral voltage represents the standard operation mode of a high-temperature electrolyzer. In contrast, in low-temperature electrolyzers, it is slightly higher than U_{tn} due to heat losses (non-adiabatic operation) and thermodynamic irreversibility.

Therefore, the final cell voltage U is defined in function of the reversible cell voltage and the overvoltages arising from ohmic resistance U_{ohm}, limitations in electrode kinetics U_{act} (activation overvoltages), and mass transport U_{con} (concentration overvoltages) [32]:

$$U = U_{rev} + U_{ohm} + U_{act} + U_{con} \quad (5)$$

These overvoltages can be analyzed through the polarization curve of an electrolytic cell, as shown in Figure 6. This curve is defined by relating current density to cell voltage. When the current density is zero, the cell potential is referred to as the Open Circuit Voltage (OCV). This parameter indicates the voltage drop caused by hydrogen crossover across the membrane, measured in the absence of applied current. The typical electrolyzers' OCV is above 1.2 V [32]. Ohmic overvoltage primarily occurs at medium current densities. It is associated with the ionic resistance of the electrolyte as well as the electrical resistance of the electrodes, current collectors, bipolar plates, and any contact from different components of the cell. Activation overvoltage refers to the electrochemical kinetic behavior and the reaction speed, and it is relevant in low current densities. Finally, concentration overvoltage arises from mass transport limitations, particularly due to a phenomenon known as bubble overvoltage. This occurs when

the products of the reaction accumulate and reduce the effective area of the electrode, leading to an increase in current density. Consequently, bubble overvoltage is more pronounced at high current densities [33].

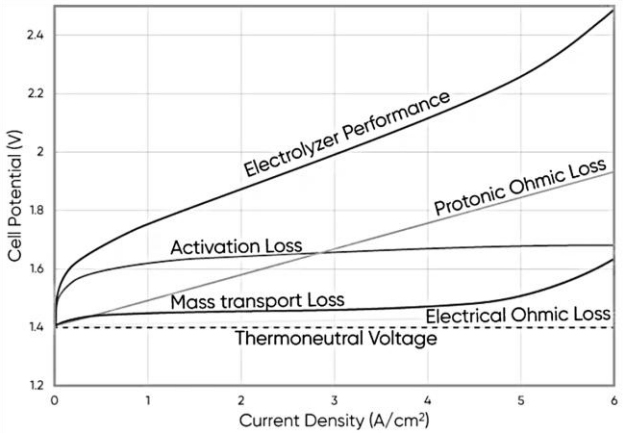

Figure 6. Polarization curve for electrolyzers [33].

From an electrochemical point of view, it is essential to evaluate both the Faradaic and energy efficiency of an electrolyzer. Faradaic efficiency is defined as the ratio between the theoretical electrical charge required to produce a given amount of hydrogen and the real electrical charge used during the electrolysis process. When this efficiency is below 0.95, the electrolyzer is operating under standard conditions; conversely, values greater than 0.95 indicate that the electrolyzer is operating under optimal conditions.

Energy efficiency (η) is another essential parameter to evaluate the electrolyzer's performance: it is calculated as the ratio between the hydrogen production rate m_{H2}, the low calorific value LHV_{H2} and the total electric power input P_{el} [34].

$$\eta = \frac{m_{H2} \cdot LHV_{H2}}{P_{el}} \tag{6}$$

II.3 Water electrolysis technologies classification

Electrolyzers can play a crucial role in producing low- or zero-emission hydrogen when supplied by nuclear or renewable energy sources. Currently, the water electrolysis technologies are employed in different applications ranging from small-scale (household, telecommunication stations) to large-scale systems (in integrated systems, both grid-connected and stand-alone) [29]. Two main electrolysis processes can be distinguished: low-temperature electrolysis such as Alkaline (AWE), Proton Exchange Membrane (PEMWE), and Anion Exchange Membrane

(AEMWE) Water Electrolyzers, and high-temperature electrolysis like Solid Oxide Electrolysis Cells (SOECs). Figure 7 shows the operating principles of electrolysis technologies.

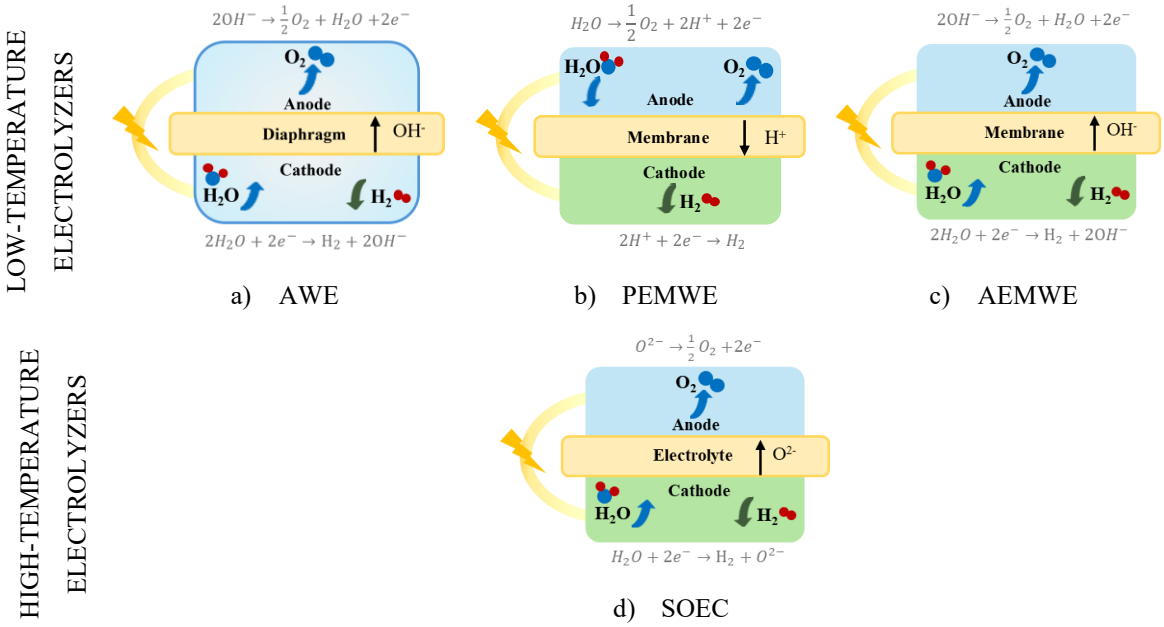

Figure 7. Classification of low and high-temperature electrolyzers: (a) AWE, (b) PEMWE, (c) AEMWE, and (d) SOEC.

Each cell stack consists of a cathode and an anode separated by a membrane containing the electrolyte. Water is split into oxygen and hydrogen when electricity runs through the electrolyte connected to a direct current power source. Due to the modular nature of these electrolyzers, it is possible to design electrolysis systems ranging from a few Watts to a MW when connecting multiple stacks.

The reactions are very similar. They differ only in the type of cation or anion in motion. Both oxygen and hydrogen must be purified, cooled, and dried before being stored or delivered to the market. The oxygen by-product can be commercialized, depending on market availability and purity requirements [35], [36].

There are benefits and drawbacks to every electrolysis technology. AWE, PEMWE, and AEMWE are widely available on the market thanks to their high maturity and Techno-Economic feasibility. These electrolysis technologies ensure safe and efficient hydrogen production, on-site generation, with modular design, fast start-up and shutdown times, and good load-following capability. Therefore, they are preferred in applications where operational flexibility is required [8], [35], [37].

However, their performance remains limited compared to high-temperature electrolyzers due to higher electrical energy consumption. Furthermore, hydrogen crossover through the membrane can occur at low-temperatures and power ranges, compromising gas purity and causing accelerated membrane and electrode degradation. They also require precious metal catalysts (e.g., platinum and iridium), resulting in higher costs [38].

High-temperature electrolyzers such as the SOECs represent a promising technology, although still in the development phase. Operating at 500–1,000°C, this electrolyzer requires approximately 35% less electricity than low-temperature electrolyzer due to improved thermodynamics. Furthermore, residual electricity can maintain the stack at operating temperature when on standby, enabling faster restart times for large-scale operations [13].

Table 1 shows the development status and typical operating conditions for water electrolysis technologies [35]. It is not possible to find all the information on AEMWE, as it is a very recent discovery.

Table 1. Technical targets for water electrolysis technologies in 2022/2024.

Parameters per stack	Unit	AWE	PEMWE	AEMWE	SOEC	Ref.
Development status	-	Market	Market	R&D	R&D	[39]
TRL	-	9	6-8	4-5	5-6	[40]
Scale	-	GW-MW	MW-kW	kW	kW	[39]
Operating Temperature	°C	70-90	50-80	40-80	700-850	[39]
Operating pressure	bar	1-30	30	<35	1	[39], [40]
Electrical consumption	kWh/kg H_2	51	51	55	34	[41], [42], [43], [44]
Current density	A/cm^2	0.5	2.0	1.0	0.6	[39], [42], [43], [44]
Voltage	V/cell	1.9	1.9	-	1.28	[42], [43], [44]
Average degradation rate	%/1,000 h	0.17	0.25	>1	0.50	[41], [42], [43], [44]
Lifetime	h	60,000	40,000	-	20,000	[42], [43], [44]
Cost	$/kW	250	450	-	300	[42], [43], [44]

Even though the stack is the primary component, it is also fundamental to consider the other Balance of Plant (BoP) components that are necessary to support efficient and safe operation of electrolysis system [36]. Typically, in low-temperature systems, the BoP consists of:

- Liquid-gas separator to separate gases from the electrolyte or water to prevent gas mixing.
- Deionized water unit to prevent potential pollution of the catalyst, diaphragm, or membrane.
- Pressure regulating valves to manage, in particular, the pressure within the alkaline systems, compensating for variations caused by gas diffusion through microporous membranes or diaphragms. They help maintain optimal operating conditions and system safety.

- Refrigeration system to control temperature rise (due to heat generated from electrical energy losses) by cooling the circulated electrolyte or water and maintaining stable operational conditions.
- Dryer and purificator to acquire hydrogen as dry and pure as possible.
- Power electronics unit to guarantee continuous current to the stacks.
- Sensors to control and monitor the electrolysis systems.

In addition to these components, for high-temperature electrolyzers, other subsystems must also be taken into account, such as:

- Heating stack subsystem that could be necessary to increase the fluid's temperature entering the electrolyzer.
- Steam production system to produce the steam required by the electrolyzer.
- Preheated air supply unit to regulate and ensure proper temperature circulation within the electrolyzer.
- Subsystem for steam and hydrogen supply necessary to combine hydrogen (about 5%) with the initially produced steam to avoid oxidation at the cathode.

In conclusion, low-temperature electrolyzers provide easy operation, compact design, and higher technology readiness levels (TRL 6-9 excluding AEMWE) while high-temperature electrolyzers demonstrate higher efficiency compared to low-temperature electrolysis systems, due to reduced internal resistance losses and enhanced kinetics of both the hydrogen evolution reaction and the oxygen evolution reaction. However, there are only a limited number of projects considering this technology due to the rapid degradation of the cells. Furthermore, regulatory barriers remain regarding the integration of high-temperature electrolyzers with nuclear thermal energy (the main candidate for supplying heat to high-temperature electrolyzers for large-scale clean hydrogen production) [13].

II.3.1 Alkaline Water Electrolyzers

AWE is the most used electrolysis technology due to its maturity and commercial availability. It offers low operating costs, extended lifetime, and the capability to produce hydrogen efficiently at multi-megawatt scales for commercial applications.

It operates at temperatures between 70°C and 90°C and pressures up to 30 bar, with an efficiency of 70%. Furthermore, it produces hydrogen with a purity between 99.5% and 99.9%. Therefore, an additional purification step is required to remove residual oxygen and achieve higher purity hydrogen (>99.999%) [36], [39].

As reported in Equations 7 and 8 [45], in the alkaline electrolysis process, water is split at the cathode to produce hydrogen and hydroxyl ions (OH^-) that travel to the anode to generate oxygen and water.

Cathode $$2H_2O + 2e^- = H_2 + 2OH^- \quad (7)$$

Anode $$2OH^- = \frac{1}{2}O_2 + H_2O + 2e^- \quad (8)$$

Aqueous solutions of potassium hydroxide (KOH) or sodium hydroxide (NaOH) are typically used as the electrolyte due to their high ionic conductivity. The electrodes, generally composed of nickel or nickel-coated stainless steel, are immersed in the electrolyte and act as the gas diffusion layer, while stainless steel and nickel-coated stainless steel are used for bipolar and end plates manufacturing, respectively [45], [46].

Industrial AWE units are commonly designed with different cell connections. These cells can be connected in parallel, or in series. In the first case, all anodes and cathodes are linked in parallel, typically using copper or aluminum busbars to minimize Ohmic losses and ensure uniform current distribution. Alternatively, cells can be connected in series, forming a bipolar assembly. In series configuration, electrical current enters and exits via end plates, with the cathode of each cell electrically connected to the anode of the adjacent cell [45].

Whatever the configuration, the AWE works at limited pressures and cannot operate under transient conditions, limiting its integration with variable renewable energy sources. In fact, it is usually deployed in a continuous mode for stationary hydrogen production in an industrial environment [13], [45], [47].

II.3.2 Proton Exchange Membrane Water Electrolyzers

In PEMWE, protons H^+ are generated at the anode and migrate through the solid polymer electrolyte membrane to the cathode where they are reduced to produce hydrogen, while oxygen is produced at the anode (Equations 9 and 10) [45].

Cathode $$2H^+ + 2e^- = H_2 \quad (9)$$

Anode $$H_2O = \frac{1}{2}O_2 + 2e^- + 2H^+ \quad (10)$$

Operating at 50-80°C and 30 bar [35], this technology produces pure hydrogen, typically achieving a purity of up to 99.9%. PEMWE offers several benefits, including high energy

efficiency, compact design, high current density operating, and a shorter response time to intermittent input of the renewable energy sources compared to AWE. These advantages translate into faster hydrogen production rates and smaller equipment footprints compared to traditional alkaline electrolyzers. However, significant challenges remain.

The materials required for PEMWE layers (the catalyst, membrane, current collector, and bipolar plates) tend to be expensive. Current electrocatalysts are based on platinum and palladium for the cathode and iridium oxide/ruthenium dioxide for the anode. The polymer electrolyte membrane is often made from costly materials such as perfluorinated sulfonic acid polymers (Nafion) [13], [29], [37]. Due to high operating pressures and current densities, these membranes are prone to durability issues, leading to frequent maintenance and replacement costs. Furthermore, another critical problem is the permeation of hydrogen through this membrane. Even small amounts of hydrogen produced at the cathode can diffuse to the anode in gaseous form. This hydrogen crossover creates a potential safety hazard by allowing hydrogen and oxygen to mix, risking explosive gas formation. For this reason, selecting materials for membrane fabrication must be done with great precision and care, balancing efficiency, cost, and safety [48]. Titanium mesh or carbon cloth usually serves as the gas diffusion layer, while platinum or gold-coated titanium is employed for bipolar plates and end plates manufacturing, respectively [46].

Despite high material costs and durability issues, this technology finds application in small-scale, such as in space and military environments, where its compact design and high efficiency justify the expense. However, recent studies have demonstrated that PEMWEs, made with cheaper alternative materials and more durable membranes, can now reach megawatt-scale power capacities, enabling larger-scale hydrogen production [13], [29], [37].

II.3.3 Anion Exchange Membrane Water Electrolyzers

AEMWE represents an emerging technology that offers a promising solution to overcome the AWE and PEMWE limitations. This innovative electrolyzer operates at high pressures with a compact design comparable to PEMWE but it does not require a separate drying unit, as hydrogen exits the stack with minimal moisture. In addition, AEMWE is composed of low-cost metal catalyst characteristic of AWE and employs its same electrochemical principle: water splitting at the cathode produces hydrogen and OH^-, which migrate throughout the ion-exchange membrane to the anode where they recombine to form water and oxygen. The oxygen produced is released from the anode.

In AEMWE technology, quaternary ammonium-based anion exchange membranes are typically employed due to their excellent ionic conductivity and chemical stability under alkaline conditions. Nickel, iron, and cobalt-based catalysts are employed for their excellent activity in both oxygen evolution (anode) and hydrogen evolution (cathode) reactions. To facilitate gas diffusion and electron transport, nickel foam or carbon cloth is used as the gas diffusion layer, ensuring high surface area and good electrical conductivity. The bipolar and end plates are usually made of stainless steel or nickel-coated stainless steel. Material selection in AEMWE design must balance mechanical integrity, corrosion resistance in alkaline environments, and efficient electron transport to optimize cell performance [49], [50].

II.3.4 Solid Oxide Electrolysis Cells

The SOEC is the best-known high-temperature electrolyzer. When electrical potential is applied to SOEC (Equations 11 and 12), steam supplied to the porous cathode undergoes electrochemical reduction, producing hydrogen gas and oxygen ions. The hydrogen produced diffuses through the cathode surface and is collected as product, while the oxygen ions are transported through the dense solid oxide electrolyte to the anode [45].

Cathode $$H_2O + 2e^- = H_2 + O^{2-} \quad (11)$$

Anode $$O^{2-} = \frac{1}{2}O_2 + 2e^- \quad (12)$$

Operating at high-temperature s (700–850°C) [39], SOEC components must meet stringent requirements. To optimize ionic conductivity, layers are fabricated with precise thicknesses, resulting in delicate cell assemblies that require careful handling [36]. Common anode materials include strontium and cobalt-based perovskites, while cathodes employ nickel and yttria-stabilized zirconia. The electrolyte typically consists of ceramic materials (e.g., yttria-stabilized zirconia or nickel-based cermets) that provide high ionic conductivity while preventing crossover of hydrogen and oxygen. An intermediate diffusion barrier layer (typically yttrium-doped ceria or gadolinium-doped ceria) is placed between the anode and the electrolyte to ensure thermal and chemical compatibility between the two layers, prevent element migration, and preserve long-term cell performance. The interconnect layer serves a crucial role as both a current collector and a physical barrier that separates the electrodes between the two adjacent cells. The materials used are chromium alloys and high chromium containing stainless steel. Thus, the choice of electrode and the electrolyte materials plays a key role in this electrolysis process [13], [35], [45].

Due to its high-temperature operation and efficiency, SOEC can be integrated with industrial processes where waste heat can be recovered to improve overall system performance or co-produce syngas via steam and CO_2 reforming. Furthermore, the SOEC is reversible and can function as a fuel cell to generate electricity through the inverse reaction [47]. However, it remains at an early development stage due to its lowest nominal capacity (150 kW) [36].

II.4 Current and future landscape of electrolysis systems installation and market outlook

In 2023, global electrolyzers manufacturing capacity increased by 3.9 GW in Europe, 4.9 GW in China, 2.1 GW in North America, 0.5 GW in India, and 3.0 GW in the rest of the world, compared to 2022. China and Europe were the world leaders in electrolyzer manufacturing capacity, with 34% and 27% respectively.

Focusing on Europe, among the available technologies, AWE and PEMWE accounted for approximately 58% and 41% of the total capacity, respectively. AEMWE, and SOEC, being relatively less mature, showed lower capacity compared to the first two electrolyzers.

Despite recent expansion, current manufacturing capacity remains insufficient to meet the EU's ambitious targets for renewable hydrogen production by 2030: to reach an annual production of 10 million tons of hydrogen, approximately 100-120 GW of installed electrolyzer capacity would be required. This implies that the annual growth rate of installed capacity needs to be at least 40% for Europe to become self-sufficient in electrolyzer manufacturing [8].

A significant challenge in electrolyzer deployment involves cost assessment, as pricing varies considerably due to several factors [45]: most electrolyzers remain in early commercial phases, technology type, design, materials and manufacturing maturity significantly impact costs, and regional manufacturing costs and rapid production scale-up affect pricing dynamics.

In percentage terms, AWE and PEMWE costs constitute 40-50% of the total capital expenditure. The remaining costs are attributed to the BoP components. Comparable cost data for AEMWE and SOEC are limited, as these technologies remain largely at the laboratory scale with few commercial manufacturers [51]. Therefore, to reduce the AWE and PEMWE stack costs, two main strategies can be employed: Substitute less critical materials, redesign stacks for improved efficiency and durability, and increase current density capability and scale up module size to achieve manufacturing economies of scale. These findings underscore the critical need to expand European electrolyzer manufacturing capacity to meet 2030 decarbonization targets while maintaining technological competitiveness.

CHAPTER 3: INNOVATIVE PROTON-CONDUCTING CERAMIC ELECTROLYZER

III.1 Characterization of Proton-Conducting Ceramic Electrolyzers

SOEC technology differs from AWE, PEMWE, and AEMWE due to its better thermodynamic and kinetic performance. However, when operating at high-temperatures, its stability can be compromised, leading to issues such as electrode degradation and delamination at the electrode-electrolyte interfaces. Moreover, the hydrogen produced requires additional purification and drying because it still contains steam.

Considerable attention is being focused on the ***Proton-Conducting Ceramic Electrolyzer*** (PCCEL), which, although still an emerging technology, may be a promising solution to these challenges. PCCEL operates at intermediate temperatures (about 400-600°C) and achieves higher efficiency than other electrolyzers. Currently, it can operate at current densities up to about 6 A/cm^2 and reach a voltage of about 1.5 V at 600 °C [52], [53], [54], [55].

Proton-conducting ceramics can also operate in a reversible mode, similar to SOEC, converting the chemical energy of fuels into electricity via Proton Ceramic Fuel Cells (PCFCs). In PCFCs, hydrogen is fed to the anode and split into protons and electrons. Protons migrate through the ceramic electrolyte to the cathode, while electrons flow through an external circuit, generating electrical power. At the cathode, protons, electrons, and oxygen from air react to form water, which is the only emission produced [56], [57].

In contrast, the electrolysis process requires both electricity and water as feed to produce hydrogen. As defined in Equations 13 and 14, the steam is sent to the anode, also called positrode or air-steam electrode, and is electrochemically split into oxygen gas, protons (H^+) and electrons (e^-). Oxygen is swept out while protons and electrons are transferred to the cathode (also defined negatrode or fuel electrode) through the proton-conducting electrolytes and to the external electrical circuit, respectively. Finally, protons and electrons are combined at the cathode to produce hydrogen [47], [52], [53].

Cathode $$4H^+ + 4e^- = 2H_2 \quad (13)$$

Anode $$2H_2O = O_2 + 4H^+ + 4e^- \quad (14)$$

Protons are not present in the lattice structure of the current materials employed in PCCELs manufacturing. Therefore, through *hydration* or *hydrogenation methods*, humid conditions

allow the feed water to interact more easily with holes or oxide ion vacancies to produce protons. Figure 8 illustrates the hydration and the hydrogenation mechanisms [55].

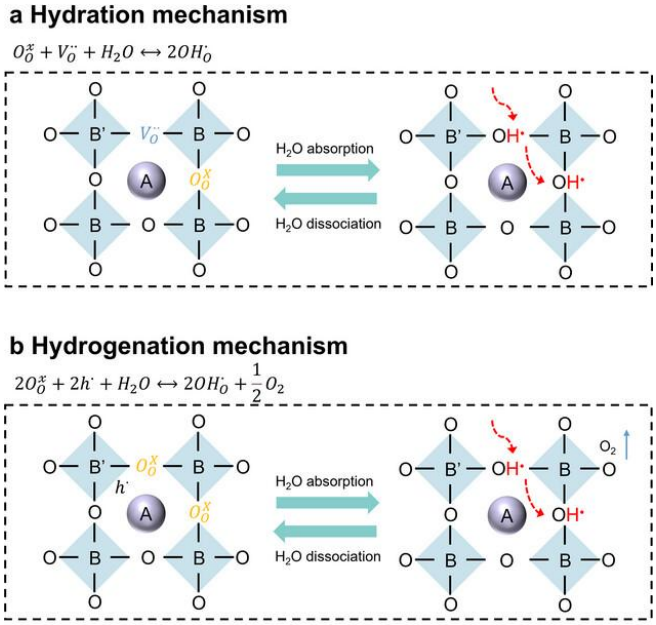

Figure 8. Simplified illustration of a) Hydration and b) Hydrogenation mechanisms [55].

The *hydration reaction* presents oxide ion vacancies. When water dissociates, hydroxide ion (OH^-) and the proton (H^+) are produced: the proton, in particular, occupies the oxygen vacancy ($V_O^{\cdot\cdot}$) and bonds with the lattice oxygen (O_O^x) at the site of the lattice oxide ion (O^{2-}). This reaction generates two mobile proton defects ($OH_O^{\cdot}$) within the lattice structure (see Figure 8a). On the other hand, the *hydrogenation reaction* occurs when both oxygen vacancies and electron holes ($h^{\cdot}$) are present in the material. These electrons react with the hydrogen incorporated into the material, producing protons and oxygen, which is released as a by-product (Figure 8b) [55]. In conclusion, although the PCCEL is in its early stage of design and development, it can play an important role in any application thanks to the production of pure, dry, and pressurized hydrogen. Separators and compressors downstream of the system are not required since the hydrogen is produced separately from the steam supplied. This reduces the size of the hydrogen production plant and, consequently, its cost. Furthermore, proton transport has a higher ionic conductivity than oxygen ion transport in SOECs, thus allowing for lower overvoltage losses and, consequently, higher thermodynamic efficiency. Finally, operating at an intermediate temperature results in less material degradation and more flexible thermal integration [52], [58].

III.1.1 Development of PCCEL in planar and tubular configurations

The PCCEL stacks can be implemented in planar or tubular configurations. The planar structure is much more compact in terms of volume and weight compared to the tubular PCCEL for equivalent electrolysis performance. As shown in Figure 9, the planar PCCEL stack design is similar to that of an oxygen-ion-conducting electrolysis stack (SOEC): the proton-ceramic membrane and electrodes are positioned between two metal interconnects. Steam is fed at the anode (air-steam electrode), while high-purity hydrogen exits at the cathode (fuel electrode) [56], [59].

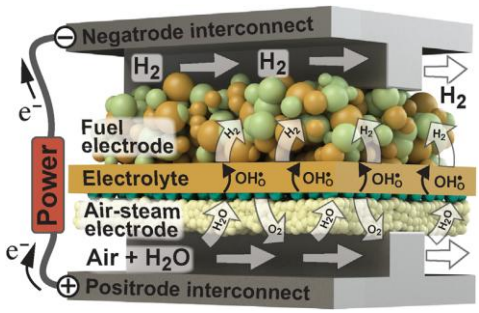

Figure 9. Planar PCCEL stack configuration [53].

In addition to being simpler to manufacture, planar PCCEL features lower internal resistance, thus improving overall system efficiency. Its configuration allows for greater flexibility in gas flow arrangements, facilitating uniform gas distribution across the cell's active surface, a crucial element for optimizing electrochemical reactions and improving performance [59]. Most planar PCCELs have a laboratory-scale button structure, with active areas of about 0.2–0.5 cm^2 [60]. However, some studies available in the literature focus on the development of bigger planar PCCELs: in Figure 10, an example of scaled-up cells compared with a button cell is illustrated [54].

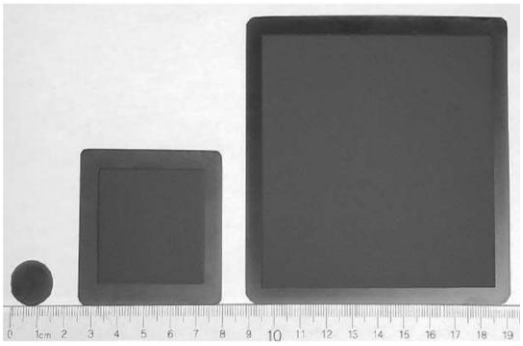

Figure 10. Comparison between the button cell and 5×5 cm^2 and 10×10 cm^2 cells [54].

Tubular PCCEL also has a similar structure to tubular SOEC. It differs in the materials used in the manufacturing process, operating conditions, and chemical compositions. In Figure 11, a

single tubular PCCEL cell is depicted: steam flows along the outside of the main tube, while hydrogen is produced on the cathode (negatrode) and collected in the space between the main electrochemical tube and the internal hydrogen sweep tube [59].

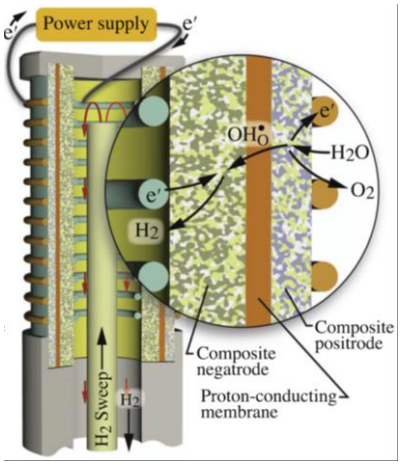

Figure 11. Tubular PCCEL cell configuration [59].

A tubular PCCEL stack typically comprises six cells connected in parallel (Figure 12a). Steam is introduced through a large central feed tube, positioned at the top, and distributed throughout the reaction chamber [59].

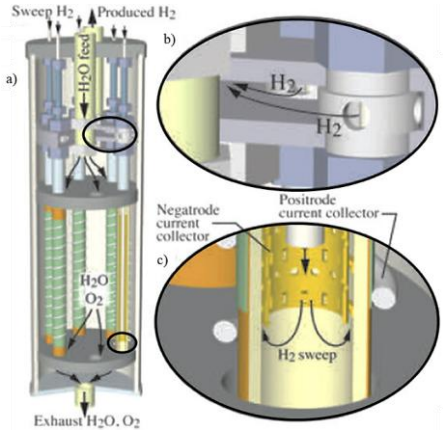

Figure 12. Tubular PCCEL stack configuration composed of six tubes [59].

Depending on the design parameters (such as tube size and spacing) and operating conditions (flow rates, temperature, voltage), the concentration distribution of feed water and oxygen within the chamber varies. It is possible to operate with 100% incoming steam and obtain nearly pure hydrogen as a product or opt for a lower steam conversion to maintain a more uniform gas. The reaction gases are expelled through annular slits in the lower collector (Figure 12b).

As shown in Figure 12c, a small-diameter central tube is inserted inside each electrochemical tube, introducing a small flow rate of hydrogen sweep. This flow is not always necessary, but it is useful for regulating flows and improving thermal and mass coupling between the negatrode structure and the moving gas [59].

The current in tubular PCCELs can be collected either internally (inside the tubes) or externally. The first method can be difficult to implement, while the second is considered an effective strategy for collecting the current. It involves a perforated annular metal structure with flexible tabs in contact with the cathode.

This technology is scalable by connecting multiple stacks in series, allowing for increased system voltage while simultaneously reducing ohmic resistive losses.

The tubular PCCEL configuration offers several advantages over the planar PCCEL configuration. In particular, it needs a smaller sealing area than a planar structure, which requires a seal along the entire perimeter of the cell. Thanks to this smaller sealing area, tubular PCCEL can withstand faster heating and cooling cycles. Furthermore, if a cell in a planar configuration fails, the entire system could be compromised; although it is sometimes possible to isolate the single cell, this leads to complex designs. Instead, replacing a single failed or defective cell in a tubular PCCEL stack is generally easier.

Finally, tubular PCCELs offer better mechanical strength and thermal cycling capacity compared to the planar configuration [59], [61].

III.1.2 Electrodes and electrolytes materials in PCCEL

PCCELs are composed of dense and proton-conducting electrolytes, porous electrodes, and interconnects.

Proton-conducting ceramic electrolytes are generally based on perovskite materials, which are considered the best materials in terms of durability and performance. These electrolytes must be gas-tight between the anode and cathode compartments while selectively transporting protons upon hydration and hydrogenation of the ceramic lattice. Thus, they need to be highly conductive for protons but also minimize electronic conductivity to avoid current leakage. Finally, they should be thin (about 10-20 μm) to provide a shorter ion path, thereby reducing ohmic overvoltages and improving electrochemical efficiency.

State-of-the-art electrolytes are mainly based on single perovskite oxides such as barium cerate ($BaCeO_3$) and barium zirconate ($BaZrO_3$), due to their high proton charge carrier concentrations. To further enhance hydration and proton conduction, it is possible to use acceptor dopants such as yttrium (Y) and ytterbium (Yb) to create oxygen vacancies. As a result,

BZY (barium zirconate doped with yttrium), BZCY (barium zirconate-cerate doped with yttrium), and BZCYYb (barium zirconate-cerate doped with yttrium and ytterbium) have become the most examined electrolytes for PCCELs [58].

Cathodes are composed of a nickel-based cermet (Ni), which serves as an electronic conductor and electrocatalyst, and a ceramic support that acts as a proton conductor (BZY, BZCY, or BZCYYb depending on the type of electrolyte used). To develop a highly stable cathode in PCCELs, doping, infiltration/impregnation, in situ exsolution, and the insertion of a functional layer between cathodes and electrolytes are required. If the electrolyte is thin, the cathode is typically thick and porous, about 0.8-1 mm [58], [62].

Anodes are commonly composed of mixed ionic-electronic conductors which offer excellent electrochemical activity under operating conditions. Therefore, double perovskites, such as barium-gadolinium-lanthanum cobalt oxide material (BGLC), or barium zirconate doped with yttrium along with cobalt and iron elements (BCFZY), can be used as they exhibit good proton and electronic activity in the presence of vapor. The anode is a thin layer, usually 1 µm - 20 µm thick. A thin layer of gadolinium-doped ceria (GDC) or lanthanum-doped ceria (LCO) is also required at the anode-electrolyte interface to reduce cell degradation [47], [53], [58].

Interconnections are necessary for electrical conductivity between the cells and the external power supply. Ferritic stainless steel (SS), based on iron (Fe), chromium (Cr), and manganese (Mn), is typically used for their manufacturing [58].

III.2 Barriers and advances in PCCEL technology

Despite their promising achievements, PCCEL use is limited to small-scale applications due to several technical, mechanical, and environmental issues that compromise their performance. Their TRL is only three or four, indicating low maturity [52], [53].

PCCELs have a relatively low Faradaic efficiency (often below 70%). This means that less than 70% of the supplied energy is converted into hydrogen production, while the remainder is lost due to transport losses or poor reaction in the electrolyte and at the anode-electrolyte interface, causing electron leakage currents [52], [58]. To improve this efficiency, it is essential to develop electrodes with improved water resistance, fuel flexibility, and greater stability [55].

The choice of raw materials used in PCCEL manufacturing is another important factor that must be considered. Current PCCELs rely heavily on rare earth elements, such as Ce, Y, Yb, La, and Gd, as well as transition metals like Ni, Co, Cr, and Mn. These materials are defined as *critical* due to their limited availability, economic value, and geopolitical and strategic situation.

Most of the critical raw materials supply for electrolyzers is concentrated in a few countries: Canada, South Africa, China, and Russia. The risk of supply chain disruptions increases due to political instability and geopolitical tensions, negatively impacting the countries that import and develop electrolyzers. Moreover, this situation can cause prices of raw materials in global markets to rise, affecting the final cost of electrolysis technologies and potentially slowing down the energy transition [58].

Technical issues and possible environmental impacts caused by these raw materials extraction or production can also occur. Ni used in the cathode is somewhat incompatible with proton-conducting materials like BZCYYb and can migrate from the cathode/electrolyte interface to the electrolyte, reducing proton conductivity and, thus, degrading cell performance. Furthermore, it is classified as a metal with a high environmental impact. To suppress Ni coarsening and migration, it is possible to employ a thin NiO-based barrier layer combined with steel [55], [60], [62]. This strategy improves environmental performance and enhances mass and charge transport properties, electrical and thermal conductivity, and mechanical and chemical stability; it also promotes sintering and improves the microstructure of ceramic electrolytes [55].

Instead, the anode is strongly influenced by Co, which improves the oxygen reduction reaction kinetics and ensures electronic conductivity, but limits the material's stability, reduces the hydration capacity, and undesirably increases the compound's thermal expansion coefficient. Therefore, Fe and Mn are considered promising alternatives [61], [62].

In addition to replacing critical materials, End-of-Life (EoL) recycling represents another potential solution to address environmental issues related to the growing demand for raw materials. The use of recycled materials is expected to significantly reduce dependence on primary supplies: for example, minerals such as nickel and cobalt could see a decrease in primary demand of approximately 10% by 2040. This contributes to greater sustainability and a reduction in the environmental impact associated with the extraction of new resources [58].

Additional challenges for PCCELs include scalability and production costs. It is difficult to develop defect-free proton-conducting electrolytes on a large scale because of the risk of cracks and structural issues during sintering. Current perovskite electrolytes, based on barium, require high-temperature s (above 1,600°C) during the sintering process, causing problems during the fabrication of electrolytes and negatively impacting their electrochemical performance. In particular, the high-temperature increases manufacturing costs and induces irregular stoichiometry due to barium evaporation, resulting in reduced electrical/electrochemical performance. For this reason, small-sized electrolytes are currently being developed.

To solve this issue, the development of double-layer cathodes containing NiO is a promising solution: the Ni sintering aid requires lower sintering temperatures (about 1,400°C) and improves the technical and chemical performance of the electrolyte [54]. Furthermore, the economic viability of PCCELs is compromised by the rising cost of raw materials (perovskite oxides and advanced ceramic materials).

In conclusion, to make PCCELs truly competitive with established technologies such as AWE and PEMWE, it is essential to develop cheaper and more efficient synthesis and assembly methods. Furthermore, for PCCELs to be successful on the market, they must offer clear advantages in both performance and cost [55].

Figure 13 summarizes the technological advancements and the current limits of the PCCELs.

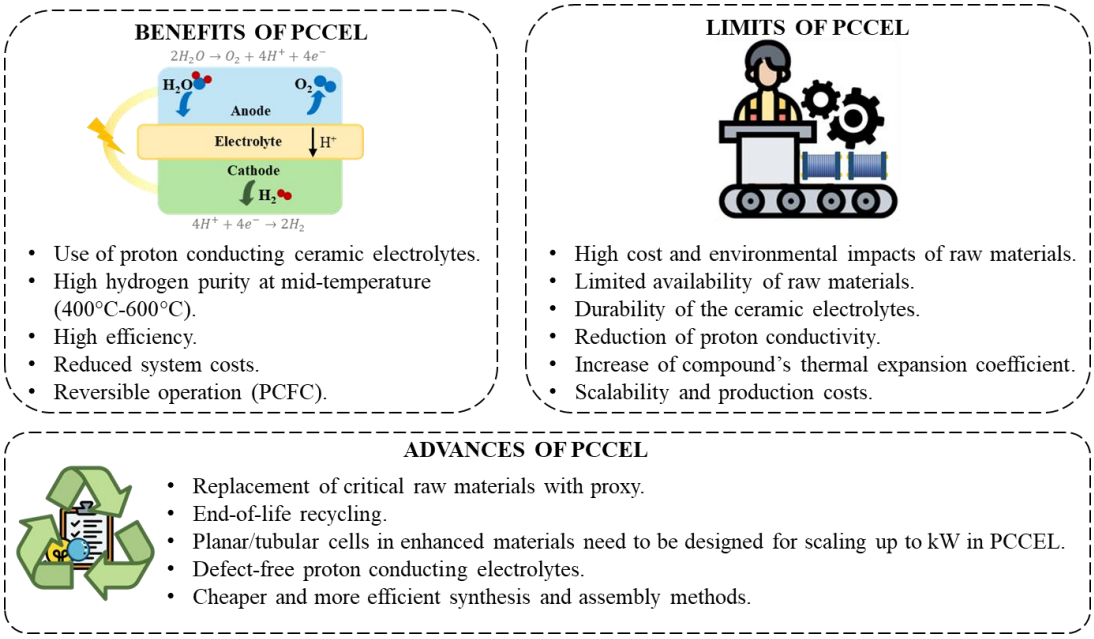

Figure 13. Advancements, limits, and future advances of PCCELs.

III.3 Literature Survey on PCCEL

Some studies have focused on improving proton cell manufacturing and performance. These works aim to improve electrolyte conductivity, chemical and mechanical stability, understanding of material properties at a basic level, low-cost manufacturability, and optimization of operating conditions [45], [53].

Le et al. [56] have investigated the degradation of ceramic proton cells. They developed in the laboratory a planar PCCEL composed of NiO-BCZYYb4411 (60 wt% NiO and 40 wt% BCZYYb) as the cathode, BCZYYb4411 as the electrolyte (spray-coated onto the cathode support), and $BaCo_{0.4}Fe_{0.4}Zr_{0.1}Y_{0.1}O_{3-\delta}$ (BCFZY) as the anode.

This study provided a detailed analysis of the durability of stacks. In particular, the operational conditions' effects on degradation were evaluated, highlighting that stability was improved at operating temperatures of 550°C and with steam feeds below 50%. Furthermore, it was possible to mitigate protonic-ceramic degradation by modifying the anode/electrolyte interface with a 10% doped gadolinium ceria (GDC) interlayer followed by high-temperature reactive sintering. However, the voltage degradation rates remain high at temperatures below 500°C.
Figure 14 shows the changes in surface morphology taken by the GDC interlayer.

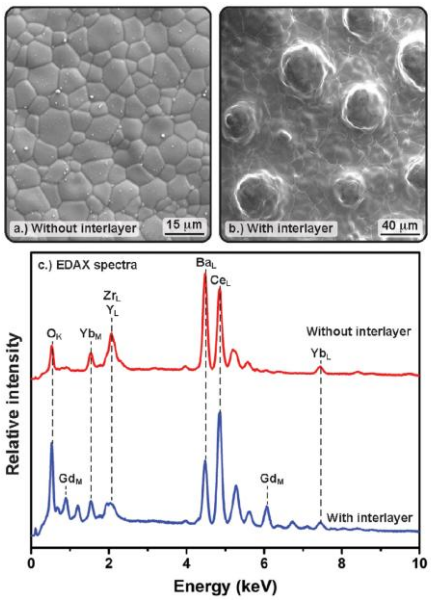

Figure 14. Surface morphology changes a) without GDC and b) with GDC interlayer. C) trend in terms of energy and relative intensity without and with GDC [56].

Compared to Figure 14a, where GDC is not present, Figure 14b illustrates how the GDC particles form well-dispersed, non-percolating islands of 15–20 µm in diameter throughout the electrolyte. In Figure 14c, it is possible to note the benefits obtained from gadolinium and cerium employment in the electrolyte surface. Although the performance and stability improvements brought about by GDC are reassuring, it is possible to use alternative interlayer materials.
Herradon et al. [53] studied the electrochemical behavior of protonic-ceramic cells at elevated pressures starting from the PCCEL developed by Le et al [56]. The electrolyzer operated at 550°C with a pressure range of 1 bar to 12 bar. A flow rate of 100 sccm of fuel (75% H_2 - 25% N_2) is sent to the cathode, and 200 sccm of air containing 10% to 30% vapor to the anode.
The electrochemical performance of the PCCEL was improved with increasing vapor concentration. However, higher vapor content also resulted in accelerated system degradation

rates. By fixing the operating potential at 1.6 V and increasing the pressure from 2.1 bar to 12.6 bar, the ohmic and transport resistances decreased by 33% and 60%, respectively, allowing higher current densities, from 375 to 600 mA/cm². At these high currents, performance improved by 60%. In terms of Faradaic efficiency, a value of 100% was obtained at 5 bar with a steam content of 15%.

Zheng et al. [63] also studied the electrochemical behavior of proton cells. Anodes characterized by high porosity and triple conductivity ($PrNi_{0.7}Co_{0.3}O_{3-\delta}$ (PNC73)) were developed in order to improve catalytic activity and interfacial stability through a self-assembly approach while maintaining scalability. The results demonstrated excellent performance, reaching a current density of 5.04 A/cm^2 at 1.6 V.

In the study by Kwati et al. [60], tape casting and screen-printing manufacturing methods were explored to produce planar PCCEL cells with dimensions up to 50 mm × 50 mm × 0.5 mm. The electrolyte used was a $BaZr_{0.44}Ce_{0.36}Y_{0.2}O_{3-\delta}$-based ceramic (BZCY44362), designed to provide high proton conductivity (10.1 mS/cm at 500 °C in wet 1% H_2) and excellent chemical stability in the presence of steam and CO_2. A NiO-$SrZr_{0.5}Ce_{0.4}Y_{0.1}O_3$ composite material was used for the cathode, chosen to minimize the crack formation during the sintering phase. The results demonstrated a good performance at 1.3 V and 1.37 A/cm² at 600°C. Furthermore, excellent durability of PCCEL was demonstrated, with over 1,000 hours of continuous hydrogen production operation without cell degradation, confirming its robustness and reliability. The authors also performed structural analyses using scanning electron microscopy (SEM), energy-dispersive spectroscopy (EDS), Raman spectroscopy, and X-ray diffraction (XRD) to study the changes induced by sintering at different temperatures. The analyses revealed that at sintering temperatures above 1,350 °C, significant structural changes occur in the electrolyte, with the formation of new defects that alter the perovskite-type structure.

In Figure 15, the schematic illustration of PCCEL cells developed by Kwati et al is reported.

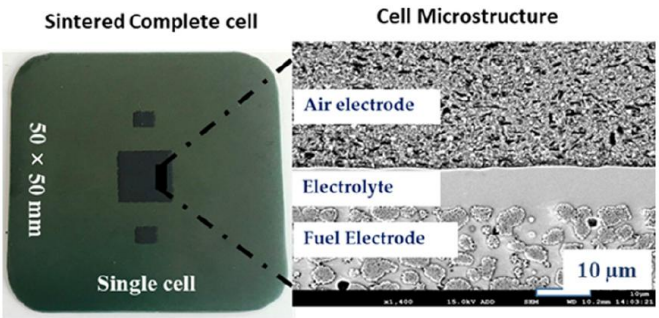

Figure 15. Planar PCCEL cells manufacturing [60].

In the study by Pirou et al. [64], two specific methods were analyzed for the manufacturing of proton cells: tape casting and co-sintering. These cells (of 135 cm^2) were composed of proton electrolytes based on $BaCe_{0.2}Zr_{O.7}Y_{O.1}O_{3-\delta}$ (BCZY27) and cermet electrodes based on BCZY27-Ni (50–50 vol%). The electrolyte and electrode layers were tape cast, laminated and co-sintered at 1,575°C. BCZY27 was chosen as the electrolyte composition due to its good performance in terms of thermodynamic stability and low grain boundary resistance. Initially, the microstructure of the cells, characterized by SEM, showed degradation, limiting their lifetime to a few days. Therefore, in order to solve this problem, a reduction heat treatment after sintering was performed.

Vøllestad et al. [52] presented the first fully operational tubular PCCEL with an active area of 10 cm^2 and a hydrogen production of 15 NmL/min. BZCY72 ($BaZr_{0.7}Ce_{0.2}Y_{0.1}O_{2.95}$) for electrolyte manufacturing was selected for high thermodynamic stability due to elevated zirconium content and low grain boundary resistance due to its moderate cerium content. BGLC ($BaGd_{0.8}La_{0.2}Co_2O_{6-\delta}$) was employed for an anode to combine p-type electronic and protonic conduction. The anode exhibited low activation energy for water splitting, polarization resistances below 1 $\Omega \cdot cm^{2,}$ and Faradaic efficiency of 100% at high steam pressures (1.5 bar), confirming the effectiveness of the selected materials. The cell also showed excellent stability over 700 hours at 600°C, maintaining a constant current density of 62.5 mA/cm^2. An important advantage of this technology was the ability to directly electrochemically compress the hydrogen, achieving a pressure difference of over 30 bar between the hydrogen and steam side. The tubular PCCEL developed by Vøllestad et al. is illustrated in Figure 16.

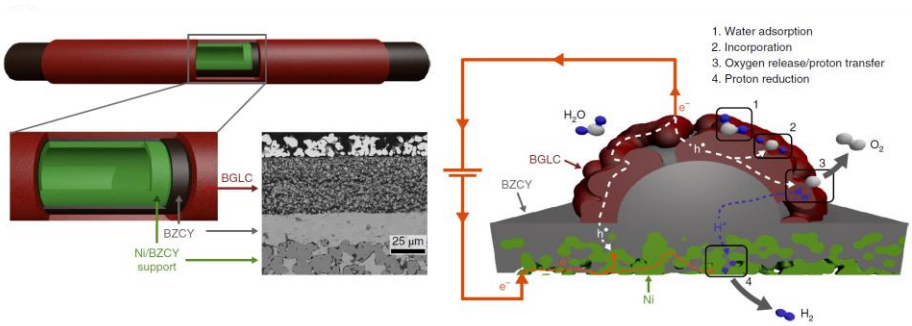

Figure 16. Illustrations of a tubular PCCEL architecture producing dry hydrogen [52].

Kee et al. [59] investigated an anode based on 50% $La_{0.6}Sr_{0.4}Co_{0.2}Fe_{0.8}O_{3-\delta}$ (LSCF) and 50% BZCY. Ni-$BaCe_{0.7}Zr_{0.1}Y_{0.16}Zn_{0.04}O_{3-\delta}$ (Ni-BCZY), with porosity of about 38% and BCZY were selected for cathode and electrolyte, respectively. As shown in Figure 17, the four tubes,

connected at current collection, have inner diameters of 12.3 mm, outer diameters of 16.9 mm, and an electrochemically active length of 306 mm, yielding an active area of 162.5 cm^2.
Tests conducted on the tubular cells showed operational stability for over 700 hours, with a Faradaic efficiency of around 67% and an energy cost of approximately 50 kWh per kg of hydrogen produced.

Figure 17. Tubular PCCEL tubes produced by Kee et al [59].

In conclusion, the few studies available in the literature focus primarily on technical and mechanical aspects. This is mainly due to the low maturity of PCCEL electrolyzers, which, being in the early stages of development, are still subject to extensive laboratory research.
However, European projects are currently starting with the aim of accelerating the large-scale production of proton-conducting ceramic electrolyzers and promoting their industrial deployment.

III.4 PCCEL Project Development

The European *ELECTRA project* (2014-2017) [65], [66] focused on tubular proton ceramic electrolyzer cells operating around 700°C for hydrogen production from steam at pressures up to 20 atm. In particular, a flexible tubular module carrying up to 18 tubes for 1 kW hydrogen production, enabling monitoring, shut-off, and replacement of individual tubes, was developed (Figure 18).

Figure 18. Tubular 1 kW PCCEL prototype developed in the Electra project [65].

Ni and cermet-based support materials for the cathode, perovskite oxide anodes, and Y- and Ce-substituted $BaZrO_2$ (BCZY) for the electrolytes were selected and optimized.

In particular, ELECTRA improved anode production, achieving an anode area-specific resistance (ASR) below 0.2 $\Omega \cdot cm^2$. Stable and sufficiently conductive current collectors and interconnections were also identified and tested, along with various seals depending on the tube generation.

The project also demonstrated co-electrolysis of steam and CO_2 to syngas, enabling highly efficient production of hydrogen and synthetic fuels using renewable heat sources. The results of this project highlighted the potential competitiveness of PCCEL technology at a moderate scale if mass production and cost targets are achieved, despite current durability challenges mainly due to anode degradation.

ELECTRA contributed significantly to scalable fabrication processes, materials development, module design, and system integration towards industrial deployment of proton ceramic electrolyzers for sustainable hydrogen production [65], [66].

The new European *GAMER project* (2018-2020) [67], [68] took into account ELECTRA's progress to realize the 10 kW PCCEL, operating for 2,000 hours, with 30 bar hydrogen production. Adopting a tube-in-shell concept, each single membrane tube was placed in a steel tube (the shell), and current collection was achieved by ensuring good electrical contact between the two (Figure 19).

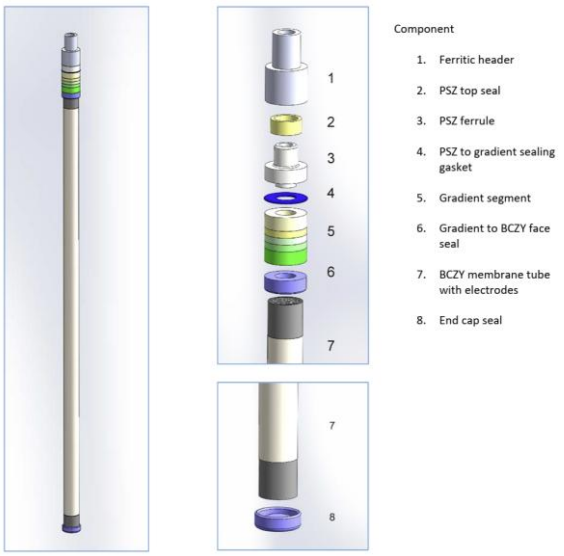

Figure 19. Tube assembly components (shell not shown) [68].

Building upon the GAMER project, the European *Winner project* (2021-2023) [69], [70] implemented PCCEL in three applications: ammonia cracking (for energy storage and usage in the form of green ammonia), dehydrogenation of hydrocarbons (to produce ethylene and pressurized hydrogen), and reversible steam electrolysis.

Novel tubular cells based on a Ni-BZCY72 electrode with BZCY81-dense electrolyte were developed. The cells met performance criteria for reversible electrolysis of ammonia to hydrogen, with a cell area-specific resistance below 1 ohm·cm² at 650°C, a Faradaic efficiency of 80–90%, and a degradation rate below 1.2% per 1,000 hours under reversible operation. A tubular cell was successfully operated reversibly for over 4,000 hours at 4 bar and 650°C [70].

In 2022, a new European project, "*PROTOSTACK*" [71], was introduced based on previous projects. In Figure 20, the PCCEL system (still in the planning phase) is depicted.

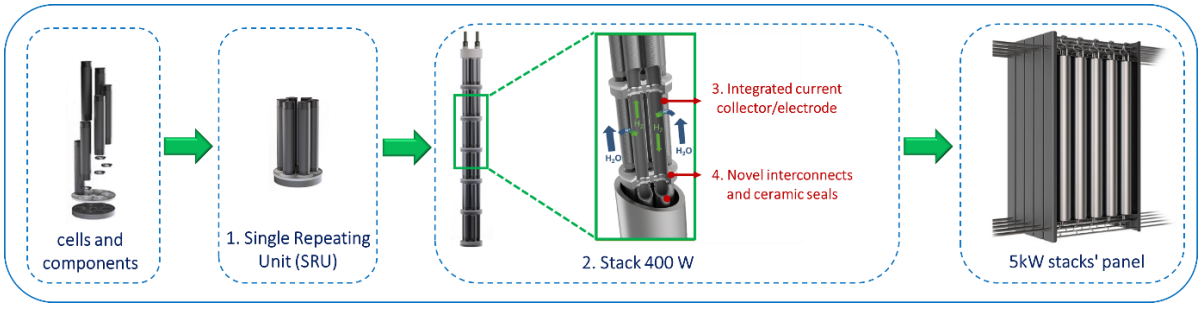

Figure 20. Stack concept in PROTOSTACK project [72]

Each 400 W stack consists of six Single Repeating Units (SRUs), which are electrically connected in series using specialized interconnects and integrated glass-ceramic sealants. Each SRU contains six tubular proton ceramic-based cells, interconnects, and seals.

The stack is demonstrated at 5 kW and provides a pathway for further scaling up to systems of hundreds of kW. The goal of this project is to create a compact and modular PCCEL stack design with an integrated hot-box for operation at 0.5 A/cm^2, with a Faradaic efficiency of at least 90% and delivery of hydrogen up to 30 bar.

In Figure 21, the comparison between Gamer, Winner, and PROTOSTACK projects in terms of current density, cell potential, and efficiency is illustrated [71], [72].

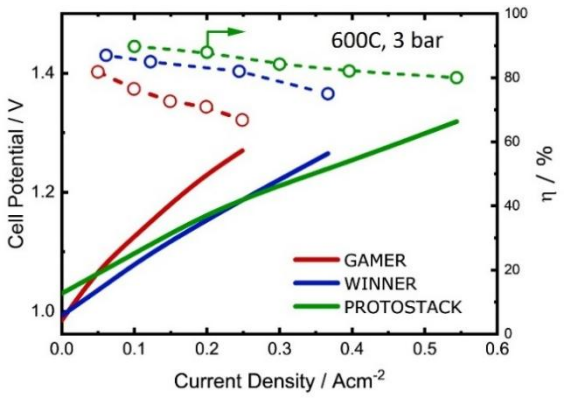

Figure 21. Cell performance evolution across three subsequent EU-projects on tubular PCE technology [71]

III.5 PCCEL feasibility study

The PCCEL is attracting considerable attention due to its high performance at relatively low-temperatures and high pressures, as well as a simpler system configuration compared to SOECs. The reactions inside this electrolyzer require lower activation energy, thus allowing for faster reaction rates and lower operating voltages. Furthermore, hydrogen is produced separately from water, avoiding the need for additional water removal steps from the hydrogen. This reduces the complexity and cost of the post-treatment unit, with the benefit of directly obtaining high-purity hydrogen.

However, operating at elevated temperatures still accelerates material degradation, resulting in reduced cell efficiency and the amount of hydrogen produced per unit of electrical energy consumed. Therefore, although this technology presents very promising characteristics, current research focuses primarily on materials and single cell studies; there are relatively few assessments of the stack/system performance, economic viability and environmental impact.

Moreover, the scalability of the PCCEL presents another challenge, requiring further research to achieve full commercialization [73].

For this reason, this thesis proposes a techno-economic and environmental assessment to analyze the performance, cost-effectiveness, and sustainability of a PCCEL system under development within the PROTOSTACK project.

CHAPTER 4: TECHNO-ECONOMIC FEASIBILITY OF A PCCEL SYSTEM

IV.1 Methodology framework for Techno-Economic Analysis

Techno-Economic Analysis (TEA) plays a crucial role in assessing innovative technologies. By integrating engineering design and process modeling with economic evaluation, this analysis allows the identification of energy-optimal layouts and the main cost drivers and potential strategies to reduce them, with the aim of ensuring the project's profitability. Therefore, there is a strong interest in estimating the system's performance and costs in the first phase of its realization, so that the project can be evaluated and optimized before manufacturing [74].

In this context, TEA is performed by evaluating the technical and economic feasibility of a PCCEL system, *currently under development as part of the PROTOSTACK project*, in order to support the exploitation of hydrogen production from the water electrolysis process using an innovative electrolyzer.

The proposed method consists of a step-by-step procedure, starting with the design and modeling of PCCEL and BoP to evaluate the optimal technical performance of the system, to define cost items related to investment, maintenance and replacement of the components, and concluding with the estimation of the *Levelized Cost of Hydrogen* ($LCOH$) taking into account electricity purchased from the grid and the revenues from oxygen sales. In Figure 22, a flowchart of the TEA methodology applied is illustrated.

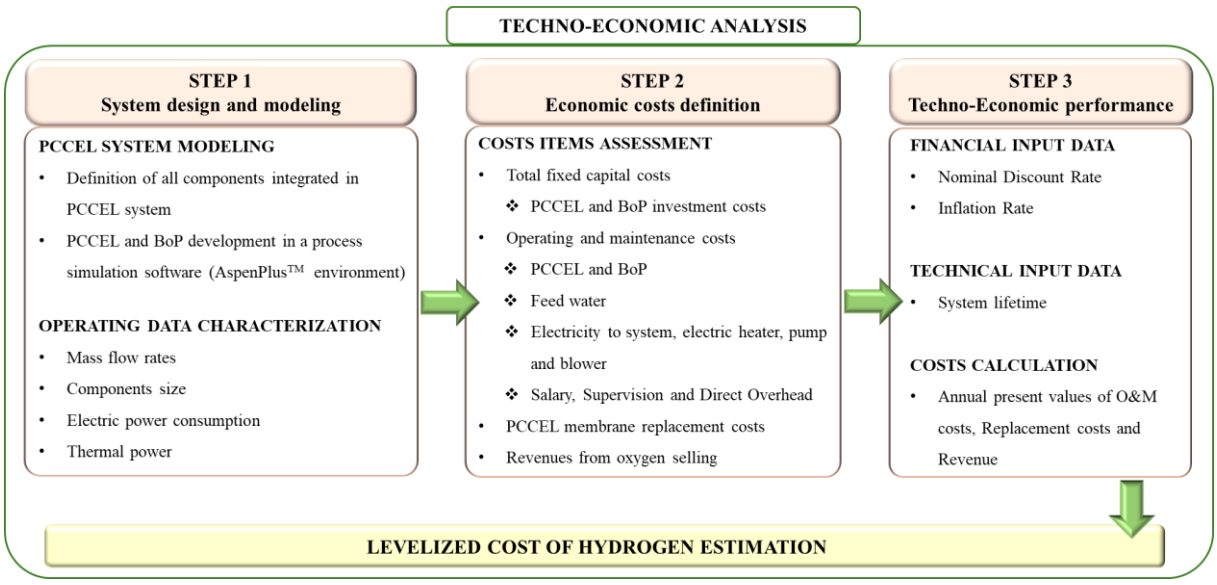

Figure 22. Detailed flowchart of the TEA Methodology.

The first step is to design and model the PCCEL system in Aspen Plus™ environment, defining all components that must be integrated in order to ensure optimal operating performance.
Taking into account the optimal layout of this system, the next step involves the definition of the investment costs, the operating and maintenance costs, and the replacement costs to evaluate the technology's potential for profitable and advantageous deployment in industrial processes. Investment costs include the expenses related to the initial purchase of the system components. Operating and maintenance costs refer to the necessary expenses for maintaining, managing, repairing, and supplying the system. Replacement costs account for the cost of replacing the PCCEL membrane. Finally, this analysis also takes into consideration the revenues obtained from the sale of the oxygen by-product.
The last step is related to the $LCOH$ calculation based on the total fixed capital costs and the annual present costs. The total fixed capital costs include the total costs of designing, purchasing, and installing the electrolysis system; they are calculated by taking into consideration the investment costs of all components and other costs related to the equipment installation (if they are not included in investment costs), expressed as cost factors. The annual present values of the operating and maintenance costs, replacement costs, and revenue are calculated according to the financial data assumed in terms of nominal discount rate and inflation rate, and the system lifetime [75].
The methodology just described is specific to this study, but since a standard framework relating to TEA implementation is not present [74], it can be used as a guideline.
It is clear that, in order to ensure consistent $LCOH$ calculation, some cost drivers like investment costs, the engineering equipment costs, the operating and maintenance costs, the replacement costs, and, finally, the electricity and feed water prices have to be taken into account. Furthermore, it is fundamental to consider technical information related to the specific energy consumption of the electrolysis system and the stack degradation, the system lifetime, and the discount rate useful for calculating the $LCOH$.
The fixed operating expenses, the contingency, the funding, the hydrogen transport and storage, the land costs, and the revenues can be considered as individual decisions. Therefore, it is possible not to assume these cost items in the $LCOH$ estimation [71], [72].

IV.2 PCCEL system design and modeling

The simplified illustration of the PCCEL system is shown in Figure 23.

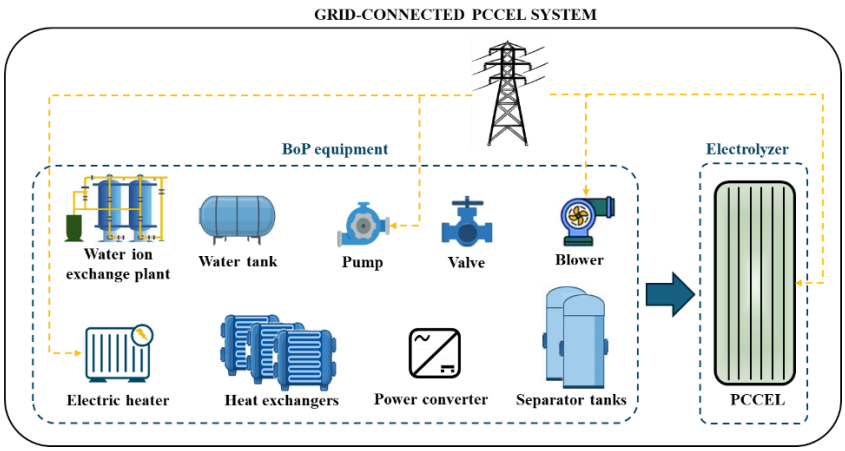

Figure 23. Simplified illustration of the PCCEL system.

The PCCEL has a tubular structure as illustrated in Figure 24 [71]: each SRU contains 6 cells connected in parallel, interconnected, and sealed. Different SRUs, electrically connected in series, form a stack. Finally, multiple stacks can be arranged in a hotbox to maximize electrical efficiency and thermal management [72].

Figure 24. First tubular PCCEL stack prototype in *PROTOSTACK project* [71].

A water ion exchange plant is considered to replace undesirable ions in feed water with more favorable ones by employing synthetic resins. Pumps and valves regulate and control the flow of fluids and gases within the system. The blower provides gases at controlled pressures to sustain the electrochemical reactions. Heat exchangers are essential for recovering heat from the PCCEL exhaust gases and for vaporizing the feed water. An electric heater ensures that specific thermal requirements are met. Finally, separators located downstream of the system separate the liquid water from the produced oxygen and hydrogen.

This system is connected to the European electricity grid to power both the PCCEL and the components of the BoP that require electricity for proper operation (i.e., electric heater, blower, and pump).

IV.2.1 Modeling description

A thermo-electrochemical model of the PCCEL system in the Aspen Plus™ environment is developed in order to calculate key parameters, including mass flow rates (hydrogen, and oxygen), electrical power consumption, and thermal power requirements.

Figure 25 illustrates the system layout: the PCCEL is designed to produce pure, dry, pressurized hydrogen, while the BoP includes essential auxiliary components (a pump, heat exchangers, valve, blower, and separator tanks) for control, regulation, and proper operation of the system.

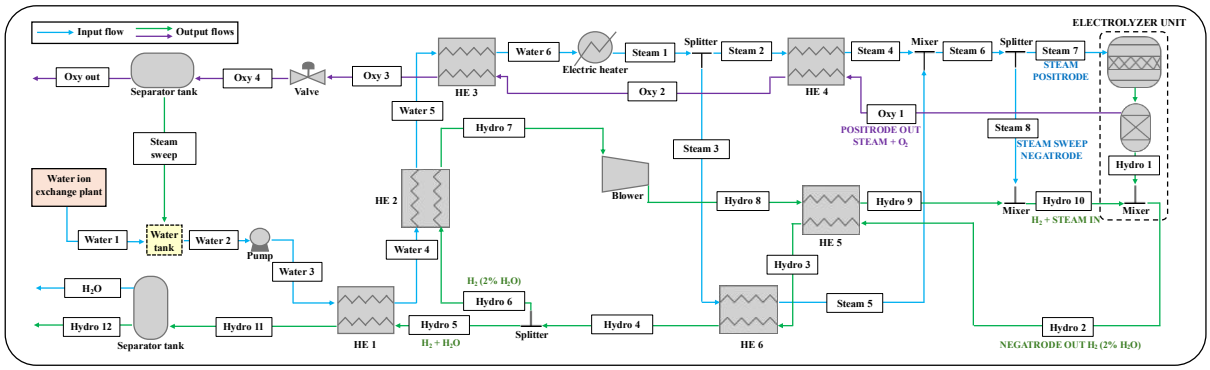

Figure 25. Layout of the PCCEL system developed in Aspen Plus.

Water is treated in an ion exchange plant before being pumped into the system and preheated. Subsequently, this flow (identified as Water 1), at standard pressure and temperature conditions, is mixed with recycled water (Steam sweep) and fed into a circulation pump (inlet flow Water 2). Once it reaches 23.5°C and 30 bar, it is preheated in the heat exchangers HE 1 (outlet flow Water 4) and HE 2 (outlet flow Water 5). In both units, heat is transferred from a hot mixture of steam and hydrogen (inlet flows Hydro 5 and Hydro 6).

At the outlet of the second heat exchanger, the water (at a temperature of 113°C) is further heated in a third heat exchanger (HE 3), reaching a temperature of about 225°C (outlet flow Water 6).

Subsequently, it is vaporized through an electric heater powered by an external energy source (outlet flow Steam 1). The generated steam is split and simultaneously sent to the heat exchangers HE 4 (inlet flow Steam 2) and HE 6 (inlet flow Steam 3) for further heating.

HE 4 utilizes heat from a hot mixture of oxygen and steam coming from the steam positrode (inlet flow Oxy 1), while HE 6 uses heat from hot hydrogen produced at the negatrode (inlet flow Hydro 3). This separation is essential to reach the operating temperature required by the PCCEL for its correct operation.

Finally, steam (identified as Steam 6) is further split into two streams: 98% of it (Steam 7) is sent to the steam positrode, and 2% (Steam 8) is recycled to the negatrode.

The outlet flow from the positrode consists of steam and oxygen (Oxy 1). This mixture is cooled down to 30°C at 1.3 bar and separated into a tank to produce recycled water (outlet flow Steam sweep) and oxygen as a by-product (outlet flow Oxy out).

On the other hand, the Hydro 2 flow, containing 2% steam and 98% hydrogen, comes out of the negatrode. After multiple cooling stages, this flow is split. About 95% (Hydro 5), still containing 2% water, is sent to a separator to remove moisture, obtaining pure hydrogen (Hydro 12) at 30°C and 30 bar while the remaining 5% of the flow (Hydro 6) which also contains 2% water, is further cooled and fed into a blower to be recycled to the negatrode along with Steam 8. In principle, sweeping hydrogen is not necessary. However, if considered, it can be useful to avoid the negatrode oxidation, to improve gas management within the electrolytic cell, and to promote better thermal balance and more efficient removal of the formed gas. This helps improve the performance and durability of the electrolytic cell [59].

The electrolyzer is modeled using two main components: a stoichiometric reactor, where the electro-oxidation reaction takes place, is employed for the steam positrode, and a separator block, where oxygen is separated from hydrogen, is used for the negatrode.

The PCCEL system operates in a thermoneutral mode; therefore, no additional heat input is required. Table 2 summarizes the nominal operating data for the 1 MW PCCEL system.

Table 2. Technical characteristics of the PCCEL system.

Parameters	Values
Operating PCCEL Temperature (°C)	600 [52][a]
Operating PCCEL pressure (bar)	30 [72][a]
Steam utilization (%)	80 [b]
Water recirculation (%)	20 [b]
Faradaic efficiency (%)	92 [52] [b]
PCCEL degradation rate (% per 1,000h)	1.2 [b]
PCCEL stack electrical consumption (kWh/kg)	38.2 [b]
System Area (m^2)	152 [b]
System water consumption (kg/h)	239.1 [b]
System power (MW)	1[a]
System Lifetime (y)	20 [76] [a]
System operational hours (h)	8,000 [76] [a]

[a] Values fixed [b] Values assumed/declared

IV.2.2 Mass and energy balance results

The technical feasibility evaluation is structured in two key phases.

In the first phase, the thermo-electrochemical conditions of the PCCEL system in terms of the mass flow rates, temperature, pressure, and flow composition are defined. This estimation is based on the model developed in the software. Table 3 summarizes these data.

Table 3. Mass balance results of the PCCEL system.

	Flows	Mass flow rate (kg/h)	T (°C)	P (bar)	Composition (%)
Input flows	Water 1	239.1	20.0	1.00	100 - Liquid
	Water 2	297.6	22.0	1.00	100 - Liquid
	Water 3	297.6	23.5	30.0	100 - Liquid
	Water 4	297.6	110	30.0	100 - Liquid
	Water 5	297.6	113	30.0	100 - Liquid
	Water 6	297.6	225	30.0	100 - Liquid
	Steam 1	297.6	234	30.0	100 - Vapor
	Steam 2	148.8	234	30.0	100 - Vapor
	Steam 3	148.8	234	30.0	100 - Vapor
	Steam 4	148.8	550	30.0	100 - Vapor
	Steam 5	148.8	550	29.9	100 - Vapor
	Steam 6	297.6	550	30.0	100 - Vapor
	Steam 7	292.8	550	30.0	100 - Vapor
	Steam 8	4.786	550	30.0	100 - Vapor
Output flows	Hydro 1	26.21	600	30.0	100 - Vapor
	Hydro 2	32.63	600	29.9	100 - Vapor
	Hydro 3	32.63	575	29.9	100 - Vapor
	Hydro 4	32.63	323	29.9	100 - Vapor
	Hydro 5	31.00	323	29.9	100 - Vapor
	Hydro 6	1.630	323	29.9	100 - Vapor
	Hydro 7	1.630	122	29.9	100 - Vapor
	Hydro 8	1.630	123	30	100 - Vapor
	Hydro 9	1.630	550	30	100 - Vapor
	Hydro 10	6.416	550	30	100 - Vapor
	Hydro 11	31.00	48.0	29.9	98 – Vapor, 2 - Liquid
	Hydro 12	26.21	30.0	30.0	100 - Vapor
	H_2O	4.790	30.0	30.0	100 - Liquid
	Oxy 1	266.5	600	30.0	100 - Vapor
	Oxy 2	266.5	297	30.0	100 - Vapor
	Oxy 3	266.5	123	30.0	72 – Vapor, 28 - Liquid
	Oxy 4	266.5	62.0	1.30	78 – Vapor, 22 - Liquid
	Oxy out	208.0	30.0	1.30	100 - Vapor
	Steam sweep	58.50	30.0	1.30	100 - Liquid

The 1 MW PCCEL system produces 26.21 kg/h of hydrogen and 208.0 kg/h of oxygen by consuming 297.6 kg/h of water. The energy consumption of this system is 0.045 MWh/kg; it is calculated by considering the energy consumption of PCCEL (0.0381 MWh/kg) and BoP auxiliary (0.0067 MWh/kg).

The second phase consists of the estimation of the BoP operating parameters in terms of electrical power consumption (E), and thermal power (Q). For the heat exchanger, the logarithmic mean temperature difference (ΔT_{LMTD}) and the overall heat transfer coefficient–area product (UA), are also determined. These results are summarized in Table 4.

Table 4. Energy balances and overall performances of the BoP components.

Equipment	E (kW)	Q (kW)	ΔT_{LMTD} (°C)	UA (J/sK)
Pump	0.814	-	-	-
Blower	0.004	-	-	-
Electric heater	175.4	-	-	-
HE 1	-	32.5	87.2	373
HE 2	-	1.15	69.3	16.5
HE 3	-	45.5	31.7	1437
HE 4	-	29.0	56.2	515
HE 5	-	2.45	177	13.8
HE 6	-	29.0	50.2	578

IV.3 Economic costs assessment

The main goal of the economic analysis is to define all costs associated with hydrogen production from water electrolysis using the PCCEL system in order to evaluate the economic performance of the system through the $LCOH$ calculation and to compare it with the $LCOH$ values of the other hydrogen production technologies. The $LCOH$ estimate, thus, includes the calculation of the investment, operating, maintenance, and replacement costs of the PCCEL system, as well as potential revenues from the sale of co-produced oxygen.

IV.3.1 Economic performance

To assess the total capital cost of the 1 MW PCCEL system, the parameter corresponding to the total fixed capital cost (C_{FC}) must be calculated as shown in Equation 15. This means that the total investment cost of the system ($CAPEX$) is multiplied by the cost factors (f_{cost}), listed in Table 5, related to the installation of the technical and engineering equipment (calculated according to Equation 16) [77]. These cost factors are not applied to power converter and hotbox.

$$C_{FC} = f_{cost} \cdot CAPEX \tag{15}$$

$$f_{cost} = [(1 + f_p) \cdot f_m + (f_{er} + f_{el} + f_i + f_c + f_s + f_l)] \cdot (1 + OS) \cdot (1 + D\&E + X) \tag{16}$$

Table 5. Installation factors for the estimation of total fixed capital cost [77].

Item	Factor value
Equipment erection (f_{er})	0.3
Piping (f_p)	0.8
Instrumentation and control (f_i)	0.3
Electrical (f_{el})	0.2
Civil (f_c)	0.3
Structure and buildings (f_s)	0.2
Lagging and paint (f_l)	0.1
Material Factor (f_m)	1.3
Offsites (OS)	0.3
Design and Engineering ($D\&E$)	0.3
Contingency (X)	0.1

As reported in Equation 17, the $CAPEX$ is calculated as the sum of the investment costs of each component (C_i), estimated by applying different Equations based on available data.

$$CAPEX = \sum C_i \tag{17}$$

For the PCCEL, electric heater, power converter, and hotbox, C_i is determined considering the specific costs ($C_{s,i}$) derived from the literature or estimated by project partners (Table 6), and the respective size (P).

$$C_i = C_{s,i} \cdot P \tag{18}$$

Table 6. Specific costs of electrolyzer, electric heater, power converter, and hotbox.

Components	Specific investment costs ($C_{s,i}$)	Ref.
PCCEL	500 €/kW	PROTOSTACK project*
Electric heater	65,450 €/MW	[78]
Power converter	100 €/kW	PROTOSTACK project*
Hotbox	170.40 €/kW	PROTOSTACK project*

*Specific costs estimated by the PROTOSTACK project partners.

For other components like water ion exchange plant, heat exchangers, pump, and blower, where data are not available in the literature, the cost curve proposed by Sinnott and Towler is applied (Equation 19) to define their C_i [77].

$$C_i = a + bS^n \tag{19}$$

The parameters a, and b are cost constants while n is the exponent that varies based on the type of equipment. They are reported in Table 7 [77].

Table 7. Parameters for purchased equipment cost correction [77].

Components	Units per size (S)	a	b	n
Water ion exchange plant	m^3/h	14,000	6,200	0.75
Blower	m^3/h	4,450	57.00	0.80
Pump	l/s	8.000	240.0	0.90
HE 1	m^2	1,600	210.0	0.95
HE 2	m^2	1,600	210.0	0.95
HE 3	m^2	1,600	210.0	0.95
HE 4	m^2	1,600	210.0	0.95
HE 5	m^2	1,600	210.0	0.95
HE 6	m^2	1,600	210.0	0.95

The sizes S of the water ion exchange plant, blower, and pump are calculated in terms of volumetric and mass rate, taking into consideration the flow rates defined in Aspen Plus and reported in Table 3. Instead, the sizes of the six heat exchangers are estimated by applying the Equation 20 [77].

$$S = \frac{Q}{U \cdot \Delta T_{LMTD} \cdot F_t} \tag{20}$$

The parameters Q and ΔT_{LMTD} are extracted from Aspen Plus simulation, while the coefficient U (which depends on the geometry of the heat exchanger and the physical property of the gas) assumes different values equal to 10 W/m^2°C and 20 W/m^2°C [77]. The correction factor (F_t) of 1 is considered since the counter-current heat exchangers are used [79].

Considering the determined data, it is possible to define the component sizes that are summarized in Table 8.

Table 8. BoP components size estimation.

Equipment	Units per size (***S***)	Value
Water ion exchange plant	m^3/h	0.24
Pump	l/s	0.08
Blower	m^3/h	0.88
HE 1	m^2	18.6
HE 2	m^2	0.83
HE 3	m^2	71.8
HE 4	m^2	51.6
HE 5	m^2	1.38
HE 6	m^2	57.8

The electric heater size, as estimated using the developed model, is 175 kW.

Finally, the investment costs (C_i) of feed water tank and separator tank are assumed to be 290 € per 1,000 litres of water (assuming slight oversizing) [80] and 34,000 € per MW_{system} [81], respectively.

Most of the investment costs of the BoP components are based on 2012 and 2017 data are, therefore, updated to 2024 values using the conversion factor derived from the *Chemical Engineering Plant Cost Index* ($CEPCI$) as shown in Equation 21 [82]. The $CEPCI$ is a composite index published monthly, tracking changes in the cost of constructing chemical plants over time. It aggregates four weighted sub-indices: equipment, construction labor, buildings, and engineering/supervision

$$C_{i,2024} = C_{i,2012/2017} \cdot \frac{CEPCI_{2024}}{CEPCI_{2012/2017}} \tag{21}$$

$CEPCI_{2012}$, $CEPCI_{2017}$ and $CEPCI_{2024}$ are equal to 584.6, 567.5 and 800, respectively [83], [84]. The feed water tank, power converter, and hotbox are exceptions, as their costs already refer to 2024 values. It is clear that C_i are updated to 2024 because the annual $CEPCI$ related to 2025/2026 are not available yet.

Another important cost item that must be calculated is related to expenses associated with the operation and maintenance of the electrolysis system ($C_{O\&M}$). These costs include both fixed components (such as labor and system maintenance) and variable components (costs that vary based on the price of electricity necessary to supply the components and feed water). The replacement costs (C_{rep}) are the financial expense required to replace system components with others that have the same functionality. Finally, as previously introduced, for this analysis, the revenue obtained from oxygen sales is also considered [77]. In Table 9, these cost parameters are summarized.

Table 9. Economic data assumed for this analysis.

Parameters	Value	Ref.
Annual Specific Maintenance Costs		
Electrolyzer	1.5% of C_i/y	[85]
BoP	2% of C_i/y	[35]
Annual Operating Costs		
Feed water	3.28 €/m^3	[86]
Electricity	75 €/MWh	[87]
Salary	50,000 € full-time	PROTOSTACK project*
Supervision	25% of Salary	PROTOSTACK project*
Direct overhead	45% of Salary and Supervision	PROTOSTACK project*
Annual Replacement Costs		
PCCEL membrane replacement	1,000 €/m^2	PROTOSTACK project*
Annual Revenues		
Oxygen sold	0.13 €/m^3	[88]

*Estimated by the PROTOSTACK project partners.

The operating and maintenance costs for the PCCEL and BoP are calculated as 1.5% and 2% of the investment cost of the single component, respectively.

A feed water cost of 3.28 €/m^3 is assumed. To calculate the corresponding yearly cost, this operating expense is multiplied by the hourly water consumption (239 kg/h) and the annual operating hours of the PCCEL system (8,000 h/y).

The electricity cost considered is based on the average European price in 2024; this cost reflects the electricity generation mix, which consists of 48% renewables, 24% nuclear, and 28% fossil fuels [89]. The annual electricity consumed to power the PCCEL, electric heater, pump, and blower is estimated by multiplying the average electricity price for the component power and operating hours of the PCCEL system.

The salary is determined considering the assumption that one full-time worker is employed, while supervision and the direct overhead work are calculated as a percentage of the salary. Regarding the replacement cost, it is assumed that only the electrolyzer is replaced about every two and a half years during the system's lifetime. Finally, since water splitting produces not only hydrogen but also oxygen, it is possible to sell such oxygen.

IV.3.2 Levelized Cost of Hydrogen

To make hydrogen a sustainable energy option, it is essential to analyze the economic aspects of its production. For this purpose, estimating the $LCOH$ calculation is necessary for comparing the cost-effectiveness of hydrogen with other energy sources and assessing its market competitiveness. Among the different factors influencing the $LCOH$ value, production technology and primary energy source play a key role. Different methodologies, such as SMR, SMR combined with CCUS, or electrolysis, whether grid-connected or powered directly by renewable sources, have different costs [90].

In this study, $LCOH$, expressed in €/kg H_2, it is estimated by applying the Equation 22 [91].

$$LCOH = \frac{CRF \cdot [C_{FC} + \sum_{n=0}^{N-1}(C_{O\&M,\,n,\,an} + C_{rep,\,n=t,an} - Rev_{O_2,n,an})]}{m_{H_2,year}} \quad (22)$$

$m_{H_2,year}$ is the yearly hydrogen production through the PCCEL system.

The capital recovery factor, CRF, is applied to determine the annuity that is equivalent to a present expenditure [92]: it is expressed in function of the real interest rate (I_r) and the electrolysis system lifetime (N).

The real interest rate is based on the nominal discount rate (i) and the inflation rate (f) equal to 4% [17] and 2.5% [93], respectively. CRF and I_r are calculated applying the Equations 23 and 24, respectively [91].

$$CRF = \frac{I_r \cdot (1 + I_r)^N}{(1 + I_r)^N - 1} \quad (23)$$

$$I_r = \frac{i - f}{1 + f} \quad (24)$$

Finally, $C_{O\&M,n,an}$, $C_{rep,\mathrm{n=}t,an}$, and $Rev_{O_2,n,an}$ are the annual present values of the operating and maintenance costs, replacement costs and revenue obtained from oxygen selling,

respectively. They are discounted at the real interest rate to take into account the time value of money. They are calculated as illustrated in Equations 25-27 [91].

$$C_{O\&M,n,an} = \frac{C_{O\&M}}{(1+I_r)^n} \tag{25}$$

$$C_{rep,\mathrm{n}=t,an} = \frac{C_{rep}}{(1+I_r)^t} \tag{26}$$

$$Rev_{O_2,n,an} = \frac{p_{O_2} \cdot m_{O_2}}{(1+I_r)^n} \tag{27}$$

The annual replacement costs are calculated by assuming t as the years in which the replacement of components is suggested while the annual revenue is estimated based on the selling price (p_{O_2}) and the yearly amount of the co-produced oxygen (m_{O_2}).

To assess the relative impact of each cost item on the final $LCOH$ value (excluding the revenues), the contribution of each item is estimated using Equations 28-30:

$$cost\ item_1 = \frac{CRF \cdot C_{FC}}{m_{H_2,year}} \tag{28}$$

$$cost\ item_2 = \frac{CRF \cdot \sum_{n=0}^{N-1} C_{O\&M,n,an}}{m_{H_2,year}} \tag{29}$$

$$cost\ item_3 = \frac{CRF \cdot \sum_{n=0}^{N-1} C_{rep,n=t,an}}{m_{H_2,year}} \tag{30}$$

This estimation allows identifying which costs have the greatest influence on the overall hydrogen production cost.

IV.3.3 Economic feasibility results

The economic results for the 1 MW PCCEL system are summarized in the following Tables, presenting investment costs, operating and maintenance costs, replacement costs, and revenues. These data provide a comprehensive overview of the financial requirements associated with the system, allowing a detailed assessment of its economic performance and highlighting the main cost drivers.

Table 10. Investment costs for each component.

Component	$C_{i,2024}$ (€)
PCCEL	500,000
Electric heater	15,714
Power converter	100,000
Hotbox	170,401
Water ion exchange plant	18,754
HE 1	5,796
HE 2	2,065
HE 3	16,040
HE 4	12,206
HE 5	2,193
HE6	13,383
Pump	9,335
Blower	5,236
Water tank	290
Separators	95,859
Total $C_{i,2024}$	**967,272**

The electrolyzer, power converter, hotbox and feed water tank costs refer to 2024 values and, for this reason, they are not updated. In contrast, the separator tanks costs are updated, taking into account the $CEPCI$ for 2017. The other BoP costs are updated considering the $CEPCI$ for 2012.

Considering the economic parameters reported in Table 9, the operating and maintenance costs, replacement costs, and oxygen revenues are estimated and reported in Table 11.

Table 11. Annual O&M and Replacements costs and Revenues of the PCCEL system.

Annual costs	Total annual values	€/y
Maintenance costs	PCCEL	7,500
	Electric heater	314
	Power converter	-
	Hotbox	-
	Water ion exchange plant	375
	HE 1	116
	HE 2	41
	HE 3	321
	HE 4	244
	HE 5	44
	HE6	268
	Pump	187
	Blower	105
	Water tank	5.80
	Separators	1,917
Operating costs	Feed water	6,285
	Electricity to PCCEL	600,000
	Electricity to electric heater	105,265
	Electricity to pump	488
	Electricity to blower	2.60
	Salary	50,000
	Supervision	12,500
	Direct overhead	28,125
Replacement costs	PCCEL membrane replacement	151,515
Revenues	Oxygen	151,447

The maintenance costs of the power converter and the hotbox are not included as their lifetime is assumed to be 20 years. Furthermore, the heat source cost useful for supplying the PCCEL is not considered since it works in thermoneutral mode.

The terms used in Equation 22 to estimate the $LCOH$, together with their associated values, are summarized in Table 12.

Table 12. Terms used in Equation 14 to estimate the LCOH.

Parameters	Unit	Values
I_r	%	1.46
CRF	-	0.06
C_{FC}	€	5,013,855
$\sum_{n=0}^{N-1} C_{O\&M,n,an}$	€	14,232,874
$\sum_{n=0}^{N-1} C_{rep,n=t,an}$	€	410,546
$\sum_{n=0}^{N-1} Rev_{O_2,n,an}$	€	2,647,730
$m_{H_2,year}$	kg/y	209,754

Based on the average European electricity cost in 2024 (75 €/MWh) and the revenue from the oxygen sale, the annual $LCOH$ for the 1 MW PCCEL system is 4.71 €/kg H_2. This value reflects the combined effects of investment, operating, maintenance and replacement costs, and oxygen revenues providing a comprehensive assessment of the economic performance of the system. The estimated $LCOH$ demonstrates the potential competitiveness of the proposed PCCEL system in the current European energy market, considering the assumed generation mix and electricity pricing.

On the other hand, if oxygen is emitted into the atmosphere, the $LCOH$ value is approximately 5.44 €/kg H2. Based on this value, the contribution of individual cost items to the $LCOH$ using equations 28-30 is calculated. As shown in Figure 26, the contribution of investment, operating and maintenance, and replacement costs is about 26%, 72%, and 2% of the total $LCOH$, respectively.

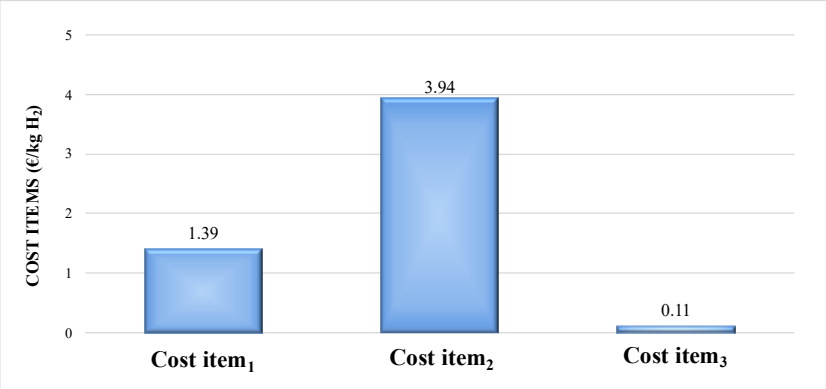

Figure 26. Contribution of costs to LCOH value (Equation 28-30).

Since the specific costs of PCCEL, power converter, and hotbox (Table 6), as well as the labor and the PCCEL replacement costs (Table 9), are estimates provided by *PROTOSTACK partners*, it is crucial to calculate the *LCOH* by considering the uncertainty of these values. In line with the Association for the Advancement of Cost Engineering (AACE) guidelines [77], these estimates are categorized as "*Class 3*", which typically has an accuracy range of -10% to +10%. Applying this variation, the *levelized cost of hydrogen* varies between 5.28 €/kg H_2 and 5.60 €/kg H_2, starting from a baseline of 5.44 €/kg H_2 excluding revenues.

The marginal variation of just 0.16 €/kg H_2 (± 3% error) confirms the robustness of the Techno-Economic model and highlights how operating and maintenance costs are the determining factor in the economic process. For this reason, a further detailed analysis of these expenses is conducted. The results are illustrated in Figure 27. Within this category, the predominant cost item is electricity consumption to power the electrolyzer, accounting for approximately 74%. The remaining items have a marginal impact, ranging from 1% to 13%.

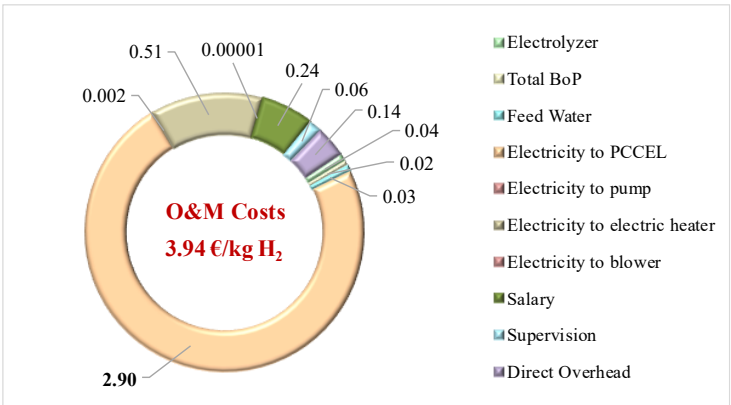

Figure 27. Operating and maintenance costs contribution.

IV.4 Electricity Cost Contribution to LCOH

As discussed above, the electricity cost influences the system's performance, particularly the $LCOH$ calculation and, consequently, its economic feasibility. To demonstrate the incidence of electricity price changes on the $LCOH$, a further sensitivity analysis is carried out.

IV.4.1 Average European electricity cost trend

To examine the impact of electricity costs on the $LCOH$ overtime, the sensitivity analysis is carried out by considering both the electricity prices in different European countries in 2024 (Table 13) and various future time scenarios (Table 14). This approach allows evaluating how geographical and temporal variations in electricity costs affect the economic performance of the PCCEL system.

As it can be observed in Table 13, in 2024, Italy had the highest electricity prices, followed by Greece, Hungary, Poland, and Slovenia, due to the continued reliance on expensive gas-fired power plants. In contrast, France, Finland, and Sweden exhibit the lowest electricity costs due to their electricity generation mix, which is dominated by low-marginal-cost sources such as nuclear and hydropower. This stable and efficient production results in lower average electricity prices compared to countries more reliant on fossil fuels [89].

Table 13. Electricity costs for different European countries in 2024 [89].

Country	European electricity cost in 2024 (€/MWh)
Italy (IT)	107
Greece (GR) and Hungary (HU)	99
Poland (PL)	94
Slovenia (SI)	89
Austria (AT) and Germany (DE)	80
Netherlands (NL)	77
Belgium (BE) and Denmark (DK)	68
Spain (ES)	61
France (FR)	55
Finland (FI)	44
Sweden (SE)	36

Regarding the temporal sensitivity analysis, three scenarios are considered. The first is the 2022 scenario, characterized by rising energy costs following the Russian invasion of Ukraine and, consequently, an increase in the price of imported natural gas. The second is the 2023 scenario, in which this average electricity cost decreased significantly, reaching a price of 100 €/MWh [94], [95]. The last is the 2030 scenario, in which electricity costs are expected to decrease as a result of the large-scale deployment of renewable energy sources.

Table 14. European average electricity costs from 2022 to 2023 and 2030 [94], [95].

Scenario	Year	European average electricity cost (€/MWh)
Case 1	2022	284
Case 2	2023	100
Case 3	2030	40

Through the sensitivity analysis conducted, this study aims to evaluate how the different electricity prices can impact the hydrogen production cost, highlighting the strategic importance of energy price variability in the European context.

IV.4.2 Sensitivity analysis results

The average electricity cost significantly influences the $LCOH$ value making it very sensitive to electricity price variations.

As reported in Table 13, each European country has different electricity prices depending on the type of energy sources employed. The sensitivity analysis conducted shows that an increase in electricity prices corresponds to a higher estimated $LCOH$ value.

As shown in Figures 28 and 29, countries like Italy, Germany, Poland, Hungary and Slovenia, still heavily dependent on fossil fuels, show very high $LCOH$ values, while countries like Austria, Germany, and Netherlands show $LCOH$ values close to the European average. Belgium, Denmark and Spain have lower $LCOH$ values between 4.39 €/kg H_2 and 4.07 €/kg H_2 considering the sale of oxygen and between 5.12 €/kg H_2 and 4.80 €/kg H_2 without the sale of oxygen. Finally, France, Finland, and Sweden, where nuclear and renewable energy are widely used, achieve significantly more competitive $LCOH$ values.

The red line represents the $LCOH$ calculated at the average European electricity price of 75 €/MWh, serving as a reference point and corresponding to the economic results obtained in this study.

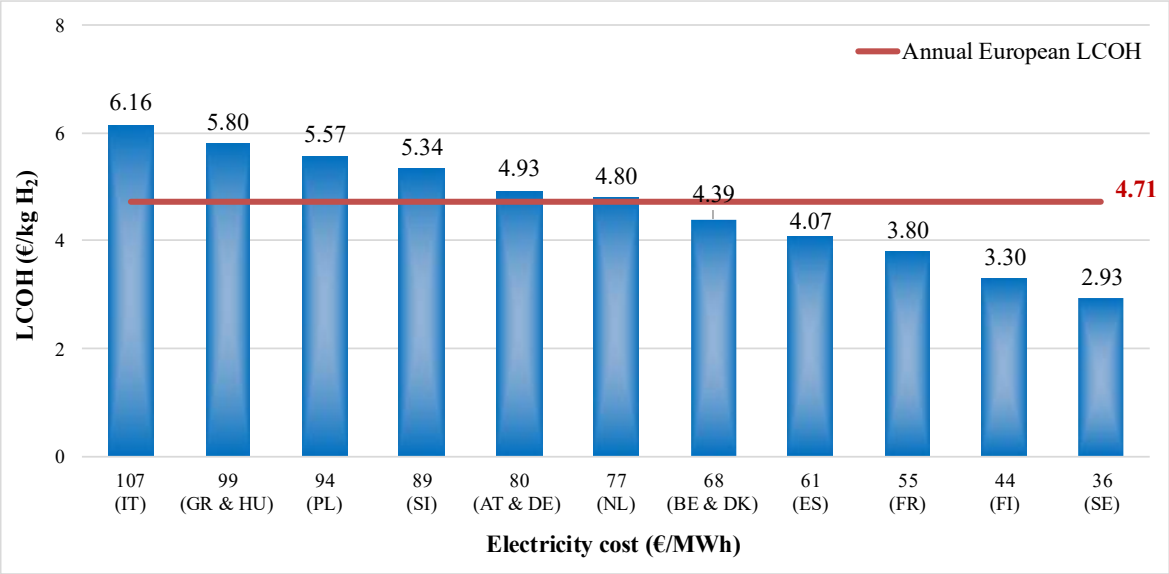

Figure 28. Effect of European electricity prices change on the LCOH considering oxygen sales in 2024.

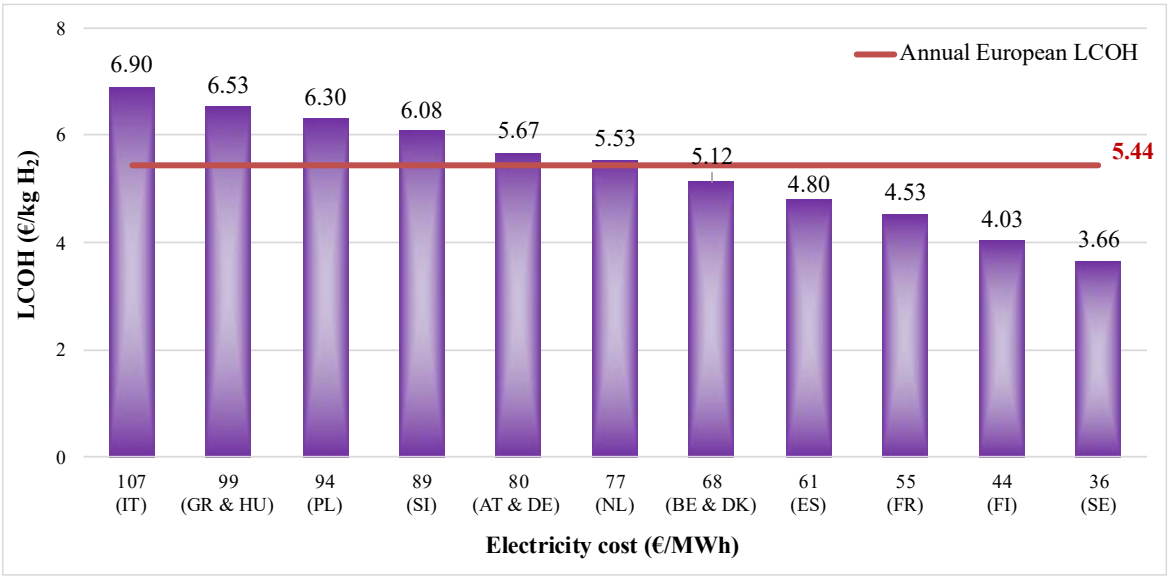

Figure 29. Effect of European electricity prices change on the LCOH without oxygen sales in 2024.

The $LCOH$ is also calculated for different time scenarios. In particular, considering the average electricity price in Europe of 284 €/MWh in 2022, 100 €/MWh in 2023, and 40 €/MWh in 2030, the $LCOH$ value is approximately 14.22 €/kg H_2, 5.84 €/kg H_2, and 3.11 €/kg H_2 of hydrogen (considering the sale of oxygen), respectively. When excluding oxygen sales (an increase of about 0.73 €), $LCOH$ values would be 14.95 €/kg H_2, 6.58 €/kg H_2, and 3.84 €/kg H_2 in 2022, 2023, and 2030, respectively. Figures 30 compares these results with the current $LCOH$ value in 2024.

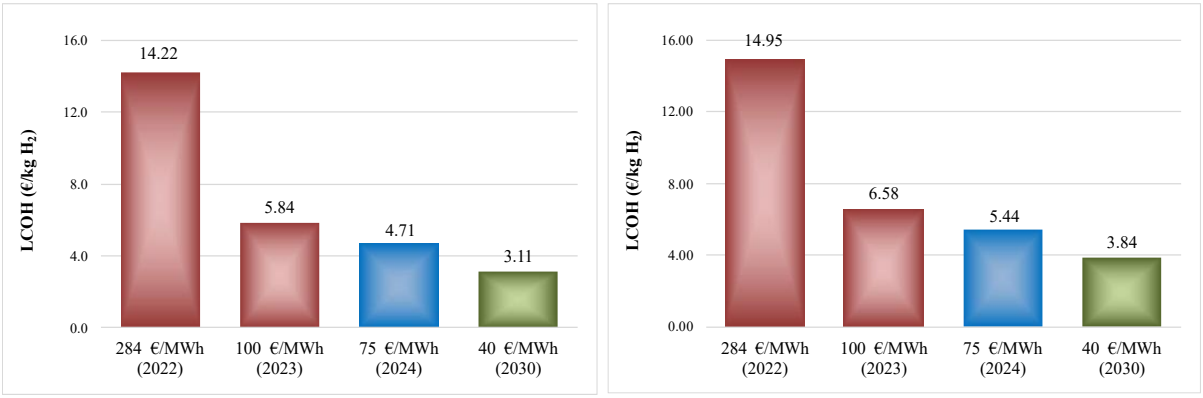

(a) (b)

Figure 30. LCOH estimation based on the different average electricity costs: (a) considering also the oxygen sales and (b) without oxygen sales.

The 2024 scenario with an average European electricity cost of 75 €/MWh is considered as a reference case. In 2022, the $LCOH$ value reached record levels due to high natural gas prices. However, although the $LCOH$ values decreased in the following years, they are still considered high due to the large-scale use of fossil fuels [95].

Assuming an average electricity cost of 40 €/MWh in 2030—enabled by continued investments in renewables and energy efficiency—$LCOH$ could drop to 3.11 €/kg H_2 with oxygen sales and 3.84 €/kg H_2 without sales, close to Hydrogen Europe's SRIA target of 3 €/kg H_2 by 2030 [96]. To achieve this goal, the total installed capacity of renewable plants must increase to 77%, up from the current 50%. It is essential that policymakers facilitate access to new investments through more effective financing mechanisms. Furthermore, it is necessary to rapidly implement smart and interconnected grids, demand response systems, and energy storage solutions to ensure a more stable and balanced renewable system [97].

IV.5 Hydrogen production costs and market competitiveness in Europe

Nowadays, the most economically viable technology for reducing GHG emissions in hydrogen production is methane reforming combined with CCS (because it is still operational and it has the lowest investment costs). In 2024, in Europe, hydrogen produced via SMR with CCS reached around 4 €/kg, considering a natural gas price of about 40 €/MWh and a cost for CO_2 storage and transport of 100 €/t. Natural gas price had the greatest impact on $LCOH$, contributing 56%, while CO_2 storage and transport costs accounted for approximately 10%. Assuming an average natural gas price of 20 €/MWh in the coming years, low-carbon hydrogen production costs could decrease to about 3 €/kg.

Another solution to reduce GHG emissions in short term is methane splitting, although this technology is currently less mature than SMR and requires significant initial investment costs. In 2024, the estimated $LCOH$ for methane splitting ranged from 5.3 €/kg to 3.3 €/kg, depending on the revenue from the sale of solid carbon produced (500-1,800 €/t).

Instead, hydrogen obtained from the gasification and/or pyrolysis of biomass waste reached a cost of 4.8 €/kg with a biomass price of 60 €/t, and revenues from the biochar by-product of 300 €/t. This process is more cost-effective than low-temperature electrolysis. Furthermore, like SMR with CCS and methane splitting, it can provide low-emission hydrogen, promoting local decarbonization and helping reduce uncontrolled agricultural emissions resulting from the decomposition of organic waste in nature.

On the other hand, the $LCOH$ estimated for hydrogen produced from non-biological and non-recyclable feedstocks reached a slightly higher value (5 €/kg) [76].

Compared to hydrogen production technologies mentioned above, the *PROTOSTACK project* is based on water electrolysis. Therefore, a literature review is necessary to evaluate and compare the results obtained in this study with those reported in the literature.

Scientific studies show that $LCOH$ varies significantly depending on the electrolyzer type used (AWE, PEMWE, or SOEC), electricity costs, and hydrogen delivery pressure. For example, Pinheiro et al. [98] estimated an $LCOH$ of 4.60 €/kg for AWE and 5.20 €/kg for PEMWE at 30 bar, using electricity at 43 €/MWh from combined wind-PV and Brazilian grid systems. Massaro et al. [99] calculated $LCOH$ >14 €/kg at 30 bar for both AWE and PEMWE using Italian grid electricity (240 €/MWh in 2023). Honig et al. [100] achieved 7.91 €/kg for high-pressure AWE (130 €/MWh) by valorizing co-produced oxygen in wastewater treatment. Hancke et al. [101] reported 9.71 €/kg at 30 bar for PEMWE connected to the grid (120 €/MWh). Bukar et al. [102] attained $LCOH$ between 6.30-14.60 €/kg at low pressure using AEMWE, AWE, PEMWE and SOEC electrolyzers (66.5 €/MWh Saudi grid plus renewables). Finally, Li et al. [102] calculated 9-10 €/kg for planar PCCEL (1.285 V, 600°C) at 54 €/MWh.

In the *PROTOSTACK project*, producing hydrogen directly at 30 bar – *without a downstream mechanical compressor* – provides more economic advantages. For a 1 MW tubular PCCEL system powered by the 2024 European grid (~75 €/MWh electricity cost), the results are 4.71 €/kg H_2, including oxygen sales, and 5.44 €/kg H_2 with oxygen emitted into the atmosphere. These results demonstrate that *PROTOSTACK project* achieves the lowest $LCOH$ among analyzed systems at equivalent delivery pressure (30 bar).

CHAPTER 5: LIFE CYCLE ASSESSMENT OF PCCEL SYSTEM

V.1 Standards and guidelines for Life Cycle Assessment

Life Cycle Assessment (LCA) is a fundamental tool for quantifying and interpreting the environmental impacts associated with a product, process, or service throughout its entire life cycle, from production to end-of-life management.

This methodology allows for the identification of the most impactful phases and processes and is a solid basis for environmental improvement, supporting more sustainable decisions at both design and strategic levels [103].

ISO 14040 and *14044*, introduced by the International Organization for Standardization, [104], [105] are the main international references for conducting LCA studies. ISO 14040, published in 1997 and updated in 2006, establishes the general principles, objectives, and framework for life cycle assessment, highlighting aspects such as transparency, consistency, and accuracy. ISO 14044, a more detailed standard, provides operational guidance for each phase of the LCA method, from data acquisition to impact analysis and interpretation of results, emphasizing the importance of data quality and uncertainty management.

Despite the effectiveness of ISO standards, their application is complex due to data variability, uncertainties, and the need for comparability between different studies.

For this reason, the *International Reference Life Cycle Data System (ILCD) Handbook* [106] and the *Specific Guidelines for Hydrogen and Fuel Cells (SH2E)* [103] are introduced, offering more detailed guidance and practical tools to address specific methodological and technical issues. The ILCD manual provides a more specific standard for managing data inventory and environmental impact assessment, offering guidance on addressing uncertainties and data gaps, as well as ensuring consistency and comparability across studies. The SH2E offers a specific LCA methodology for fuel cell and hydrogen (FCH) systems. In particular, it provides detailed procedures, customized models, and guidance for reliably and comparably assessing environmental impacts throughout the life cycle of fuel cell systems, as well as the production, storage, and use of hydrogen.

V.2 LCA methodology

The ISO standards, the ILCD, and the SH2E guidelines [103], [104], [105], [106], divide the LCA study into four phases, as illustrated in Figure 31: goal and scope definition, Life Cycle Inventory (LCI), Life Cycle Impact Assessment (LCIA), and, finally, interpretation of results.

To refine and improve the overall quality of the LCA analysis, the four phases must be closely interconnected, so that the process is iterative.

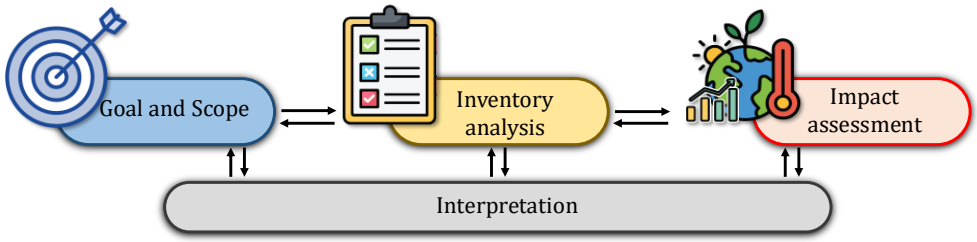

Figure 31. Phases of Life Cycle Assessment.

The first phase consists of the "*goal and scope*" definition of the study. It also involves the definition of the functional unit, life-cycle stages covered, assumptions, methodological choices, and the impact assessment method.

Defining the study's goal is essential for correctly interpreting the results: the goal must clarify the reasons for the LCA study, indicate its motivations, and, in particular, identify the decision-making context. This includes choosing the most appropriate method for structuring the inventory, such as whether to adopt an attributional or consequential approach. The attributional approach describes the existing or planned system without considering dynamic changes caused by decisions or policies. On the other hand, the consequential LCA approach aims to assess the environmental consequences of decisions or changes within a production system. In particular, it allows for the analysis of how such impacts may affect the market, consumer activities, and production chains. This model includes forecasting scenarios and considers the economic and environmental repercussions of a decision, going beyond the direct impact of the individual product.

The functional unit (FU) is a quantitative or qualitative representation of the main function of the product considered. It corresponds to a reference flow to which all the system's inputs and outputs are related. In the case of systems with more than one function (multifunctional systems), it is essential to choose the function that the study intends to target.

Furthermore, particular attention must be paid when performing comparative life cycle analyses, as the functional unit must represent a common function performed by the different analyzed products, technologies, strategies, or options.

In the goal and scope phase, the system boundaries are also defined. They correspond to all processes and flows to be included in the LCA analysis. The definition of these boundaries depends on the objectives of the study and influences the data collected, the phases included, and the overall interpretation. This step is essential for ensuring consistency in the LCA analysis. Different approaches can be applied to determine these boundaries:

- The "gate-to-gate" approach refers to the analysis of environmental impacts limited to the production phase;
- The “cradle-to-gate" approach considers the product's impacts from raw material extraction to the product's exit from the plant;
- The “cradle-to-grave" approach allows for the identification of the product's environmental impacts from raw material extraction to end-of-life included.

However, it must be remarked that for each of these approaches, the system boundaries definition concerns the complete determination of processes and phases included in the analysis.

Finally, the environmental impact assessment method is determined. There are several methods, each focusing on a different set of environmental issues, faced with different strategies.

The ReCiPe method provides indicators at both midpoint and endpoint levels (final damages such as human health, ecosystems, and resources). It is widely used in European and global studies. The TRACI method (Tool for the Reduction and Assessment of Chemical and Other Environmental Impacts), introduced by the United States Environmental Protection Agency (EPA), allows environmental impacts to be assessed in the United States. This method is based on seven impact categories. Unlike other methodologies that contain multiple impact indicators, the IPCC (Intergovernmental Panel on Climate Change) method estimates only the Global Warming Potential (GWP). Using the GWP creates a standardized approach to understanding a product's impact on climate change. Finally, the Environmental Footprint 3.1 (EF 3.1) method, developed by the European Commission and containing 16 impact categories, provides a harmonized framework for measuring environmental impact within the EU [107].

Table 15 summarizes the different methods and their distinguishing features.

Table 15. Different environmental impact assessment methods [107].

Method	N. impact categories	Impact categories
ReCiPe	Midpoint indicators: 16	**Midpoint indicators:** Particulate matter, tropospheric ozone formation, ionizing radiation, ozone stratosphere depletion, human toxicity (cancer and non), global warming, water use, freshwater ecotoxicity, freshwater eutrophication, troposphere ozone (eco), terrestrial ecotoxicity, terrestrial acidification, land use/transformation, marine ecotoxicity, mineral resources, fossil resources.
	Endpoint indicators: 3	**Endpoint indicators:** Damage to human health, damage to ecosystems, and damage to resource availability.
TRACI	7	Climate change, ozone depletion, acidification, eutrophication, smog formation, human health impacts (carcinogenic and non-carcinogenic), and ecotoxicity.
IPCC 21	1	GWP
EF 3.1	16	Climate Change; ozone depletion; human toxicity, cancer effects; human toxicity, non-cancer effects; particulate matter; ionising radiation; photochemical ozone formation; acidification; eutrophication, terrestrial; eutrophication, freshwater; eutrophication, marine; ecotoxicity, freshwater; land use; water use; resource use, fossils; resource use, minerals and metals.

The second phase is the "*Life Cycle Inventory*", which involves collecting input data, such as energy and raw material consumption, and output data, like waste and emissions, for the product being evaluated.

Based on the origin and nature of the data used for LCA, the data can be classified as primary or secondary. Primary data are collected through direct measurements or specific observations of the product, process, or system. This may include on-site measurements or experiments conducted to gather information on resource use and other relevant parameters. Primary data can also be information provided by the product manufacturer. It may include production data, material composition, energy consumption, and waste generation. On the other hand, secondary data are obtained from existing databases, literature, or previously conducted studies. These sources provide general data that can be applied to a wide range of products or processes.

The third phase, "*Life Cycle Impact Assessment*", is the step of the analysis that quantifies the product's impacts and is based on the data collected during the inventory. In this phase, the impact assessment method established during the goal and scope phase is applied to calculate the environmental impacts.

The results of these three phases are analyzed and discussed in the final phase, known as "*interpretation*". It is essential to ensure sufficient consistency of methods, assumptions, and data throughout the LCA study to ensure clear and precise interpretation [103], [104], [105], [106], [107].

However, the LCA method has some limitations and drawbacks. The nature of the choices and assumptions made in LCA (such as defining system boundaries, selecting data sources, and impact categories) can often be subjective. Furthermore, the accuracy of LCA studies can be limited by the accessibility or availability of relevant data, or by data quality (such as gaps, types, aggregation, or averaging). Finally, results from different LCA studies can only be compared if their assumptions and contexts are identical.
These assumptions should also be explicitly stated for transparency reasons [104].

V.2.1 Goal and Scope Definition

Typically, when conducting an LCA, the design or development phase is not considered, as it is assumed not to contribute significantly. However, it is important to note that decisions made during these phases can significantly influence the environmental impacts in other life cycle phases [108]. Therefore, conducting an LCA analysis of a product or system during its development stage can help to adopt solutions that lower its impact. This strategy is commonly known as eco-design and, in this study, it is applied to hydrogen production by conducting an LCA analysis of the proton-conducting ceramic electrolysis system, currently being developed as part of the *European PROTOSTACK project.*
The aim of this study is to assess the environmental impacts and identify the main hotspots along the life cycle of the PCCEL system, in order to indicate specific interventions to optimize this technology already in its design phase. To achieve this goal, the 1 MW PCCEL system, previously developed in Aspen Plus^{TM} environment, is analyzed.
LCA is performed using an attributional approach: the environmental impacts associated with the predicted PCCEL system are quantified, considering only the specific supply chain related to the analyzed product without considering possible changes outside the system boundary.
The primary function of the PCCEL system is hydrogen production: for a 1 MW system, approximately 26.21 kg/h of hydrogen and 208 kg/h of oxygen are produced, consuming about 297.6 kg/h of water, with a Faraday efficiency of 92%. Therefore, the functional unit is defined as "**the production of 1 kg of 99.99% pure hydrogen, available at 30 bar and 30°C".**
As illustrated in Figure 32, the system boundaries comprise raw materials acquisition and pre-processing, the manufacturing of the whole PCCEL system, which encompasses the electrolyzer, the hotbox and the BoP, and the use phase, that is operating stage of the system.

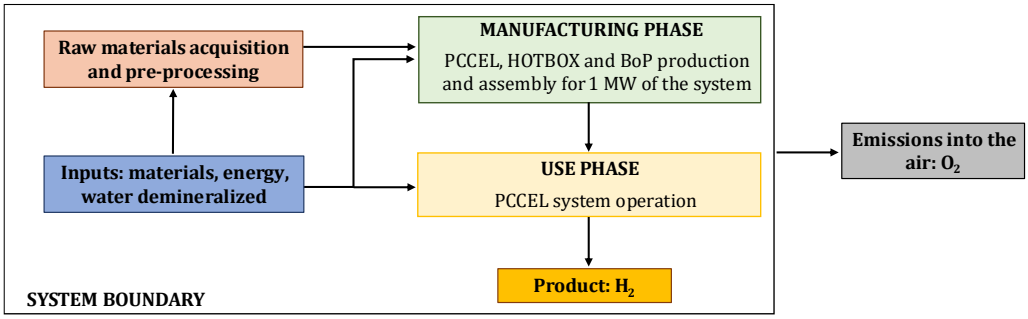

Figure 32. System boundary definition.

This makes the analysis a "cradle to gate" LCA, although it excludes from the complete life cycle solely the end-of-life treatment of the PCCEL unit. This decision is taken due to a lack of data concerning EoL management. Such circumstance is commonly encountered for technologies that are still in their developmental stages.
This analysis considers the manufacturing and use phases of the electrolyzer, hotbox, and BoP, including the raw materials acquisition and pre-processing and the energy consumption required for both the production and operation of the PCCEL system. Furthermore, in the operating phase, the two additional flows are considered: demineralized water input and the oxygen by-product output (emitted into the atmosphere).
Maintenance of these components is not considered, as they are designed for a lifetime of 20 years. Table 16 summarizes the technical data necessary to define the LCA parameters.

Table 16. Technical parameters of the PCCEL unit.

Parameters	PCCEL system
Hydrogen production [kg/h]	26.21
Pressure of H_2 produced [bar]	30
Temperature of H_2 produced [°C]	30
PCCEL system power [MW]	1
PCCEL system energy consumption [kWh/kg]	44.87
PCCEL system operating hours [h/y]	8,000
PCCEL system lifetime [h]	160,000
Faradaic efficiency [%]	92

V. 2.2 Life Cycle Inventory

The PCCEL system inventory is divided into two main sections: the first part involves the detailed data collection related to the manufacturing phase, including the quantities of materials used and the energy consumed during the system's production and assembly. The second part of the inventory focuses exclusively on energy consumption and the input and output flows during the use phase, i.e., during hydrogen production.
Distinguishing data simplifies data collection, management, and analysis, reducing errors, redundancies, and overlaps.

V. 2.2.1 LCI for PCCEL system manufacturing phase

The LCI is a fundamental step in environmental analysis, providing a detailed and quantified account of all material flows, energy use, emissions, and waste within the PCCEL system, from raw material acquisition and pre-processing through system operation.
Table 17 summarizes the types and quantities of materials required to produce the 1 MW PCCEL system, including the tubular electrolyzer, hotbox, and BoP.

Table 17. Inventory of materials used in the manufacturing phase for PCCEL system.

Component	Materials	Mass [kg]
PCCEL		
Cathode & Electrolyte	BZCY/NiO	2,604
Anode	BZCY/BGLC	76.6
Seal	Ceramic	879
Current Collector system	Composite ceramic materials, additives, and steel	272
Interconnects	precious metals	448
Reactor	Steel	5,092
HOTBOX		
Housing	Sheet metal S235	3,944
	Insulating fire brick	16,800
Bicycle racks	Stainless steel 304	624
BOP COMPONENTS		
Water tank	Stainless Steel 304	20.8
Plate and frame HE 1	Stainless Steel 304	139.8
Plate and frame HE 2	Stainless Steel 304	4.93
Plate and frame HE 3	Stainless Steel 304	196
Plate and frame HE 4	Stainless Steel 304	125
Plate and frame HE 5	Stainless Steel 304	10.5
Plate and frame HE 6	Stainless Steel 304	125
Electric heater	Mild Steel	1,894
Separator tank 1	Stainless Steel 304	11.0
Separator tank 2	Stainless Steel 304	23.5

For the electrolyzer, values are calculated based on the production of a tubular PCCEL stack. These estimates are obtained by collecting performance data in terms of mass per unit surface area (kg/m²) at the stack level and are scaled to the total surface area for a 1 MW system.
Data for the cathode, electrolyte, seal, and reactor come from publicly available sources in previous projects (for example, Gamer and WINNER [109], [110]), while data for the anode, current collector system, and interconnects are based on primary information from the PROTOSTACK project, withheld due to confidentiality. Therefore, the materials used for the current collector and the interconnections manufacturing are not specified in Table 17, while for the anode, it is possible to assume the same material used in Moranti's study [73].

The electrolyte material BZCY is a proton-conducting ceramic widely studied for its high proton conductivity and stability at intermediate temperatures (600°C). It consists of barium zirconate-cerate doped with yttrium, which enables efficient proton transport through the ceramic frame. 60% NiO is used as the electrode support in combination with BZCY for enhanced electrochemical performance.
The anode uses the same BZCY proton-conducting ceramic and blends with BGLC, a proton conductor with mixed ionic-electronic conductivity, which improves electrode kinetics and stability. BGLC provides good chemical compatibility and mechanical strength for the anode side [73], [109], [110].
Ceramic sealing material is chosen for its thermal stability, ensuring gas-tight separation between different compartments of the electrolyzer under high-temperature conditions without degrading or reacting with other components [111].
The current collector system integrates composite ceramic materials with additives (for example, manganese and cobalt nitrates) that serve as precursors in the synthesis of conductive coatings or catalysts. A ferritic stainless-steel alloy is used for its high corrosion resistance and compatible thermal expansion, ensuring mechanical integrity and long-term performance under oxidizing environments.
Precious materials are applied in interconnects manufacturing due to their excellent electrical and thermal conductivity, as well as their chemical inertness in reducing environments found inside the cell, facilitating efficient electron transport between cells [112].
Finally, the reactor, containing the stack, is constructed from steel to provide mechanical strength and resistance to the corrosive environments typical of high-temperature electrochemical systems.
For the hotbox too, primary data regarding the materials used for its manufacturing are obtained from the *PROTOSTACK project* and subsequently sized for a 1 MW system. The hotbox, designed to ensure efficient thermal insulation, is made of S235 steel sheet on the outside and refractory insulating bricks on the inside. Inside the hotbox, structural supports (bicycle racks) are made of 304 stainless steel. This material is chosen for its high resistance to corrosion and high temperatures, offering durable and stable support for the stacks.
Finally, the data collection for the BoP components is defined based on data obtained from the model developed in Aspen Plus and secondary data available in the literature.
The water tank is composed of AISI 304 stainless steel and is designed for storing water at atmospheric pressure [113]. To prevent the formation of corrosion residues, the use of stainless steel or PVC fittings is recommended. The amount of stainless steel 304 required for the tank manufacturing is estimated based on the water flow to be stored, approximately 297.6 kg/h.
According to the Sinnott and Towler method (described in the previous chapter) [77], the configuration of the heat exchangers varies depending on the inlet flows, operating conditions, and size. In this study, all plate and frame heat exchangers, consisting of corrugated plates with high-efficiency gaskets arranged alternately and mounted on frames that separate the hot and cold fluids, are assumed. These exchangers are mainly realized in 304 stainless steel [114]. The amount of this steel is estimated based on the heat exchanged: 27,959 kcal/h for HE 1, 985.8 kcal/h for HE 2, 39,142 kcal/h for HE 3, 24,933 kcal/h for HE 4, 2,106 kcal/h for HE 5, and 24,937 kcal/h for HE 6.

For the electric heater, mild steel is assumed: based on data from ref. [115], where about 350 kg of mild steel is used for a 55 kg/h water flow, the material required is calculated considering an inlet water flow of 297.6 kg/h.
Separator tanks 1 and 2 are designed to separate respectively oxygen and hydrogen from water. They are mainly developed in 304 stainless steel to ensure safety and reliability. For a 720 m^3/h gas flow, 54 kg of 304 stainless steel are used [116]. For the flows of 146 m^3/h and 313 m^3/h considered in this study, 11 kg and 23.5 kg of 304 stainless steel are estimated for separators 1 and 2, respectively.
The estimation of material quantities for the production of the pump, blower, and power converter is carried out using the most appropriate datasets from the Ecoinvent v3 database. Starting from the production processes selected in Ecoinvent, the data are scaled to fit the specific sizes of each component. For the pump, a production process for a 22 kW pump is referenced and scaled to 0.814 kW. The blower, designed in Aspen Plus for a hydrogen flow of approximately 18.1 m^3/h, is implemented in SimaPro using an Ecoinvent dataset for a blower with a flow of 120 m^3/h, adapting it to the case study conditions. Finally, for the power converter, a production process for a 100 kW converter weighing 45 kg is selected and scaled for a 1 MW converter.
The procedure adopted for the BoP inventory allows for obtaining the most accurate data possible regarding the actual production of the components associated with the electrolyzer developed in the *PROTOSTACK project*.
The manufacturing data for the PCCEL system are implemented in SimaPro software using the Ecoinvent v3 database. Table 18 shows selected datasets on the materials used in the PCCEL, hotbox, and BoP manufacturing phase.
Since detailed information on the production methods and geographic origin of the materials is not available, market-type datasets for most components are used. These datasets encompass all flows related to the production, transport, and materials losses, averaged on a market basis, thus ensuring a more complete and representative environmental assessment.
Where market-type datasets are not available, the closest appropriate dataset available in the Ecoinvent v3 database is chosen.

Table 18. Inventory of materials used in the manufacturing phase for PCCEL, hotbox, and BoP.

	Ecoinvent dataset
PCCEL ELECTROLYZER	
Cathode & Electrolyte	Nickel, class 1 {GLO}| market for nickel, class 1 | Cut-off, U
	Barite {GLO}| market for barite | Cut-off, U
	Zirconium oxide {GLO}| market for zirconium oxide | Cut-off, U
	Cerium oxide {GLO}| market for cerium oxide | Cut-off, U
	Yttrium oxide {GLO}| market for yttrium oxide | Cut-off, U
Anode	Barium oxide {GLO}| market for barium oxide | Cut-off, U
	Zirconium oxide {GLO}| market for zirconium oxide | Cut-off, U
	Cerium oxide {GLO}| market for cerium oxide | Cut-off, U
	Yttrium oxide {GLO}| market for yttrium oxide | Cut-off, U
	Gadolinium oxide {GLO}| market for gadolinium oxide | Cut-off, U
	Lanthanum oxide {GLO}| market for lanthanum oxide | Cut-off, U
	Cobalt oxide {GLO}| market for cobalt oxide | Cut-off, U

Seal	Silica sand {GLO}| market for silica sand | Cut-off, U
	Magnesium oxide {GLO}| market for magnesium oxide | Cut-off, U
	Calcium carbonate, precipitated {GLO}| market for calcium carbonate, precipitated | Cut-off, U
	Aluminium oxide {GLO}| market for aluminium oxide | Cut-off, U
Current Collector system	Composite ceramic materials
	Additives
	Steel, chromium steel 18/8{GLO}|market for steel, chromium steel 18/8 |Cut-off, U
Interconnects	Precious metals
Reactor	Steel, chromium steel 18/8{GLO}|market for steel, chromium steel 18/8 |Cut-off, U
HOTBOX	
Housing	Steel, low-alloyed, hot rolled{GLO}|market for steel, low-alloyed, hot rolled |Cut-off, U
	Refractory, fireclay, packed {GLO}| market for refractory, fireclay, packed | Cut-off, U
Bicycle racks	Steel, chromium steel 18/8{GLO}|market for steel, chromium steel 18/8 |Cut-off, U
BoP COMPONENTS	
Water tank	Steel, chromium steel 18/8{GLO}|market for steel, chromium steel 18/8 |Cut-off, U
Plate and frame HE 1	Steel, chromium steel 18/8{GLO}|market for steel, chromium steel 18/8 |Cut-off, U
Plate and frame HE 2	Steel, chromium steel 18/8{GLO}|market for steel, chromium steel 18/8 |Cut-off, U
Plate and frame HE 3	Steel, chromium steel 18/8{GLO}|market for steel, chromium steel 18/8 |Cut-off, U
Plate and frame HE 4	Steel, chromium steel 18/8{GLO}|market for steel, chromium steel 18/8 |Cut-off, U
Plate and frame HE 5	Steel, chromium steel 18/8{GLO}|market for steel, chromium steel 18/8 |Cut-off, U
Plate and frame HE 6	Steel, chromium steel 18/8{GLO}|market for steel, chromium steel 18/8 |Cut-off, U
Electric heater	Steel, unalloyed {GLO}| market for steel, unalloyed | Cut-off, U
Separator tank 1	Steel, chromium steel 18/8{GLO}|market for steel, chromium steel 18/8 |Cut-off, U
Separator tank 2	Steel, chromium steel 18/8{GLO}|market for steel, chromium steel 18/8 |Cut-off, U
Pump	Water pump, 22kW {GLO}| water pump production, 22kW | Cut-off, U
Blower	Blower and heat exchange unit, Storkair G 90 {RER}| blower and heat exchange unit production, Storkair G 90 | Cut-off, U
Power converter	Converter, for electric passenger car {GLO}| converter production, for electric passenger car | Cut-off, U

NiO, used in the production of the electrolyzer cathode, is not present in the Ecoinvent v3 database; therefore, it is replaced with an equivalent amount of elemental nickel (1:1 ratio), which is used as a proxy [117]. Similarly, because the quartz used for the seal is not available in the database, silica sand, which contains over 85% quartz, is selected.

Finally, whereas Ecoinvent does not have specific datasets for manganese nitrate and cobalt nitrate, used in the production of the current collector system, a dedicated calculation is applied to simulate the production of these chemical compounds. The procedure involves the chemical reaction of formation, starting from the respective oxides (manganese oxide and cobalt oxide) and nitric acid, and delivering the desired nitrates. The reaction is supposed to be stochiometric, calculating the masses required to obtain 1 kg of product with a 100% yield. Next, the reaction energy is estimated, calculating the standard enthalpy of reaction from the formation enthalpies of products and reactants. It is important to note that this is the theoretical value and, in the case of endothermic reactions, it corresponds to the minimum energy required for the reaction to occur successfully. Since the formation reactions of manganese nitrate and cobalt nitrate are

exothermic, the assumption of no additional external heat is applied. However, energy equal to the required activation energy must be supplied. It is, then, assumed that the heat is supplied from the combustion of natural gas.
The S235 steel sheet and mild steel used in the production of the hotbox and electric heater, respectively, are steel-based materials characterized by a low carbon content (up to 0.17), manganese (0.5–1.4%), copper, and phosphorus (up to 0.55%). Since these specific materials are not included in the database, they are substituted with unalloyed steels as proxies [118], [119].
The energy consumed for the production and assembly of 1 MW electrolyzer, according to the PROTOSTACK project, amounts to 180,451 kWh. In the Ecoinvent v3 database, the "Electricity, medium voltage {RER}| market group for electricity, medium voltage | Cut-off, U" dataset is chosen, in order to account for the fact that the production stage is located in the European Union.
For all components made of steel, i.e., current collector, hotbox, BoP components, and reactor, the precise metalworking is not considered, because out of scope, and a generic process that includes all metalworking energy and inputs is used. This generic metalworking dataset is selected from Ecoinvent as "Metal working, average for steel product manufacturing {RER}| metal working, average for steel product manufacturing | Cut-off, U".

V. 2.2.2 LCI for PCCEL system use phase

During the operating phase, the consumption of the European electricity mix required to power the electrolyzer, pump, blower, and electric heater for a total of 160,000 operating hours (20 years) is considered. Specifically, the Ecoinvent dataset "Electricity, medium voltage {RER}| market group for electricity, medium voltage | Cut-off, U", which refers to the average European electricity market mix for the period 2015–2023, is selected.
The amount of demineralized water consumed for hydrogen production over 20 years is also taken into account. The oxygen generated as a by-product is considered to be emitted into the atmosphere.
It is important to note that the PCCEL operates in thermoneutral mode, therefore requiring no additional heat input. The parameters considered for the LCA model of the use phase are summarized in Table 19.

Table 19. Input flows and energy consumption of the PCCEL system in operating phase.

Parameters	Data
PCCEL energy consumption [MWh/20y]	160,000
Pump energy consumption [MWh/20y]	130
Blower energy consumption [MWh/20y]	0.64
Electric heater energy consumption [MWh/20y]	28,053
Demineralized water [ton/20y]	38,256
Oxygen [ton/20y]	33,296

V.2.3 Life Cycle Impact Assessment

The LCIA phase is the step that translates the inventory results (resources and emissions) into environmental impacts.

For the present study, LCIA is performed using SimaPro software, which offers several methodologies for assessing environmental impact. Each method relies on a specific set of impact categories, and the choice of the most appropriate method also depends on which environmental problems the study aims to assess. In this context, the Environmental Footprint 3.1 method, containing 16 distinct impact categories, as listed in Table 15 and described in Table 20, is chosen [120].

These categories represent specific environmental aspects or areas affected by the entire life cycle of the product, process, or activity.

Table 20. Description of impact categories contained in the EF 3.1 method [120].

Impact categories	Description	Unit
CLIMATE CHANGE	Increase in global average temperature due to GHG.	kg CO2 eq
OZONE DEPLETION	Depletion of the ozone layer with harmful effects on human health (e.g., skin cancer) and plants.	kg CFC-11 eq
HUMAN TOXICITY (cancer and not)	Potential harm to human health caused by toxic substances absorbed through air, water, or soil.	CTUh
PARTICULATE MATTER	Adverse effects of fine particles and precursors on respiratory health.	Disease incidence/kg PM2.5
IONISING RADIATION	Adverse effects due to exposure to ionizing radiation.	kg U235 eq
PHOTOCHEMICAL OZONE FORMATION	Harmful effects on soil, plants, and health caused by photochemical smog.	kg NMVOC eq
ACIDIFATION	Negative impacts on forests and aquatic fauna caused by acidifying substances.	mol H+ eq
EUTROPHICATION, MARINE	Excessive growth of vegetation in terrestrial ecosystems due to the effect of nitrogen and phosphorus.	mol N eq
EUTROPHICATION, TERRESTRIAL	Excessive algae/plant growth in freshwater caused by nutrients.	kg P eq
EUTROPHICATION, FRESHWATER	Increase in nutrients (mainly nitrogen) that alters marine ecosystems.	kg N eq
ECOTOXICITY, FRESHWATER	Potential toxic damage to aquatic species and ecosystems.	CTUe
LAND USE	Impacts on biodiversity, soil structure, and function caused by human activities.	Pt (punti)

WATER USE	Water abstraction and assessment of local water scarcity.	m^3
RESOURCE USE, FOSSILS	Consumption of fossil resources such as coal, oil, and gas, with impacts on their depletion.	MJ
RESOURCE USE, MINERALS AND METALS	Extraction of minerals and metals, with impacts on their depletion.	kg Sb eq

According to the EF method [120], the life cycle impact assessment includes four mandatory phases. Classification allows potential environmental impacts to be categorized and assigned to specific impact categories. The purpose of classification is to organize several environmental impacts into distinct groups based on their nature and characteristics.

Characterization refers to calculating the contribution of each input and output and aggregating the contributions within each category. The inventoried values are then multiplied by the characterization factors for each impact category considered.

Normalization and weighting are recommended because they support the interpretation and communication of the results. They facilitate the decision-making process, allowing results to be analyzed both in absolute terms and in aggregate form. These steps combined the different environmental impact categories into a single score, facilitating direct comparisons between products or scenarios, including all indicators considered. During normalization, the results obtained with the characterization step are multiplied by normalization factors (Table 21) [20], transforming them into dimensionless data. The purpose of this step is to calculate the magnitude of the environmental impacts and compare them to a reference level, which represents a standardized quantity of a resource or a common environmental impact.

Table 21. Normalization factors for 16 impact categories *[20]*.

Impact category	**Normalization factor**
Climate change	7.55E+03
Resource Use, fossils	6.50E+04
Resource Use, minerals, and metals	6.36E-02
Ionising Radiation	4.22E+03
Ozone Depletion	5.23E-02
Human Toxicity, cancer	1.73E-05
Human Toxicity, non-cancer	1.29E-04
Particulate Matter	5.95E-04
Photochemical Ozone	4.09E+01
Acidification	5.56E+01
Eutrophication, terrestrial	1.77E+02
Eutrophication, freshwater	1.61E+00
Eutrophication, marine	1.95E+01
Ecotoxicity, freshwater	5.67E+04
Land Use	8.19E+05
Water Use	1.15E+04

The normalized results are then multiplied by weighting factors, which reflect the relative importance of each environmental impact category, thus allowing the aggregation of the different impact categories into a unique indicator. In this way, although the overall uncertainty increases, the results of the LCA study are more clearly interpreted, and environmental communication becomes easier. The set of weighting factors is reported in Table 22, showing, for instance a higher perceived importance for climate change with respect to the other impact categories [121].

Table 22. Weighting factors for 16 impact categories as recommended by the EF method [121].

Impact category	Weighting factor (%)
Acidification	6.20
Climate change	21.06
Ecotoxicity, freshwater	1.92
Particulate matter	8.96
Eutrophication, marine	2.96
Eutrophication, freshwater	2.80
Eutrophication, terrestrial	3.71
Human toxicity, cancer	2.13
Human toxicity, non-cancer	1.84
Ionising radiation	5.01
Land use	7.94
Ozone depletion	6.31
Photochemical ozone formation	4.78
Resource use, fossils	8.32
Resource use, minerals, and metals	7.55
Water use	8.51

In conclusion, the impact categories estimation is essential for quantifying and classifying potential environmental effects, providing a solid basis for an in-depth analysis of overall environmental sustainability [122].

V.2.4 Life Cycle Interpretation

The final step of the LCA involves interpreting the results, which are presented relative to the FU and understood in relation to the goal and scope of the study.

Table 23 presents the absolute environmental impact results for both the manufacturing and operating phases of the PCCEL system over its entire 20 year lifetime (equivalent to 160,000 operating hours) based on the FU defined previously, that is, environmental impact per 1 kg of H_2 produced.

The results demonstrate that environmental impacts are predominantly driven by the operating phase, primarily due to electricity consumption based on the Ecoinvent dataset representative of the European energy mix for the period 2015-2023.

Table 23. Absolute results for manufacturing and operating phases of the PCCEL system based on FU.

Impact category	Unit/kg H_2 produced	PCCEL SYSTEM MANUFACTURING	PCCEL SYSTEM OPERATING
Acidification	mol H+ eq	1.47E-03	7.41E-02
Climate change	kg CO2 eq	9.52E-02	14.61
Ecotoxicity, freshwater	CTUe	4,448	44.67
Particulate matter	disease inc.	6.96E-09	2.59E-07
Eutrophication, marine	kg N eq	2.49E-04	1.28E-02
Eutrophication, freshwater	kg P eq	1.65E-04	1.30E-02
Eutrophication, terrestrial	mol N eq	2.60E-03	1.12E-01
Human toxicity, cancer	CTUh	9.74E-10	2.92E-08
Human toxicity, non-cancer	CTUh	2.29E-09	1.11E-07
Ionising radiation	kBq U-235 eq	1.84E-02	9,601
Land use	Pt	8.25E-01	58,456
Ozone depletion	kg CFC11 eq	1.17E-09	2.53E-07
Photochemical ozone formation	kg NMVOC eq	7.08E-04	3.70E-02
Resource use, fossils	MJ	1.38	344
Resource use, minerals and metals	kg Sb eq	8.53E-05	3.19E-05
Water use	m^3 depriv.	4.99E-02	4.28

The electrolyzer's electricity consumption represents the largest contributor to environmental impacts, accounting for 77% to 85% across all categories analyzed. The electric heater is the second largest contributor, responsible for 13% to 15% of the impacts. In contrast, auxiliary equipment such as the pump and blower contributes minimally, with negligible environmental impacts. Demineralized water consumed for hydrogen production also results in very limited impacts.

Although the manufacturing phase has a lower overall impact than the operating phase, analyzing manufacturing helps to identify critical materials used and focus reduction efforts. The manufacturing of the PCCEL accounts for between 44% (Human toxicity, cancer) and 99% (Resource use, minerals and metals) of the impact, primarily due to crucial metals and materials used in components that have considerable environmental issues, especially mining activities and production of high-impact chemicals.

A notable exception is the "Human toxicity, cancer" category, where the hotbox and the BoP components show impacts of 31% and 24% respectively, comparable to PCCEL's 44%. This is due to materials and processes involving carcinogenic substances in these components.

To support a comprehensive interpretation, the Environmental Footprint 3.1 method requires normalization and weighting of impact data [121]. After normalization to average annual global per capita emissions, results are multiplied by weighting factors to obtain a final single score, as presented in Table 24. According to the Product Environmental Footprint Category Rules Guidance [123], impact categories that cumulatively account for at least 80% of the total environmental impact are classified as most relevant categories and should be selected for

detailed analysis. Therefore, in this Table, the impact categories are organized in descending order to identify those reaching this threshold. With a cumulative contribution of 80.6%, the following five categories are selected: "Resource use, fossils" (26.7%), "Climate change" (24.8%), "Eutrophication, freshwater" (13.8%), "Resource use, minerals and metals" (8.4%), and "Ionising radiation" (6.9%). The remaining categories are aggregated and categorized as "Others.

Table 24. Single score results for manufacturing and operating phases of the PCCEL system based on FU.

Impact categories	PCCEL SYSTEM MANUFACTURING (%)	PCCEL SYSTEM OPERATING (%)
Most relevant categories		
Resource use, fossils	0.11	26.59
Climate change	0.16	24.62
Eutrophication, freshwater	0.17	13.65
Resource use, minerals and metals	6.12	2.29
Ionising radiation	0.01	6.89
Others		
Acidification	0.10	5.00
Photochemical ozone formation	0.05	2.62
Particulate matter	0.06	2.36
Human toxicity, cancer	0.07	2.18
Water use	0.02	1.92
Eutrophication, terrestrial	0.03	1.42
Eutrophication, marine	0.02	1.18
Ecotoxicity, freshwater	0.09	0.91
Human toxicity, non-cancer	0.02	0.96
Land use	0.005	0.34
Ozone depletion	0.0001	0.02
Total	7.10	92.9

The results of the LCA analysis show that the manufacturing phase contributes 7.10% of the total impact, corresponding to 0.117 mPt on the functional unit considered, while the operating phase represents 92.9% of the total impact, quantitatively equal to 1.54 mPt.

Figure 33 illustrates the single scores for manufacturing and operating phases, highlighting the operating phase's dominant impact. The analysis reveals that, based on the Ecoinvent dataset representative of the European energy mix for the period 2015-2023, significant variations exist among European countries in their contribution to different impact categories. In the "Resource use, fossils" category, France and Germany emerge as principal contributors due to the intensive use of nuclear energy in France and lignite-based electricity generation in Germany. France also appears as a major emitter in the "Ionizing radiation" category, confirming the predominant role of nuclear energy in its electricity mix. In the "Climate change" category, Italy and Germany exhibit the highest emissions, primarily attributable to natural gas combustion in Italy and hard coal use in Germany. Finally, in the "Eutrophication, freshwater" category, the most significant

impacts are associated with copper mining activities in Germany and hard coal utilization in Poland. France and Germany account for the highest emissions in almost all impact categories. Being among the most populous and highly industrialized countries, they have significantly higher energy demand, thus accounting for a higher percentage of the European average mix. These country-specific variations underscore how national energy policies and resource endowments significantly influence the environmental profile of hydrogen production via electrolysis.

Although the manufacturing impacts are lower, they remain significant, especially in the "Resource use, minerals and metals" category, where they contribute 6.12% out of 8.41% of total impact. This indicates that, while the majority of environmental impacts derive from the energy consumed during system use, the manufacturing phase plays an important role, primarily in the abiotic depletion of minerals and metals.

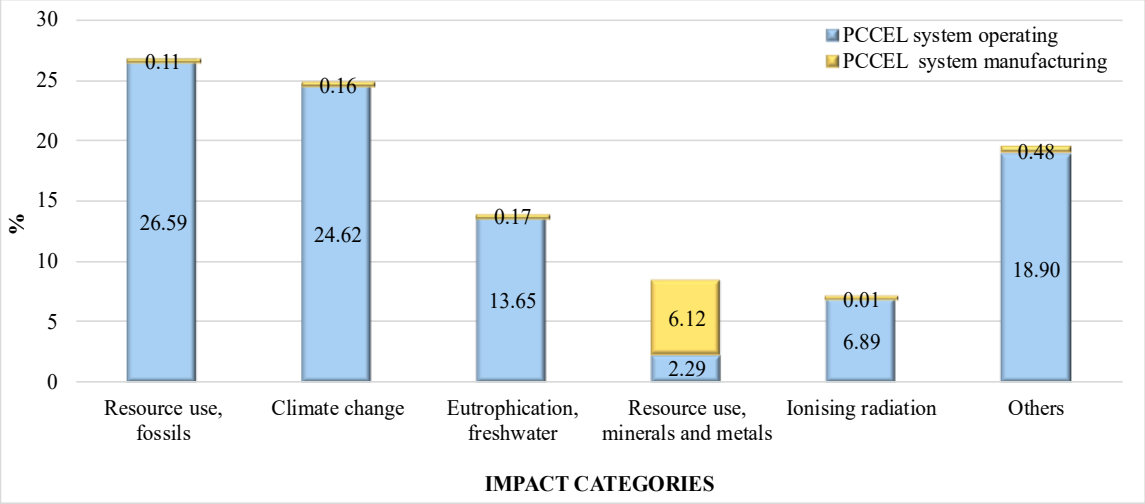

Figure 33. Single score results for PCCEL system manufacturing and operating phases based on FU.

A detailed disaggregation of operating phase results in terms of single scores (Figure 34) reveals that, as previously mentioned, the electrolyzer's energy consumption (160,000 MWh over 20 years) contributes most significantly to environmental impacts, exceeding 20% in both the "Resource use, fossils" and "Climate change" categories. These values emphasize the crucial role of energy requirements in electrolysis operations and highlight the imperative for transitioning to low-carbon electricity sources to achieve meaningful reductions in hydrogen production impacts.

The electric heater, with an energy requirement of 28,053 MWh over 20 years, contributes 4.26%, 3.95% and 2.19% in “Resource use, fossils”, “Climate change”, and “Eutrophication,

freshwater" categories, respectively. The pump and blower, with energy consumption of 130.6 MWh over 20 years, demonstrate impacts below 0.03% across all analyzed categories and are, therefore, aggregated due to their negligible contribution relative to other components. Finally, the consumption of demineralized water (38,256 tons over 20 years) has a marginal impact on all the impact categories.

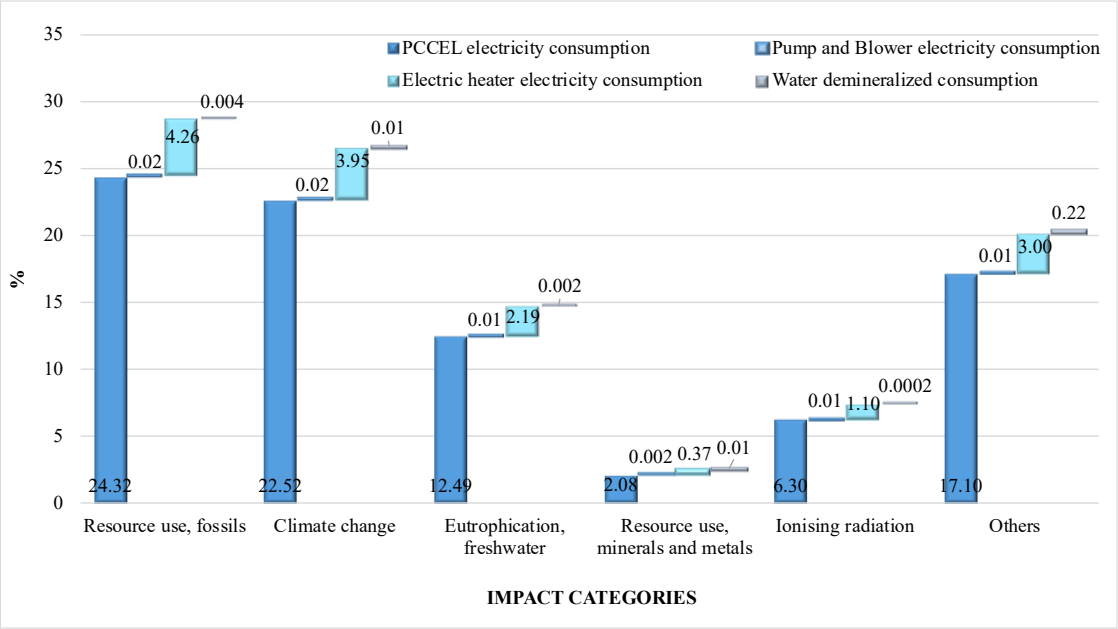

Figure 34. Single score results for the PCCEL system operating phase based on FU. The percentages are relative to the weighted results considering only the PCCEL operating phase.

Further investigation is warranted in the manufacturing phase to assess the efficiency and environmental sustainability of materials employed in system fabrication. As illustrated in Figure 35, single-score results indicate that the electrolyzer manufacturing exerts the greatest impact in the "Resource, use, minerals and metals" category, accounting for approximately 86.60% of manufacturing phase impact. Hotbox and BoP contribute significantly less to all categories.

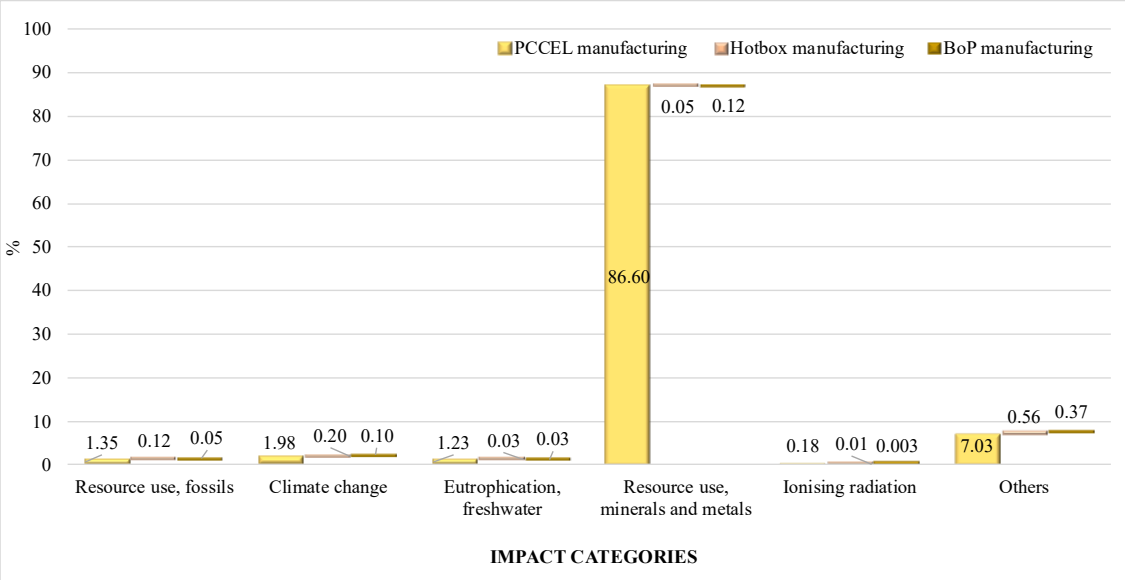

Figure 35. Single score results for the PCCEL system manufacturing phase based on FU. The percentages are relative to the weighted results considering only the PCCEL manufacturing phase.

A further analysis of each manufacturing component is presented in Table 25, with single-score results expressed in micropoints on the FU (µPt/kg H_2 produced). This detailed breakdown enables the identification of crucial materials and facilitates targeted improvement strategies.

Table 25. Single score results, expressed in µPt/kg H_2 produced, for the PCCEL system's manufacturing phase.

Impact category (µPt/kg H_2 produced)	**Resource use, fossils**	**Climate change**	**Eutrophication, freshwater**	**Resource use, minerals, and metals**	**Ionising radiation**	**Others**
ELECTROLYZER						
Cathode & Electrolyte	1.40E-01	2.15E-01	1.05E-01	9.42E-01	1.85E-02	1.49E+00
Anode	7.62E-03	1.17E-02	3.18E-03	4.98E-02	3.64E-03	6.90E-02
Seal	1.41E-03	3.60E-03	4.73E-04	8.61E-04	2.84E-05	5.49E-03
Current Collector system	3.23E-02	4.72E-02	5.62E-03	7.80E-02	4.45E-03	1.03E-01
Interconnects	8.46E-01	1.41E+00	2.42E+00	9.97E+01	6.37E-02	4.35E+00
Reactor	1.23E-01	2.29E-01	4.90E-02	1.96E-01	8.56E-03	5.40E-01
Electricity consumption	4.19E-01	3.88E-01	2.15E-01	3.59E-02	1.09E-01	2.95E-01
HOTBOX						
Housing	1.25E-01	2.08E-01	3.43E-02	3.46E-02	5.51E-03	5.85E-01
Bicycle racks	1.51E-02	2.81E-02	6.00E-03	2.40E-02	1.05E-03	6.62E-02
BoP COMPONENTS						
Water Tank	5.06E-04	9.39E-04	2.01E-04	8.02E-04	3.51E-05	2.21E-03
Pump	1.74E-04	3.28E-04	2.62E-04	2.50E-03	8.68E-06	1.50E-03
Plate and frame HEs	2.24E-02	4.17E-02	9.67E-03	1.42E-02	1.57E-03	1.61E-01

Electric Heater	2.43E-02	4.57E-02	1.08E-02	6.32E-03	1.71E-03	2.01E-01
Blower	1.12E-04	1.67E-04	6.18E-05	5.40E-04	5.05E-06	6.01E-04
Separator Tanks 1, 2	8.34E-04	1.55E-03	3.31E-04	1.32E-03	5.78E-05	3.65E-03
Power converter	6.41E-03	1.24E-02	7.88E-03	1.17E-01	3.83E-04	2.16E-02

Starting with the production of the proton-conducting ceramic tubular electrolyzer, the primary environmental impact is attributable to the extensive use of precious materials - including copper, silver, and/or gold (specific materials withheld due to confidentiality constraints related to the *PROTOSTACK project*) in the manufacturing of interconnects. Although these materials are appreciated for their high thermal and electrical conductivity, their extraction entails significant environmental consequences, including soil contamination, water pollution, and adverse impacts on biodiversity. These critical issues arise from intensive mining operations and the deployment of toxic chemicals in extraction and refining processes, which can cause persistent environmental contamination [124].

Excluding interconnects from the analysis, Figure 36 better shows the other components' impacts. Among the top five contributing categories, "Resource use, fossils" and "Climate change" impacts related to the energy consumed for producing and assembling the different layers of the electrolyzer (180.451 kWh), are relatively elevated. This result reflects the energy mix characteristics dominated by suppliers from countries generating electricity primarily through fossil fuels.

Regarding the "Resource use, minerals and metals" category, significant contributions arise from cathode and electrolyte manufacturing, attributable to materials such as nickel (used as a proxy for nickel oxide) and cerium oxide. Nickel mining and processing, particularly the thermal smelting and refining processes for pure nickel metal, involve high energy consumption and significant emissions. Cerium oxide, widely used in nanotechnology applications including catalysts, fuel cells, and fuel additives, is associated with high toxicity to aquatic ecosystems, water resources, and human health. [125], [126].

The results indicate that, although the anode composed of BZCY/BGLC exhibits a lower environmental impact compared to the cathode, normalizing the impacts by the respective weights of the materials allows for the estimation of the specific impact per kilogram of material used. In this context, the cathode demonstrates a lower value equal to 1.12 nPt/kg material*FU compared to the anode, which totals 1.89 nPt/kg material*FU.

Therefore, optimization strategies should focus on both reducing the amount of material used for the cathode, such as decreasing its thickness to lower its overall environmental impact, and on improving the performance of anode materials. The latter approach, which could involve

enhancements in microstructure or performance, may significantly lower the anode's specific environmental impact, thus narrowing the gap in the overall environmental performances of the two electrodes.

However, it is important to underline that, based on data provided by partners in the PROTOSTACK project, the environmental impacts attributed to the cathode also include the portion related to the electrolyte. For confidentiality reasons, it is not possible to determine precisely how much of the impact is attributable to the cathode versus the electrolyte. This uncertainty should be considered during interpretation and when devising optimization strategies, as a more detailed allocation of impacts could alter priorities for actions targeted to specific materials.

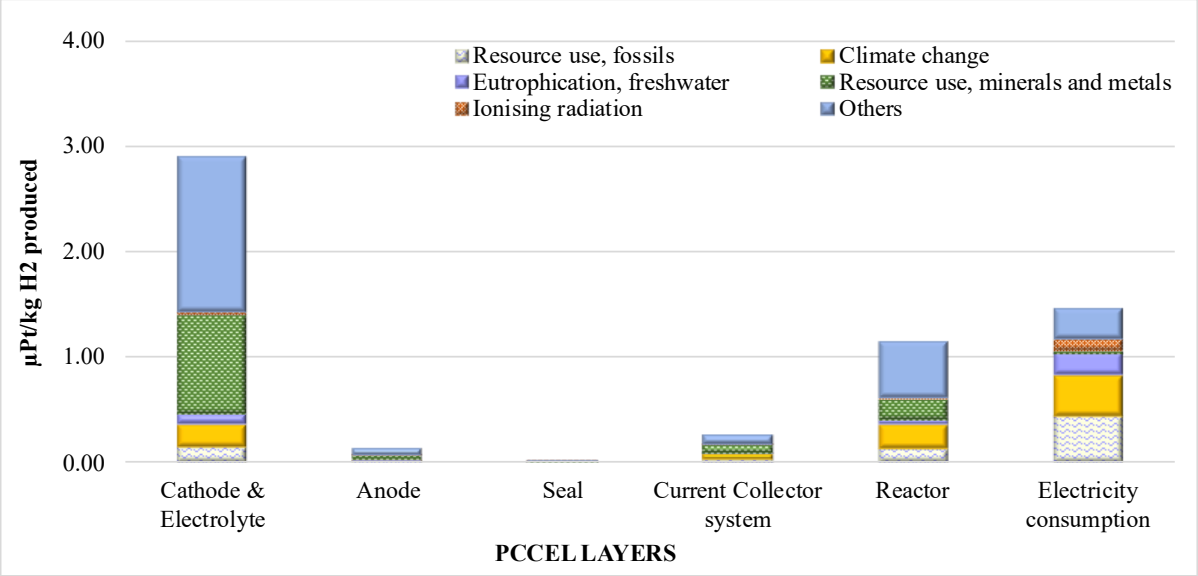

Figure 36. Single score results, expressed in µPt/kg H_2 produced, for the electrolyzer's manufacturing phase.

Analysis of hotbox production phase results (Figure 37) reveals that "Resource use, fossils" and "Climate change" categories exhibit the highest contributions, particularly for housing components (0.12 µPt/kg H_2 produced and 0.21 µPt/kg H_2 produced, respectively), compared to other impact categories. This indicates that a part of the environmental impact derives from elevated consumption of mild steel used for sheet metal production (3.944 kg).

The "Eutrophication, freshwater", "Ionizing radiation", and "Others" impact categories show lower single score values but still need to be considered in the overall assessment, especially for housing, which registers an "Others" value of 0.59 µPt/kg H_2 produced, suggesting the presence of minor yet significant impacts for the overall sustainability of the component. Thermal management represents a critical design consideration for high-temperature

electrochemical systems, with hotbox insulation materials (including refractory firebricks totaling 16,800 kg) contributing to both thermal efficiency and material-related environmental burdens. Optimization of insulation thickness and material selection presents opportunities for reducing manufacturing impacts while maintaining requisite thermal performance.

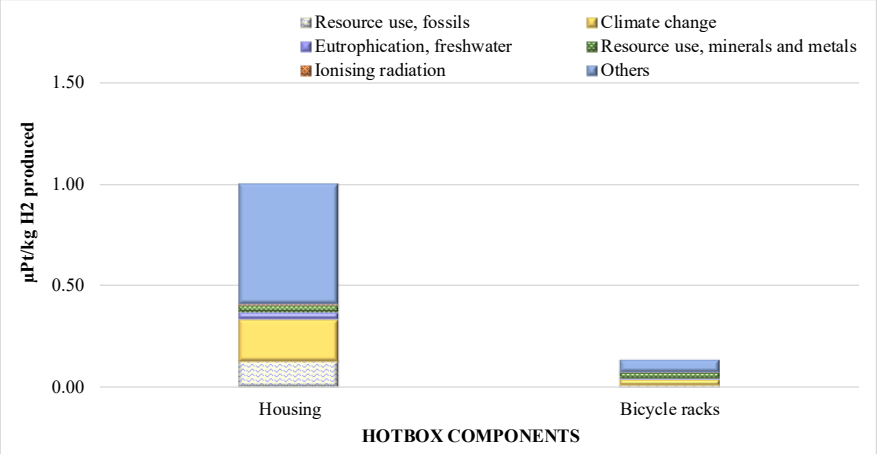

Figure 37. Single score results, expressed in µPt/kg H_2 produced, for the hotbox's manufacturing phase.

From Figure 38, it is clear that in all impact categories, the potential environmental effects related to the manufacturing of the BoP are significantly lower than those associated with the hotbox and the PCCEL.

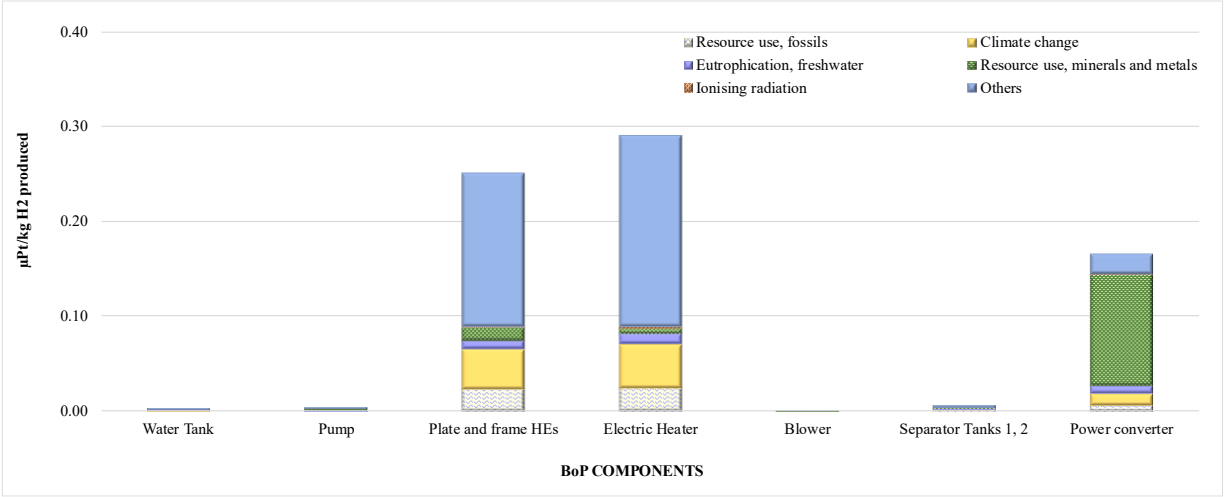

Figure 38. Single score results, expressed in µPt/kg H_2 produced, for the BoP manufacturing phase.

The components with the greatest environmental impact are the plate and frame heat exchangers, the electric heater, and the power converter. The plate and frame heat exchangers and the electric heater are characterized by notable impacts in "Climate change", "Resource

use, and fossils" and "Others" categories. This is due to the extensive use of 304 stainless steel (for a total of 601.2 kg), a material known for its robustness, but it also requires intense energy for its processing and refining. The power converter, a key component for converting electrical power from AC to DC needed to power the electrolyzer, has a high impact, especially in the "Resource use, minerals, and metals" category. This is due to the presence of several crucial materials within it, such as rare earths, precious metals, and other special alloys used in electronic circuits and power modules.

It is also important to note that these results represent estimates, influenced by the dataset selection and may therefore exhibit slight variations. This consideration applies equally to the other results presented in the study.

V.3 Comparative Context and Improvement Strategies

According to ISO 14040 and ISO 14044, comparisons between LCA studies are only valid when assessment methodology and functional unit are equivalent. Consequently, the results of this study cannot be *directly* compared with those available in the literature, as no specific LCA exist for PCCEL systems, and studies on other electrolysis technologies adopt different assessment methods, functional units and inventory databases, limiting environmental results comparability [104], [105].

Comparisons with other LCA studies on electrolysis systems should therefore be interpreted with caution. Although environmental impact categories vary by methodology, only the "Climate Change" category (kg CO_2 equivalent) is reported for each study below, as it is consistently present across all works. This choice enables targeted quantitative comparison for this specific impact category.

Gerloff et al. [127] assesses hydrogen production impacts from AWE, PEMWE, and SOEC, focusing on manufacturing and operating phases, assuming German electricity. System boundaries include raw material extraction, manufacturing, and operation over a useful life of more than 20 years (at 50% load factor), excluding end-of-life treatment. The functional unit is 1 kg of H_2 produced at 30 bar. The LCA is modeled with SimaPro 9.0 and the Ecoinvent v3.6 database, applying the ILCD 2011 Midpoint+ method (16 impact categories).

The results show that the operating phase generates over 90% of the total impacts, dominated by electricity consumption, while production contributes just over 5%. In particular, the AWE has an impacts of 22.5 kg CO_2 eq/kg H_2 (lowest, due to less critical materials like nickel and

steel), PEMWE of 25.1 kg CO_2 eq/kg H_2 (slightly higher due to platinum catalysts), and SOEC of 32.8 kg CO_2 eq/kg H_2 (highest, owing to high-temperature ceramics and nickel-YSZ).

Barei et al. [128] estimate the environmental impact of hydrogen production via PEMWE powered by the German electricity mix. The goal is to quantify the environmental impacts of H_2 from PEMWE in current and future energy scenarios, identifying hotspots and improvement opportunities. The analysis follows a cradle-to-gate approach modeled in SimaPro, including the electrolyzer and the BoP; datasets are chosen from Ecoinvent v3.3. The functional unit is defined as 1 kg of dried H_2. Using the ReCiPe method (endpoint and midpoint), key results show a climate change impact of 29.5 kg CO_2eq/kg H_2.

Magnaval et al. [129] conduct an LCA for a 20 kW SOEC system, taking into account both the manufacturing and operating phases. The functional unit is defined as the production of 1 kg of 99.9% pure hydrogen produced at 25 bar, considering European energy consumption in 2024. The Impact World+ v2.0 method is used to assess environmental impacts. OpenLCA 2.0.3 software is used to calculate the potential impacts associated with the inventoried emissions.

The results show that the operating phase dominates all impact categories, contributing 67%-89%, followed by the BoP (7%-22%), while stack production remains minor (4%-11%). In particular, the SOEC system production and operating impact 15.4 kg CO_2 eq/kg H_2 in climate change category.

In the ELY4OFF project [130], an LCA analysis is conducted on a 62 kW PEMWE system with a maximum hydrogen production of 28 kg/day, assuming continuous operation. The functional unit used is 1 kg of hydrogen produced at 99.999% purity, at 20 bar and 55°C. The ReCiPe method, considering seven midpoint impact categories, including Climate change, Ozone depletion, Non-carcinogenic Human toxicity, Terrestrial acidification, Fine particulate matter formation, Photochemical oxidant formation (ecosystem), and Mineral resource scarcity, is adopted for the environmental assessment. The study highlights that the PEMWE system manufacturing process represents the most critical phase in terms of emissions (1.89 kg CO_2 eq/kg H2 in climate change category). The contribution of different electricity generation technologies to the use phase is also assessed: the use of wind turbines, followed by solar panels, has the least impact in all impact categories, while the grid electricity mix is the least sustainable choice.

Mehmeti et al. [131] evaluate the environmental impact of hydrogen production via high-temperature SOEC powered by different electrical energy sources. The functional unit is 1 kg of H_2 produced in a 100 kg H_2/day plant operating at 750°C with a steam/water input of 80% H_2O/20% H_2 and a conversion rate of 83%. Using a cradle-to-grave approach, the boundaries

system include the construction, operation, and maintenance of the SOEC system (electrolyzer and Balance of Plant). The ReCiPe 2016 LCA method is applied for environmental life cycle assessment. For average estimate of the impacts calculated in the countries such as Italy, Germany, Denmark, Finland, France, Switzerland, the Netherlands, Norway, Poland, and Sweden, the approximate result is climate change 17.00 kg CO_2 eq/kg H_2.

Also in this study, the LCA assessment of the PCCEL system shows that the operating phase, particularly fossil-fuel electricity consumption, is the primary driver of overall environmental impacts, accounting for over 90%. System production accounts for only approximately 7% of impacts, primarily in the "Resource use, minerals, and metals" category due to the use of precious metals in interconnects and the manufacturing of ceramic components. These findings are consistent with the literature, which recognizes production impacts as secondary to operational impacts. Furthermore, by comparing only the results related to the "climate change" category with the available studies, it is clear that the PCCEL system examined has a lower impact in terms of kg CO2 eq.

However, the PCCEL system's results have limitations: PCCEL production outcomes are based on estimates from small-scale prototypes and confidential primary data, which introduce uncertainty regarding the actual impact. Real efficiency and production processes may vary when scaling up to commercial levels. Additionally, the analysis uses the European electricity mix dataset for 2015–2023, which does not account for ongoing decarbonization trends. In the future, as renewable technologies become more prevalent, the operational impacts of PCCEL systems will likely decrease. Lastly, end-of-life treatment is not included due to a lack of data, despite the potential for recycling precious metals and ceramic components.

To effectively reduce the environmental impact of the PCCEL system, it is therefore recommended to prioritize renewable sources, optimize the design of critical components such as the cathode, electrolyte, and interconnects, and adopt circular economy strategies that promote the recovery and recycling of critical end-of-life materials – aspects that will be explored in future studies.

These results offer basic guidance for developing PCCEL technology in the *PROTOSTACK project*. Ongoing monitoring and reassessment of environmental performance will be crucial to ensure that optimization efforts effectively target the most significant environmental hotspots while remaining technically and economically feasible.

REFERENCE

[1] I. Energy Agency, “World Energy Outlook 2024,” 2024. [Online]. Available: www.iea.org/terms

[2] R. Martin, “GHG EMISSIONS OF ALL WORLD COUNTRIES JRC SCIENCE FOR POLICY REPORT,” 2024. doi: 10.2760/0115360.

[3] European Environment Agency, “Trends and projections in Europe 2024”, doi: 10.2800/7574066.

[4] “World Energy Outlook 2023 – International Energy Agency - https://www.iea.org/reports/world-energy-outlook-2023/executive-summary [Accessed 8 June 2025]”.

[5] “Compliance of Parties to the Kyoto Protocol in the first Commitment Period.”

[6] “The Kyoto Protocol - Global Gateway Forum - https://climate.ec.europa.eu/eu-action/international-action-climate-change/kyoto-protocol_en [Accessed 8 June 2025]”.

[7] “Key aspects of the Paris Agreement - UN Climate Change - https://unfccc.int/most-requested/key-aspects-of-the-paris-agreement [Accessed 8 June 2025] ”.

[8] M. Kuhn *et al.*, “Matus Muron (Ch. 2), Grzegorz Pawelec,” Ivan Petar Yovchev.

[9] “The Europen hydrogen policy landscape - extensive update of the April 2024 report - January 2025”.

[10] “Clean Hydrogen JOINT UNDERTAKING (Clean Hydrogen JU) WORK PROGRAMME 2025.”

[11] Mariette. Hagglund, *Rebuilding Sweden’s crisis preparedness : lack of clarity impedes implementation*. Finnish Institute of International Affairs, 2020.

[12] J. A. Riera, R. M. Lima, and O. M. Knio, “A review of hydrogen production and supply chain modeling and optimization,” Apr. 30, 2023, *Elsevier Ltd*. doi: 10.1016/j.ijhydene.2022.12.242.

[13] M. Fallah Vostakola, H. Ozcan, R. S. El-Emam, and B. Amini Horri, “Recent Advances in High-Temperature Steam Electrolysis with Solid Oxide Electrolysers for Green Hydrogen Production,” Apr. 01, 2023, *MDPI*. doi: 10.3390/en16083327.

[14] D. Saygin and D. Gielen, “Zero-emission pathway for the global chemical and petrochemical sector,” *Energies (Basel).*, vol. 14, no. 13, Jul. 2021, doi: 10.3390/en14133772.

[15] I. Renewable Energy Agency, *Decarbonising hard-to-abate sectors with renewables: Perspectives for the G7*. 2024. [Online]. Available: www.irena.org

[16] L. M. Pastore and L. de Santoli, “100% renewable energy Italy: A vision to achieve full energy system decarbonisation by 2050,” *Energy*, vol. 317, Feb. 2025, doi: 10.1016/j.energy.2025.134749.

[17] P. Marocco, M. Gandiglio, D. Audisio, and M. Santarelli, “Assessment of the role of hydrogen to produce high-temperature heat in the steel industry,” *J. Clean. Prod.*, vol. 388, Feb. 2023, doi: 10.1016/j.jclepro.2023.135969.

[18] P. J. Megia, A. J. Vizcaino, J. A. Calles, and A. Carrero, “Hydrogen Production Technologies: From Fossil Fuels toward Renewable Sources. A Mini Review,” Oct. 21, 2021, *American Chemical Society*. doi: 10.1021/acs.energyfuels.1c02501.

[19] T. Geißler *et al.*, “Experimental investigation and thermo-chemical modeling of methane pyrolysis in a liquid metal bubble column reactor with a packed bed,” *Int. J. Hydrogen Energy*, vol. 40, no. 41, pp. 14134–14146, 2015, doi: 10.1016/j.ijhydene.2015.08.102.

[20] A. Constantin, “Nuclear hydrogen projects to support clean energy transition: Updates on international initiatives and IAEA activities,” *Int. J. Hydrogen Energy*, vol. 54, pp. 768–779, Feb. 2024, doi: 10.1016/j.ijhydene.2023.09.250.

[21] A. Ajanovic, M. Sayer, and R. Haas, “The economics and the environmental benignity of different colors of hydrogen,” *Int. J. Hydrogen Energy*, vol. 47, no. 57, pp. 24136–24154, Jul. 2022, doi: 10.1016/j.ijhydene.2022.02.094.

[22] N. Hydrogen Council, “Information Paper: Hydrogen transport,” 2021.

[23] C. Smith, A. K. Hill, and L. Torrente-Murciano, “Current and future role of Haber-Bosch ammonia in a carbon-free energy landscape,” *Energy Environ. Sci.*, vol. 13, no. 2, pp. 331–344, Feb. 2020, doi: 10.1039/c9ee02873k.

[24] “Lowering your emissions through innovation in transport and energy infrastructure REPORT PROJECT CT PROJECT An Introduction to Hydrogen Fuel Cell Electric Vehicles and Refuelling Stations.”

[25] L. van Biert, M. Godjevac, K. Visser, and P. V. Aravind, “A review of fuel cell systems for maritime applications,” Sep. 30, 2016, *Elsevier B.V.* doi: 10.1016/j.jpowsour.2016.07.007.

[26] K. Oesingmann, W. Grimme, and J. Scheelhaase, “Hydrogen in aviation: A simulation of demand, price dynamics, and CO2 emission reduction potentials,” *Int. J. Hydrogen Energy*, vol. 64, pp. 633–642, Apr. 2024, doi: 10.1016/j.ijhydene.2024.03.241.

[27] S. A. Grigoriev, V. N. Fateev, D. G. Bessarabov, and P. Millet, “Current status, research trends, and challenges in water electrolysis science and technology,” *Int. J. Hydrogen Energy*, vol. 45, no. 49, pp. 26036–26058, Oct. 2020, doi: 10.1016/j.ijhydene.2020.03.109.

[28] “Greig Chisholm, Tingting Zhao and Leroy Cronin. Hydrogen from water electrolysis”.

[29] D. M. F. Santos, C. A. C. Sequeira, and J. L. Figueiredo, “Hydrogen production by alkaline water electrolysis,” *Quim. Nova*, vol. 36, no. 8, pp. 1176–1193, 2013, doi: 10.1590/S0100-40422013000800017.

[30] E. Katz, “Electrochemical contributions: William Nicholson (1753–1815),” Feb. 01, 2021, *John Wiley and Sons Inc*. doi: 10.1002/elsa.202160003.

[31] S. Finger, M. Piccolino, and F. W. Stahnisch, “Alexander von Humboldt: Galvanism, animal electricity, and self-experimentation part 2: The electric eel, animal electricity, and later years,” *J. Hist. Neurosci.*, vol. 22, no. 4, pp. 327–352, Oct. 2013, doi: 10.1080/0964704X.2012.732728.

[32] A. Buttler and H. Spliethoff, “Current status of water electrolysis for energy storage, grid balancing and sector coupling via power-to-gas and power-to-liquids: A review,” Feb. 01, 2018, *Elsevier Ltd*. doi: 10.1016/j.rser.2017.09.003.

[33] “What are PEM Fuel Cells and Electrolyzers - Biologic - Latest updated: November 18, 2024 - https://www.biologic.net/topics/what-are-pem-fuel-cells-and-electrolyzers/ [Accessed 25 June 2025].”

[34] “Alfredo Ursúa, Luis M. Gandia and Pablo Sanchis. IEEE - Hydrogen production from water electrolysis: current status and future trends”.

[35] D. Jang, J. Kim, D. Kim, W. B. Han, and S. Kang, “Techno-economic analysis and Monte Carlo simulation of green hydrogen production technology through various water electrolysis technologies,” *Energy Convers. Manag.*, vol. 258, Apr. 2022, doi: 10.1016/j.enconman.2022.115499.

[36] S. G. Nnabuife, A. K. Hamzat, J. Whidborne, B. Kuang, and K. W. Jenkins, “Integration of renewable energy sources in tandem with electrolysis: A technology review for green hydrogen production,” *Int. J. Hydrogen Energy*, vol. 107, pp. 218–240, Mar. 2025, doi: 10.1016/j.ijhydene.2024.06.342.

[37] A. Khataee, A. Shirole, P. Jannasch, A. Krüger, and A. Cornell, “Anion exchange membrane water electrolysis using Aemion™ membranes and nickel electrodes,” *J. Mater. Chem. A Mater.*, vol. 10, no. 30, pp. 16061–16070, Jul. 2022, doi: 10.1039/d2ta03291k.

[38] E. E. Nzaba Madila, A. Makhsoos, M. M. Shanbhag, and B. G. Pollet, “Advancements in electrolyser stack performance: A comprehensive review of Latest technologies and efficiency strategies,” *Int. J. Hydrogen Energy*, vol. 144, pp. 1168–1189, Jul. 2025, doi: 10.1016/j.ijhydene.2025.04.047.

[39] K. Ham, S. Bae, and J. Lee, “Classification and technical target of water electrolysis for hydrogen production,” Aug. 01, 2024, *Elsevier B.V.* doi: 10.1016/j.jechem.2024.04.003.

[40] W. Li, H. Tian, L. Ma, Y. Wang, X. Liu, and X. Gao, “Low-temperature water electrolysis: fundamentals, progress, and new strategies,” May 17, 2022, *Royal Society of Chemistry*. doi: 10.1039/d2ma00185c.

[41] “JRC report - Water electrolysis and hydrogen in the European Union 2023 - ISSN 1831-9424”.

[42] “U.S. DEPARTMENT OF ENERGY - Technical Targets for Liquid Alkaline Electrolysis - https://www.energy.gov/eere/fuelcells/technical-targets-liquid-alkaline-electrolysis [Accessed 2 July 2025].”

[43] “U.S. DEPARTMENT OF ENERGY - Technical Targets for Proton Exchange Membrane Electrolysis - https://www.energy.gov/eere/fuelcells/technical-targets-proton-exchange-membrane-electrolysis [Accessed 2 July 2025].”

[44] “U.S. DEPARTMENT OF ENERGY -Technical Targets for High Temperature Electrolysis - https://www.energy.gov/eere/fuelcells/technical-targets-high-temperature-electrolysis [Accessed 2 July 2025]”.

[45] M. Chatenet *et al.*, “Water electrolysis: from textbook knowledge to the latest scientific strategies and industrial developments,” May 16, 2022, *Royal Society of Chemistry*. doi: 10.1039/d0cs01079k.

[46] S. Shiva Kumar and H. Lim, “An overview of water electrolysis technologies for green hydrogen production,” Nov. 01, 2022, *Elsevier Ltd*. doi: 10.1016/j.egyr.2022.10.127.

[47] Jonathan. Davies, Francesco. Dolci, and Eveline. Weidner, *Historical analysis of FCH 2 JU electrolyser projects : evaluation of contributions towards advancing the state of the art*. Publications Office of the European Union, 2021.

[48] N. Norazahar, F. Khan, N. Rahmani, and A. Ahmad, "Degradation modelling and reliability analysis of PEM electrolyzer," *Int. J. Hydrogen Energy*, vol. 50, pp. 842–856, Jan. 2024, doi: 10.1016/j.ijhydene.2023.07.153.

[49] A. Pozio, "Development perspectives on low-temperature electrolysis," 2021, doi: 10.12910/EAI2021-014.

[50] A. Kumar, A. K. Tiwari, and D. Milani, "Decarbonizing hard-to-abate heavy industries: Current status and pathways towards net-zero future," Jul. 01, 2024, *Institution of Chemical Engineers*. doi: 10.1016/j.psep.2024.04.107.

[51] T. International Renewable Energy Agency, *GREEN HYDROGEN COST REDUCTION SCALING UP ELECTROLYSERS TO MEET THE 1.5°C CLIMATE GOAL H 2 O 2*. 2020. [Online]. Available: www.irena.org/publications

[52] E. Vøllestad *et al.*, "Mixed proton and electron conducting double perovskite anodes for stable and efficient tubular proton ceramic electrolysers," *Nat. Mater.*, vol. 18, no. 7, pp. 752–759, Jul. 2019, doi: 10.1038/s41563-019-0388-2.

[53] C. Herradon *et al.*, "Proton-conducting ceramics for water electrolysis and hydrogen production at elevated pressure," *Front. Energy Res.*, vol. 10, Oct. 2022, doi: 10.3389/fenrg.2022.1020960.

[54] H. Il Ji, J. H. Lee, J. W. Son, K. J. Yoon, S. Yang, and B. K. Kim, "Protonic ceramic electrolysis cells for fuel production: a brief review," Sep. 01, 2020, *Springer*. doi: 10.1007/s43207-020-00059-4.

[55] Z. Liu *et al.*, "Advanced Electrode Materials for Efficient Hydrogen Production in Protonic Ceramic Electrolysis Cells," 2025, *John Wiley and Sons Inc*. doi: 10.1002/adma.202503609.

[56] L. Q. Le *et al.*, "Performance degradation in proton-conducting ceramic fuel cell and electrolyzer stacks," *J. Power Sources*, vol. 537, Jul. 2022, doi: 10.1016/j.jpowsour.2022.231356.

[57] X. Chen *et al.*, "Advanced Air Electrodes for Reversible Protonic Ceramic Electrochemical Cells: A Comprehensive Review," 2025, *John Wiley and Sons Inc*. doi: 10.1002/adma.202418620.

[58] E. Eikeng, A. Makhsoos, and B. G. Pollet, "Critical and strategic raw materials for electrolysers, fuel cells, metal hydrides and hydrogen separation technologies," Jun. 19, 2024, *Elsevier Ltd*. doi: 10.1016/j.ijhydene.2024.05.096.

[59] R. J. Kee, S. Ricote, H. Zhu, R. J. Braun, G. Carins, and J. E. Persky, "Perspectives on Technical Challenges and Scaling Considerations for Tubular Protonic-Ceramic Electrolysis Cells and Stacks," *J. Electrochem. Soc.*, vol. 169, no. 5, p. 054525, May 2022, doi: 10.1149/1945-7111/ac6c4e.

[60] L. Kwati *et al.*, "Toward highly efficient protonic electrolysis cells for large-scale hydrogen production at moderate temperatures," *Mater. Adv.*, vol. 6, no. 10, pp. 3253–3263, Apr. 2025, doi: 10.1039/d5ma00028a.

[61] C. Meisel, Y. D. Kim, D. Diercks, R. O'Hayre, and N. P. Sullivan, "Advancing proton-conducting ceramic electrochemical devices: perspectives on benchmarking and barriers to progress," *Front. Energy Res.*, vol. 13, 2025, doi: 10.3389/fenrg.2025.1565315.

[62] H. Su and Y. H. Hu, "Degradation issues and stabilization strategies of protonic ceramic electrolysis cells for steam electrolysis," May 01, 2022, *John Wiley and Sons Ltd*. doi: 10.1002/ese3.1010.

[63] S. Zheng *et al.*, "Enhancing surface activity and durability in triple conducting electrode for protonic ceramic electrochemical cells," *Nature Communications* , vol. 16, no. 1, Dec. 2025, doi: 10.1038/s41467-025-59477-9.

[64] S. Pirou *et al.*, "Planar proton-conducting ceramic cells for hydrogen extraction: Mechanical properties, electrochemical performance and up-scaling," *Int. J. Hydrogen Energy*, vol. 47, no. 10, pp. 6745–6754, Feb. 2022, doi: 10.1016/j.ijhydene.2021.12.041.

[65] "ELECTRA High Temperature Electrolyser with Novel Proton Ceramic Tubular Modules of Superior Efficiency, Robustness and Lifetime Economy."

[66] "European Commission - High temperature electrolyser with novel proton ceramic tubular modules of superior efficiency, robustness, and lifetime economy - https://cordis.europa.eu/project/id/621244/reporting [Accessed 1 September 2025]."

[67] "Sintef - GAMER - Game changer in high temperature steam electrolysers with novel tubular cells and stacks geometry for pressurized hydrogen production - https://www.sintef.no/en/projects/2018/gamer-game-changer-in-high-temperature-steam-electrolysers-with-novel-tubular-cells-and-stacks-geometry-for-pressurized-hydrogen-production/ - [Accessed 1 September 2025]".

[68] "Deliverable 2.1 GAMER - Delivery of individual components and assemblies for qualification tests in WP3".

[69] "Sintef - WINNER - World class Innovative Novel Nanoscale optimized electrodes and electrolytes for Electrochemical Reactions - https://www.sintef.no/en/projects/2021/winner/ [Accessed 1 September 2025]."

[70] "WINNER: World class innovative novel nanoscale optimized electrodes and electrolytes for electrochemical reactions".

[71] "European Commission - Tubular proton conducting ceramic stacks for pressurized hydrogen production - https://cordis.europa.eu/project/id/101101504/reporting [Accessed 1 September 2025]."

[72] "Protostack project - https://protostack.eu/objectives."

[73] A. Moranti, F. Riva, T. M. Bachmann, and J. Dailly, "Environmental performance of a metal-supported protonic ceramic cell and an electrolyte-supported solid oxide cell for steam electrolysis," *Int. J. Hydrogen Energy*, vol. 92, pp. 1284–1297, Nov. 2024, doi: 10.1016/j.ijhydene.2024.10.221.

[74] Z. Barahmand and M. S. Eikeland, "Techno-Economic and Life Cycle Cost Analysis through the Lens of Uncertainty: A Scoping Review," Oct. 01, 2022, *MDPI*. doi: 10.3390/su141912191.

[75] “Factorial Techniques applied in Chemical Plant Cost Estimation: A Comparative Study based on Literature and Cases.”

[76] “CLEAN HYDROGEN PRODUCTION PATHWAYS REPORT 2024.”

[77] G. P. . Towler and R. K. . Sinnott, *Chemical engineering design : principles, practice and economics of plant and process design*. Butterworth-Heinemann is an imprint of Elsevier, 2022.

[78] E. A. Harvego, J. E. O’brien, and M. G. Mckellar, “System Evaluations and Life-Cycle Cost Analyses for High-Temperature Electrolysis Hydrogen Production Facilities,” 2012. [Online]. Available: http://www.inl.gov

[79] “Aspen Plus User Models V8_2 - Heat Exchanger Dynamic Modeling - https://lhd52.wordpress.com/wp-content/uploads/2011/09/group-1-heat-exchanger.pdf”.

[80] “Acquademi Price https://www.acquademi.com/product/17497941/acqua-demineralizzata-in-cisterna-da-1000-litri [Accessed at October 2025].”

[81] M. Ruth, A. Mayyas, and M. Mann, “CEMAC-Clean Energy Manufacturing Analysis Center Manufacturing Competitiveness Analysis for PEM and Alkaline Water Electrolysis Systems Fuel Cell Seminar and Energy Expo CEMAC-Clean Energy Manufacturing Analysis Center 2,” 2017.

[82] S. Pratschner, F. Radosits, A. Ajanovic, and F. Winter, “Techno-economic assessment of a power-to-green methanol plant,” *Journal of CO2 Utilization*, vol. 75, Sep. 2023, doi: 10.1016/j.jcou.2023.102563.

[83] “Chemical Engineering - Economic Indicators CEPCI 2024 - www.CHEMENGONLINE.COM”.

[84] “Department of Chemical Engineering - Chemical Engineering Plant Cost Index - https://www.training.itservices.manchester.ac.uk/public/gced/CEPCI.html?reactors/CEPCI/index.html [Accessed 24 April 2025].”

[85] E. Vartiainen *et al.*, “True Cost of Solar Hydrogen,” *Solar RRL*, vol. 6, no. 5, May 2022, doi: 10.1002/solr.202100487.

[86] “D5.1 REINVENTING WATER PRICING Accelerate Innovation in urban wastewater management for Climate Change- ALICE PROJECT.”

[87] “Ffe - European day-ahead electricity prices in 2024 - https://www.ffe.de/en/publications/european-day-ahead-electricity-prices-in-2024/ [Accessed 24 April 2025].”

[88] Y. Zhou and S. Searle, “COST OF RENEWABLE HYDROGEN PRODUCED ONSITE AT HYDROGEN REFUELING STATIONS IN EUROPE,” 2022. [Online]. Available: www.theicct.orgcommunications@theicct.org

[89] “Ffe - European day-ahead electricity prices in 2024 - https://www.ffe.de/en/publications/european-day-ahead-electricity-prices-in-2024/#:~:text=The%20European%20price%20average%20in,above%20the%20pre%2Dcrisis%20level - [Accessed 24 April 2025].”

[90] “Levelised Cost of Hydrogen (LCOH) Calculator Manual,” 2024. [Online]. Available: https://observatory.clean-

[91] A. Perna, E. Jannelli, S. Di Micco, F. Romano, and M. Minutillo, “Designing, sizing and economic feasibility of a green hydrogen supply chain for maritime transportation,” *Energy Convers. Manag.*, vol. 278, Feb. 2023, doi: 10.1016/j.enconman.2023.116702.

[92] “Economics of Traditional Planning Methods - https://home.engineering.iastate.edu/jdm/ee552/EngrEconomics.pdf.”

[93] “EUROSTAT - EU key indicators - Inflation rate https://ec.europa.eu/eurostat [Accessed 24 April 2025].”

[94] “Electricity prices in Europe fell significantly in January 2023. https://gmk.center/en/posts/electricity-prices-in-europe-fell-significantly-in-january-2023/.”

[95] “STATISTA - Average monthly electricity wholesale price in Italy from January 2019 to September 2025 -https://www.statista.com/statistics/1267548/italy-monthly-wholesale-electricity-price/#statisticContainer [Accessed 24 April 2025].”

[96] H. Europe, “Strategic Research and Innovation Agenda Final Draft,” 2020.

[97] “How renewables could cut energy prices by 57% across Europe - https://www.rinnovabili.net/environment/scientific-reports/energy-prices-down-57-by-2030-renewables/ [Accessed 24 April 2025].”

[98] F. P. Pinheiro *et al.*, “Techno-economic analysis of green hydrogen generation from combined wind and photovoltaic systems based on hourly temporal correlation,” *Int. J. Hydrogen Energy*, vol. 97, pp. 690–707, Jan. 2025, doi: 10.1016/j.ijhydene.2024.11.429.

[99] F. Massaro, M. Ferraro, F. Montana, E. Riva Sanseverino, and S. Ruffino, “Techno-Economic Analysis of Clean Hydrogen Production Plants in Sicily: Comparison of Distributed and Centralized Production,” *Energies* , vol. 17, no. 13, Jul. 2024, doi: 10.3390/en17133239.

[100] F. Hönig, G. D. Rupakula, D. Duque-Gonzalez, M. Ebert, and U. Blum, “Enhancing the Levelized Cost of Hydrogen with the Usage of the Byproduct Oxygen in a Wastewater Treatment Plant,” Jun. 01, 2023, *MDPI*. doi: 10.3390/en16124829.

[101] R. Hancke, T. Holm, and Ø. Ulleberg, “The case for high-pressure PEM water electrolysis,” *Energy Convers. Manag.*, vol. 261, Jun. 2022, doi: 10.1016/j.enconman.2022.115642.

[102] Z. Li *et al.*, “A techno-economic analysis of protonic ceramic electrolysis cells (PCECs) for advancing the future of large-scale green hydrogen production,” *Renew. Energy*, vol. 254, Dec. 2025, doi: 10.1016/j.renene.2025.123703.

[103] E. Bargiacchi, G. Puig-Samper, F. Campos-Carriedo, D. Iribarren, and J. Dufour, “SUSTAINABILITY ASSESSMENT OF HARMONISED HYDROGEN ENERGY SYSTEMS D2.2 Definition of FCH-LCA guidelines WP2 Reformulation of current guidelines for Life Cycle Assessment DELIVERABLE LEADERS.”

[104] Derek, *Environmental management-Life cycle assessment-Requirements and guidelines*. 2010.

[105] “Environmental management-Life cycle assessment-Principles and framework Management environnemental-Analyse du cycle de vie-Principes et cadre.”

[106] *International Reference Life Cycle Data System (ILCD) Handbook : general guide for life cycle assessment : detailed guidance*. Publications Office, 2010.

[107] “CarbonBright. LCIA Methods: Measuring Impact Beyond Carbon. https://www.carbonbright.co/insight/lcia-methods-a-guide-to-measuring-what-matters [Accessed 7 October 2025].”

[108] G. Rebitzer *et al.*, “Life cycle assessment Part 1: Framework, goal and scope definition, inventory analysis, and applications,” 2004, *Elsevier Ltd*. doi: 10.1016/j.envint.2003.11.005.

[109] D. Clark *et al.*, “Single-step hydrogen production from NH 3 , CH 4 , and biogas in stacked proton ceramic reactors,” 2022. [Online]. Available: https://www.science.org

[110] M. Tarach *et al.*, “D3.2; Report on individual components qualification tests Public Summary Contractual date of delivery to COM M10 Actual date of delivery to COM M12.”

[111] F. Da Prato, S. Anelli, A. Moranti, D. Ferrero, M. Santarelli, and F. Smeacetto, “Progress in the study of glass-based systems as sealants for proton ceramic electrolysis cell assembly,” *Int. J. Hydrogen Energy*, vol. 140, pp. 119–130, Jun. 2025, doi: 10.1016/j.ijhydene.2025.05.286.

[112] F. Stepniak, P. A. Kohl, and S. A. Bidstrup, “Silver Metallization For Advanced Electronic Interconnections.”

[113] “Feed Water tank. Di camillo tanks. www.di-camillo.com”.

[114] “Technical Specifications.” [Online]. Available: www.aecinternet.com

[115] “Ascent Machineries & Engg. Services Mumbai, Maharashtra. Electric 55 kg/hr Steam Boilerhttps://www.ascentmachineries.com/electrical-electrode-non-ibr-boiler.html [Accessed 1 September 2025].”

[116] “Hypersep BioEnergy Separator tank. https://ph.parker.com/it/it/product/hypersep-bioenergy-water-separators/csb720-304 [Accessed 1 September 2025].”

[117] S. Lundberg, “Comparative LCA of Electrolyzers for Hydrogen Gas Production SCHOOL OF ARCHITECTURE AND THE BUILT ENVIRONMENT,” 2019.

[118] “S235JR unalloyed steel structure. Bettinelli Acciai”.

[119] “DieCasting-Mould. What is Mild Steel https://www.diecasting-mould.com/news/what-is-mild-steel-ms-definition-composition-properties-grade-gauge-uses-types-vs-stainless-steel [Accessed 1 September 2025].”

[120] “European COmmission. Life Cycle Assessment & the EF methods. https://green-forum.ec.europa.eu/green-business/environmental-footprint-methods/life-cycle-assessment-ef-methods_en [Accessed 10 September 2025].”

[121] “Environmental life cycle assessment (LCA) comparison of hydrogen delivery options within Europe,” doi: 10.2760/5459.

[122] V. De Laurentiis, A. Amadei, E. Sanyé-Mengual, and S. Sala, “Exploring alternative normalization approaches for life cycle assessment,” *International Journal of Life Cycle Assessment*, vol. 28, no. 10, pp. 1382–1399, Oct. 2023, doi: 10.1007/s11367-023-02188-4.

[123] J. Felix Aigner, “EPPA-European Paper Packaging Alliance Date Ramboll Italy Rome Office COMPARATIVE LIFE CYCLE ASSESSMENT (LCA) SINGLE-USE AND MULTIPLE-USE TABLEWARE SYSTEMS FOR TAKE-AWAY SERVICES IN QUICK SERVICE RESTAURANTS,” 2022.

[124] M. B. Memon, M. Tao, T. Ahmed, Z. Yang, M. Ibrahim, and S. Ullah, “Towards greener metal production: A life cycle assessment model for copper-gold-silver mining and mineral processing operations,” *Process Safety and Environmental Protection*, vol. 197, May 2025, doi: 10.1016/j.psep.2025.107069.

[125] J. T. Dahle and Y. Arai, “Environmental geochemistry of cerium: Applications and toxicology of cerium oxide nanoparticles,” Jan. 23, 2015, *MDPI*. doi: 10.3390/ijerph120201253.

[126] W. Wei, P. B. Samuelsson, A. Tilliander, R. Gyllenram, and P. G. Jönsson, “Wenergy consumption and greenhouse gas emissions of nickel products,” *Energies (Basel).*, vol. 13, no. 21, Nov. 2020, doi: 10.3390/en13215664.

[127] N. Gerloff, “Comparative Life-Cycle-Assessment analysis of three major water electrolysis technologies while applying various energy scenarios for a greener hydrogen production,” *J. Energy Storage*, vol. 43, Nov. 2021, doi: 10.1016/j.est.2021.102759.

[128] K. Bareiß, C. de la Rua, M. Möckl, and T. Hamacher, “Life cycle assessment of hydrogen from proton exchange membrane water electrolysis in future energy systems,” *Appl. Energy*, vol. 237, pp. 862–872, Mar. 2019, doi: 10.1016/j.apenergy.2019.01.001.

[129] G. Magnaval, T. Debonnet, and M. Margni, “Integrated LCA and Eco-design Process for Hydrogen Technologies: Case Study of the Solid Oxide Electrolyser,” in *Proceedings of the 35th European Symposium on Computer Aided Process Engineering (ESCAPE 35)*, PSE Press, Jul. 2025, pp. 674–680. doi: 10.69997/sct.171756.

[130] “ELY4OFF: PEM electrolysers for operation with offgrid renewable installations. Deliverable 2.6-LCA and cost analysis”.

[131] A. Mehmeti, A. Angelis-Dimakis, C. B. Muñoz, M. Graziadio, and S. J. McPhail, “Eco-thermodynamics of hydrogen production by high-temperature electrolysis using solid oxide cells,” *J. Clean. Prod.*, vol. 199, pp. 723–736, Oct. 2018, doi: 10.1016/j.jclepro.2018.07.166.

RINGRAZIAMENTI

Desidero ringraziare il *Prof. Elio Jannelli* per avermi accolta come dottoranda, facendomi sentire fin da subito un membro prezioso del suo gruppo di ricerca. Grazie alle opportunità da lui offerte, ho potuto collaborare e confrontarmi costantemente con dottorandi e ricercatori, in un percorso di continua e stimolante crescita professionale. Inoltre, grazie al suo supporto e alla fiducia dimostratami, ho avuto l'onore di partecipare a diverse conferenze nazionali ed internazionali, esperienze che hanno rafforzato la mia passione per la ricerca.

Un ringraziamento speciale è riservato alla *Prof. Mariagiovanna Minutillo*, alla quale va la mia gratitudine più profonda e sincera per tutto ciò che ha fatto e continua a fare per me.
La sua presenza è stata ed è tuttora una costante illuminante in questo lungo percorso: un mentore empatico, capace di bilanciare l'approccio scientifico con quello umano. La ringrazio per avermi guidata con una competenza straordinaria, una dedizione instancabile, ma soprattutto per aver saputo trasformare i momenti di incertezza in occasioni di crescita attraverso il suo costante incoraggiamento. Le discussioni approfondite, le innumerevoli opportunità di ricerca che mi ha offerto fin dai primi giorni, e la fiducia che ha riposto in me sono state il vero motore che mi ha spinta a superare i miei limiti. Il suo sostegno, tanto tecnico quanto emotivo, è stato un pilastro fondamentale per il successo della mia ricerca.

Ringrazio anche i ricercatori *Viviana Cigolotti, Giuseppe Di Florio, Claudio Carbone ed Alessandro Agostini dell'Agenzia nazionale ENEA*. Lavorare con loro è stato un privilegio: il loro impegno vigoroso, la sinergia nell'affrontare problemi complessi, le sessioni di brainstorming e lo spirito di squadra hanno reso questo dottorato un'esperienza collettiva e arricchente. Grazie per le condivisioni di conoscenze, per il supporto tecnico nelle simulazioni e per avermi insegnato il valore della collaborazione interdisciplinare.

Ringrazio il ricercatore *Alessandro Arrigoni del JRC - Joint Research Centre della Commissione Europea di Petten (Olanda)*. Gli sono profondamente grata per la calorosa accoglienza riservatami durante il mio periodo di permanenza presso il loro centro di ricerca, per il supporto costante e la pazienza infinita con cui ha accompagnato ogni passo di questo cammino. Lo ringrazio per avermi guidata con dedizione negli studi condotti insieme e per le numerose opportunità professionali che ha creato per me.

Ringrazio tutti i partner del *progetto Europeo PROTOSTACK*. È stato per me un grande onore poter partecipare e lavorare in prima linea a questo progetto, seguendone da vicino gli sviluppi e le dinamiche. Sono grata per l'opportunità ricevuta e per aver potuto offrire il mio contributo scientifico all'avanzamento di un progetto così prestigioso.

Infine, ma non per importanza, rivolgo un ringraziamento colmo di affetto e stima alla *Prof.ssa Simona Di Micco*. In questi anni, il nostro rapporto è cresciuto passo dopo passo, consolidandosi in un legame che supera la sfera accademica. Grazie per essere stata non solo una costante guida professionale e un'instancabile stimolatrice di idee, ma anche una grande amica e una sostenitrice sincera. La sua presenza è stata un punto di riferimento fondamentale su cui ho potuto contare, personalmente e scientificamente, in ogni momento di questo lungo cammino insieme.